GENETIC ALGORITHM-ASSISTED EMBEDDED HEAT SPREADER RADIATOR DESIGN FOR LIGHTWEIGHT AND THERMAL PERFORMANCE IN GEO SPACECRAFT

GIRAY ÖZEN

ÖZYEĞİN UNIVERSITY

NOVEMBER, 2025

GENETIC ALGORITHM-ASSISTED EMBEDDED HEAT SPREADER RADIATOR DESIGN FOR LIGHTWEIGHT AND THERMAL PERFORMANCE IN GEO SPACECRAFT

by
Giray Özen

Thesis
Submitted in Partial Fulfillment of the
Requirements for the Degree of

Master of Science

in
Mechanical Engineering

Advisor: Asst. Prof. Altuğ Melik Başol

Graduate School of Science and Engineering
Özyeğin University
İstanbul

November, 2025

GENETIC ALGORITHM-ASSISTED EMBEDDED HEAT SPREADER RADIATOR DESIGN FOR LIGHTWEIGHT AND THERMAL PERFORMANCE IN GEO SPACECRAFT

Approved by:

Asst. Prof. Altuğ Melik Başol, Advisor
Department of Mechanical Engineering
Özyeğin University

Assoc. Prof. Dr. Özgür Ertunç
Department of Mechanical Engineering
Özyeğin University

Prof. Dr. Barbaros Çetin
Department of Mechanical Engineering
Bilkent University

Approval Date: October 10, 2025

To my family and to all who have believed in me

DECLARATION OF ORIGINALITY

I hereby declare that I am the sole author of this thesis and that this is the true copy of my thesis, including the final revisions, approved by my thesis committee. All data and information have been obtained, produced, and presented in accordance with the rules of research ethics and principles of academic honesty. As required by these rules, to the best of my knowledge I have acknowledged ideas, thoughts, and any copyrighted material in accordance with the standard referencing rules. I certify that any part of this thesis has not been submitted for a degree or diploma in another educational institution.

Giray Özen

ABSTRACT

In spacecraft, radiators cool electronic equipment by conducting waste heat away from components and radiating it into space. They are essential for maintaining component temperatures within allowable operational limits. While radiators must provide adequate heat transfer area to manage thermal loads, minimizing their mass is equally important to ensure feasibility in space applications. This study presents an optimization methodology employing a genetic algorithm (GA) for the thermal design of embedded heat spreader radiators and equipment layout in Geostationary Earth Orbit (GEO) spacecraft. The optimized radiator design and equipment layout for the case studies were validated through thermal analysis using SIEMENS SIMCENTER 3D Space Systems Thermal (SST). Unlike traditional methods, the developed tool concurrently assesses all relevant design variables to determine the optimal radiator and equipment layout, thereby streamlining the design process. The case study results highlight that GA parameters affect GA outcomes. Larger populations and higher mutation rates increase computation time but improve accuracy, making the evaluation of multiple GA parameter sets essential for identifying optimal configurations.

Keywords: *Spacecraft Radiator, Thermal Design, Genetic Algorithm, Equipment Layout, Heat Spreader*

ÖZETÇE

Uzay araçlarında, elektronik ekipmanların atık ısısını uzaklaştırıp, uzaya atmak için radyatörler kullanılmaktadır. Radyatörler, ekipmanların izin verilen operasyonel sıcaklık sınırları içinde çalışmasını sağlamak açısından kritik öneme sahiptir. Isıl yükleri yönetebilmek için radyatörlerin yeterli ısı transfer alanına sahip olması gerekirken, kütlelerinin de minimumda tutulması uzay uygulamalarında fizibilite açısından son derece önemlidir. Bu çalışma, Yer Sabit Yörünge (GEO) uzay aracı için ısı yayıcı gömülü radyatörlerin ve ekipman yerleşiminin ısıl tasarımında genetik algoritma (GA) tabanlı bir tasarım metodolojisi sunmaktadır. Optimize edilmiş radyatör tasarımı ve ekipman yerleşimi, SIEMENS SIMCENTER 3D Space Systems Thermal (SST) yazılımı kullanılarak gerçekleştirilen ısıl analizle doğrulanmıştır. Geleneksel yöntemlerin aksine, geliştirilen bu araç ile tüm ilgili tasarım değişkenleri aynı anda değerlendirilmekte ve böylece optimal radyatör ve ekipman yerleşimi hızlı ve etkin bir şekilde belirlenebilmektedir. Gerçekleştirilen vaka çalışmaları, GA parametrelerinin elde edilen sonuçlar üzerinde önemli bir etkisi olduğunu göstermektedir. Daha büyük popülasyonlar ve daha yüksek mutasyon oranları, hesaplama süresini artırmakla birlikte, çözüm kalitesini de iyileştirmekte; bu nedenle, optimal konfigürasyonların belirlenmesi için birden fazla GA parametre setinin değerlendirilmesi gerekmektedir.

Anahtar Kelimeler: *Uzay Aracı Radyatörü, Isıl Tasarım, Genetik Algoritma, Ekipman Yeterliliği, Isı Yayıcılar*

ACKNOWLEDGMENTS

I would like to express my deepest gratitude to my thesis advisor, Asst. Prof. Altuğ Melik Başol, for his unwavering guidance, patience, and invaluable expertise. Despite his demanding schedule, he generously shared his time with me, allowing me to benefit from his vast knowledge and learn immensely throughout this process.

I would like to express my gratitude to Turkish Aerospace for their valuable support throughout the course of this study.

I am sincerely thankful to my beloved wife, Duygu Özen, whose constant belief in me and unyielding support gave me the strength to keep moving forward. Her presence has been my greatest source of motivation.

Finally, I would like to thank my dear friend, Süleyman Kaancan Ataer, for his technical insights and generous help. His strong academic background and encouragement helped me overcome many challenges along the way.

TABLE OF CONTENTS

DECLARATION OF ORIGINALITY iv
ABSTRACT v
ÖZETÇE vi
ACKNOWLEDGMENTS vii
TABLE OF CONTENTS viii
LIST OF TABLES x
LIST OF FIGURES iii
1. INTRODUCTION 1
1.1 GEO Spacecraft Thermal Design Overview 2
1.1.1 Spacecraft Radiator Applications 21
1.1.1.1 Passive Structure Radiators 22
1.1.1.1.1 Thermal Doublers 23
1.1.1.1.2 Heat Spreaders 24
1.1.1.2 Deployable Radiators 26
1.1.1.3 Body-Mounted Radiators 27
1.1.1.4 Structural Panels with Heat Pipes 28
1.1.1.4.1 Heat Pipes 30
1.2 Engineering Optimization 33
1.2.1 Definition of Genetic Algorithm 38
2. LITERATURE REVIEW 41
2.1 Thermal Modelling of Spacecraft Radiators 41
2.2 Genetic Algorithms for Optimization-Based Engineering Design 44
2.3 Objective of Thesis 47
2.4 Outline of Thesis 48
3. METHODOLOGY 49
3.1 Thermal Design of Embedded Heat Spreader GEO Radiators 49
3.1.1 Radiator Sizing and Dimensioning 51
3.1.2 Fin Efficiency Approach and Equations 53
3.2 Genetic Algorithm 63
3.2.1 Operators of the Genetic Algorithm 64

3.2.1.1 Population Size 64
3.2.1.2 Encoding and Decoding 66
3.2.1.2.1 Binary Representation of Discrete Design Variables in GAs 68
3.2.1.2.2 Binary Representation of Continuous Design Variables in GAs 69
3.2.1.3 Generation Gap and Elitism 70
3.2.1.4 Selection in Genetic Algorithms 72
3.2.1.5 Crossover in Genetic Algorithms 75
3.2.1.6 Mutation in Genetic Algorithms 78
3.2.1.7 Fitness Evaluation in Genetic Algorithms 81
3.2.1.8 Stopping Criteria in Genetic Algorithms 82
3.3 Application of GA in Radiator and Equipment Layout Optimization 84
3.3.1 Problem Statement for Optimizing Embedded HS GEO Radiators 85
3.3.2 Problem Statement for Optimizing Equipment Layout 90
3.3.3 Workflow of the Developed Radiator Optimization Code 94
4. RESULTS AND DISCUSSION 100
4.1 Finite Element-Based Thermal Modelling 100
4.1.1 Geometric Modelling 100
4.1.2 Meshing 101
4.1.3 Thermal Analysis 104
4.2 Case Study Analysis 113
4.2.1 Case Study-1 113
4.2.1.1 Problem Statement for Case Study-1 113
4.2.1.2 Results for Case Study-1 116
4.2.1.3 Verification Using Finite Element Method for Case Study-1 120
4.2.2 Case Study-2 125
4.2.2.1 Problem Statement for Case Study-2 125
4.2.2.2 Results for Case Study-2 127
4.2.2.3 Verification Using Finite Element Method for Case Study-2 131
4.3 Discussion 137
5. CONCLUSION 140
6. FUTURE WORK 141
7. REFERENCES 142

LIST OF TABLES

Table 1.1: Thermo-Optical Properties of Different Materials 6
Table 1.2: Thermal Requirements Example 10
Table 1.3: Comparison of Thermal Simulation Software 14
Table 1.4: Shape Function and Graphical Representations 17
Table 1.5: Classification of Optimization Problems... 34
Table 3.1: Comparison of Common GA Encoding Schemes 67
Table 3.2: Decoding Discrete Variables with Two-Stage Three-Bit Mapping 69
Table 3.3: Comparison of Different Selection Techniques 73
Table 3.4: Comparison of Different Crossover Techniques 76
Table 3.5: Comparison of Different Mutation Techniques... 79
Table 3.6: Example of Sorted Candidate Solution Sets Based on Mass........................ 98
Table 3.7: Sorted Candidate Equipment Layouts by HS Heat Load Std. Dev. 99
Table 4.1: Equipment Information for Case Study-1.. 114
Table 4.2: Material Properties Used in Case Study 114
Table 4.3: Design Space for Radiator Design Variables for Case Study-1 116
Table 4.4: Equipment Temperature Limits for Case Study-1..................................... 117
Table 4.5: GA Parameters Set for the DROC 117
Table 4.6: Best Radiator Configurations with GA Variations for Case Study-1......... 118
Table 4.7: Best Equipment Layouts with GA Variations for Case Study-1 119
Table 4.8: Design Parameters of Selected Radiator Configuration – Case Study-1.... 121
Table 4.9: Selected Equipment Layout Design Parameters – Case Study-1 122
Table 4.10: Heat Distribution Across Radiator Sections – Case Study-1.................... 124
Table 4.11: Results of Thermal Analysis – Case Study-1 125
Table 4.12: Equipment Information – Case Study-2 126
Table 4.13: Design Space for Radiator Design Variables – Case Study-2.................. 127
Table 4.14: Equipment Temperature Limits for Case Study-2................................... 128
Table 4.15: Best Radiator Configurations with GA Variations – Case Study-2 129
Table 4.16: Best Equipment Layouts with GA Variations for Case Study-2.............. 130
Table 4.17: Design Parameters of Selected Radiator Configuration – Case Study-2.. 132
Table 4.18: Selected Equipment Layout Design Parameters – Case Study-2 133
Table 4.19: Heat Distribution Across Radiator Sections – Case Study-2.................... 136

Table 4.20: Results of Thermal Analysis – Case Study-2 136

LIST OF FIGURES

Figure 1.1: Annual Number of Objects Launched.. 1
Figure 1.2: Space Thermal Environment.. 3
Figure 1.3: Thermal Balance of a Radiator in Steady State in Space............................ 4
Figure 1.4: Solar Illumination on the North and South Faces of a GEO Satellite........... 7
Figure 1.5: Bent Heat Pipe Profile.. 7
Figure 1.6: Equinox Eclipse Condition in Geostationary Orbit 9
Figure 1.7: NASA Temperature Margin Philosophy.. 11
Figure 1.8: ESA Temperature Margin Philosophy 11
Figure 1.9: Thermal Control Subsystem Design Flowchart 13
Figure 1.10: Integration Path Between Elements i and j 19
Figure 1.11: Thermal Vacuum Test Profile.. 20
Figure 1.12: Passive Structure Radiator 23
Figure 1.13: Radiator Panel with Integrated Thermal Doubler 24
Figure 1.14: Radiator Panel with Embedded HS.. 25
Figure 1.15: Deployable Radiator Components 26
Figure 1.16: Body Mounted Radiator.. 27
Figure 1.17: Typical HPs and Radiator Panel Configurations 28
Figure 1.18: Temperature Profile of Radiator with Embedded HP 30
Figure 1.19: Flanged Axially Grooved HP... 31
Figure 1.20: Working Principle of HP.. 32
Figure 1.21: Classification of Numerical Optimization Techniques 36
Figure 1.22: Classification of Metaheuristic Algorithms 37
Figure 1.23: Flowchart of Genetic Algorithm 39
Figure 1.24: Operators of Genetic Algorithm... 40
Figure 3.1: Equipment Placement on Embedded HS GEO Radiator Panel 50
Figure 3.2: Thermal Resistance Diagram of Embedded HS GEO Radiator.................. 51
Figure 3.3: Simplified Thermal Resistance Diagram of Embedded HS GEO Radiator 56
Figure 3.4: Schematic Diagram of a Radiator with Embedded HS 57
Figure 3.5: HS and Fin in Radiator.. 58
Figure 3.6: Honeycomb Structure and Heat Transfer Pathways 59
Figure 3.7: Longitudinal Radiating Fin of Flat Shape 61

Figure 3.8: Population Sizing in Genetic Algorithms ... 65
Figure 3.9: Chromosome Structure – 34-Bit String with 6 Genes ... 68
Figure 3.10: Roulette Wheel for Fitness-Based Population Selection ... 74
Figure 3.11: Mixed Two-Point Crossover Operator ... 77
Figure 3.12: Bitwise Mutation Operator ... 80
Figure 3.13: Chromosome Representation of Radiator Design Variables ... 85
Figure 3.14: Chromosome Representation of Equipment Layout Variables ... 85
Figure 3.15: Design Parameters of Embedded HS Radiators ... 86
Figure 3.16: Design Variables of Equipment Layout ... 91
Figure 3.17: Flowchart of the Developed Radiator Optimization Code ... 95
Figure 3.18: Inputs and Outputs of the Developed Radiator Optimization Code ... 97
Figure 4.1: Geometric Model of Radiator and Equipment ... 101
Figure 4.2: 2D Mesh Creation ... 102
Figure 4.3: Assembly-Level Finite Element Model of Radiator and Equipment ... 102
Figure 4.4: Sub-Level Finite Element Model of Radiator and Equipment ... 103
Figure 4.5: Mesh Collector Information ... 104
Figure 4.6: Simulation Objects and Thermal Loads ... 105
Figure 4.7: Solution Parameters ... 106
Figure 4.8: Radiation Definition ... 107
Figure 4.9: Thermal Coupling Between Equipment and Inner FS ... 108
Figure 4.10: Solar Heating Space Definition ... 109
Figure 4.11: Thermal Coupling Between Inner FS and HS Top ... 110
Figure 4.12: Thermal Coupling Between Outer FS and HS Bottom ... 111
Figure 4.13: Thermal Coupling Between Top and Bottom of HS ... 112
Figure 4.14: Heat Load Definition for Equipment ... 113
Figure 4.15: GA-5 Convergence Curve – Case Study-1 Equipment Layout Design ... 120
Figure 4.16: Radiator Geometric Model in Siemens NX – Case Study-1 ... 122
Figure 4.17: Radiator Thermal Model in Simcenter 3D – Case Study-1 ... 122
Figure 4.18: Inner FS Temperature in Simcenter 3D SST – Case Study-1 ... 123
Figure 4.19: Temperatures of Equipment in Simcenter 3D SST – Case Study-1 ... 124
Figure 4.20: GA-9 Convergence Curve – Case Study-2 Equipment Layout Design ... 131
Figure 4.21: Radiator Geometric Model in Siemens NX – Case Study-2 ... 134

Figure 4.22: Radiator Thermal Model in Simcenter 3D – Case Study-2 134
Figure 4.23: Inner FS Temperature in Simcenter 3D SST – Case Study-2 135
Figure 4.24: Temperatures of Equipment in Simcenter 3D SST – Case Study-2 135

LIST OF ACRONYMS AND ABBREVIATIONS

1D: One-Dimensional Domain

2D: Two-Dimensional Domain

ACO: Ant Colony Optimization

APG: Annealed Pyrolytic Graphite

AR: Aspect Ratio

BA: Bat Algorithm

BB-BC: Big Bang-Big Crunch Algorithm

BOL: Beginning of Life

CAD: Computer-Aided Design

CPL: Capillary Pumped Loop

CS: Cuckoo Search

CSS: Charged System Search

DROC: Developed Radiator Optimization Code

EOL: End of Life

ESA: European Space Agency

ESARAD: European Space Agency Radiative Analysis Design Tool

ESATAN: European Space Agency Thermal Analysis Network

FFA: Firefly Algorithm

FA: Flight Acceptance

FDM: Finite Difference Method

FEM: Finite Element Method

FLUINT: Fluid Integrator

FS: Facesheet

GA: Genetic Algorithm

GEO: Geostationary Earth Orbit

HC: Honeycomb

HP: Heat Pipe

HSA: Harmony Search Algorithm

HS: Heat Spreader

IR: Infrared

KH: Krill Herd

LEO: Low Earth Orbit

MEO: Medium Earth Orbit

MLI: Multilayer Insulation

NASA: National Aeronautics and Space Administration

OSR: Optical Solar Reflector

PC: Personal Computer

PCM: Phase Change Material

PSO: Particle Swarm Optimization

QUAD4: Four-Node Quadrilateral Element

RadCAD: Radiation Computer-Aided Design

RadK: Radiation Kernel

SA: Simulated Annealing

SINDA: Systems Improved Numerical Differencing Analyzer

SST: Space Systems Thermal

Std. Dev.: Standard Deviation

TFAWS: NASA Thermal & Fluids Analysis Workshop

TMM: Thermal Mathematical Model

TS: Tabu Search

TSS: Thermal Synthesizer System

TVC: Thermal Vacuum Chamber

UV: Ultraviolet

1. INTRODUCTION

A spacecraft is a vehicle or device designed for travel or operation in outer space. Spacecraft play a vital role in improving human life by enhancing communication, enabling navigation, monitoring the Earth's environment, advancing scientific knowledge, driving technological innovation, and inspiring future generations to explore and discover the wonders of the universe.

In the past few decades, there has been a remarkable increase in competition within the space industry. Countries, private companies, and international groups are all vying to lead in space exploration, satellite launches, and commercial ventures. As shown in Figure 1.1, the total number of objects sent into space has risen significantly. This trend reflects how space is becoming more accessible and is being used for a wide range of purposes.

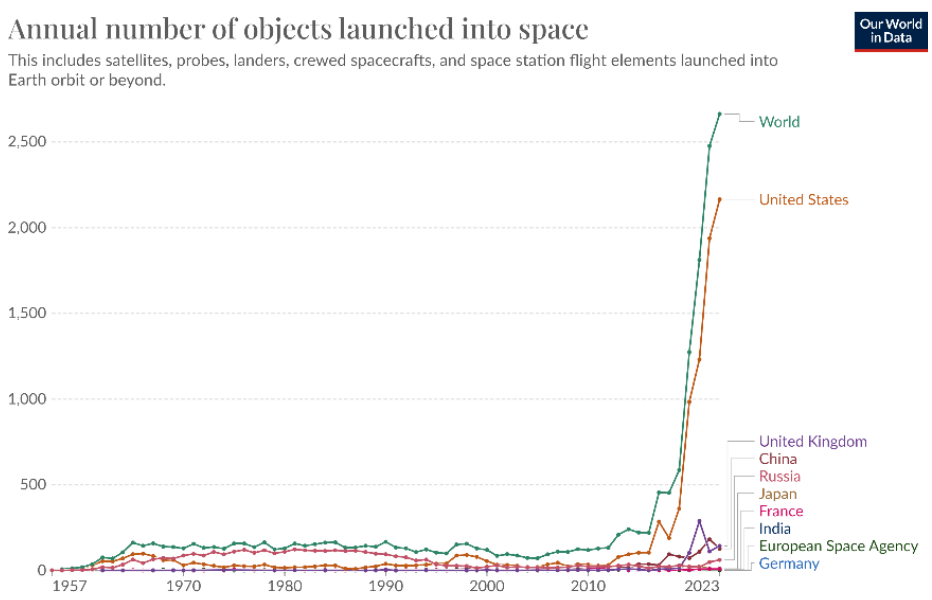

Figure 1.1: *Annual Number of Objects Launched (Source: Our World in Data [1])*

In order to succeed in the competitive space industry, companies focus on developing more competitive spacecraft designs. One critical aspect involves the diligent management of costs, particularly those stemming from the dimensions and weight of spacecraft. This emphasis on cost control is vital for enhancing competitiveness and ensuring the economic viability of space exploration endeavors. Therefore, reducing the size and mass of spacecraft components is a crucial objective for all subsystems within the spacecraft. To address these challenges, optimization techniques are frequently employed during the design and development phases. These techniques enable engineers to systematically evaluate trade-offs among multiple design variables, ultimately leading to solutions that minimize mass and volume while maintaining or enhancing system performance.

1.1 GEO Spacecraft Thermal Design Overview

Spacecraft are equipped with various instruments, propulsion systems, and communication devices to fulfill their specific missions and objectives. This equipment is exposed to harsh environmental conditions in space and must maintain allowable flight temperatures to avoid performance issues that could jeopardize the mission. Therefore, thermal design engineers employ passive and/or active thermal hardware to meet this requirement. As with other subsystems, thermal design engineers are also expected to pursue for lightweight and compact thermal control designs in addition to sufficient thermal performance.

The objective of spacecraft thermal control is to maintain a balance between incoming and outgoing energy to ensure that the equipment temperatures remain within the allowable range for the flight. Orbital heating, comprising direct solar radiation, reflected solar energy (albedo), and planetary infrared thermal radiation, as shown in

Figure 1.2, along with the heat produced by equipment operation, represents the incoming energy. The spacecraft releases heat through infrared radiation into space, which constitutes the outgoing energy.

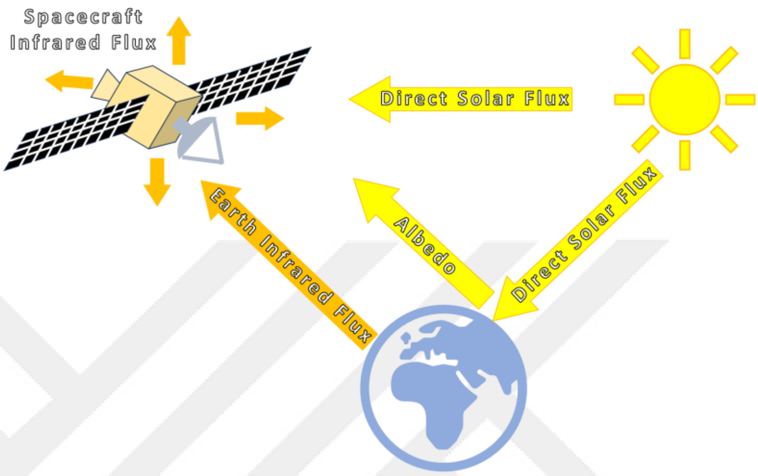

Figure 1.2: *Space Thermal Environment*

Thermal design engineers must achieve a sophisticated balance in managing heat exchange, heat transfer directions, and heat transfer processes both within the satellite and between its internal and external environments. Regulating the elements that affect energy input and output on a spacecraft, as shown in Figure 1.3, is essential for efficient thermal management. Heat transfer in spacecraft occurs through conduction, convection, and radiation. However, the primary methods of heat transfer are radiation and conduction. In space applications, convection is not a concern because of the vacuum conditions. The only medium present inside the spacecraft is the fluid within the heat pipe (HP), which helps transfer heat from the evaporator to the condenser.

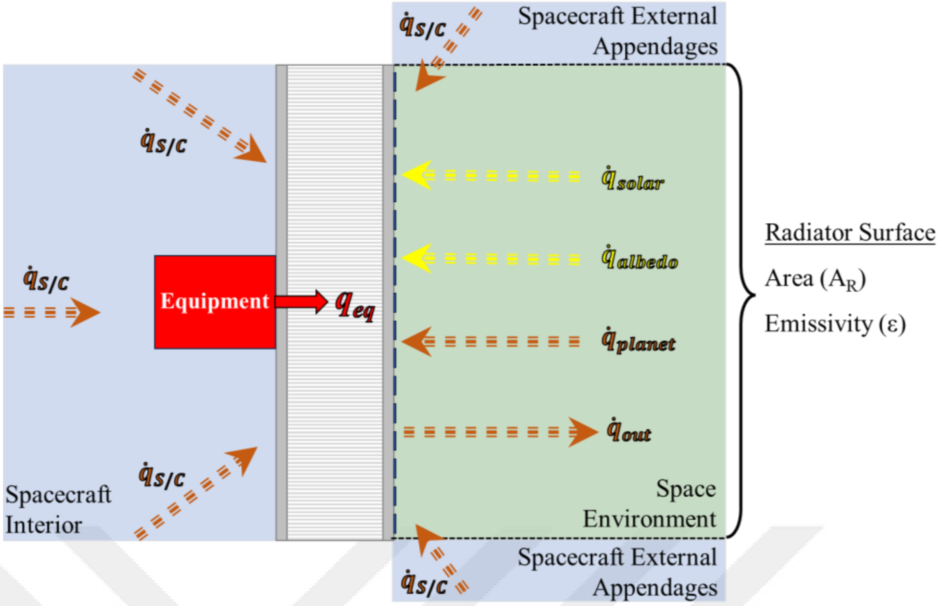

Figure 1.3: *Thermal Balance of a Radiator in Steady State in Space*

A methodology based on the first law of thermodynamics is employed to evaluate the thermal performance of the spacecraft and to verify that the radiator design meets the required heat rejection capability. This analysis considers all incoming ($\dot{q}_{in}$) and outgoing ($\dot{q}_{out}$) heat fluxes affecting the spacecraft. The incoming heat fluxes to the radiator include internal radiative exchange between the radiator and surrounding components with a non-zero view factor, as well as heat generated by accommodated dissipative equipment $\left(q_{eq}\right)$. In addition, orbital heat fluxes, are albedo ($\dot{q}_{albedo}$), solar ($\dot{q}_{solar}$), planetary ($\dot{q}_{planet}$), and heat fluxes from spacecraft appendages and interior surfaces of the spacecraft $\left(\dot{q}_{S/C}\right)$ contribute to the total input. The outgoing heat flux corresponds to radiative heat rejection to space ($\dot{q}_{R\,HRC}$), which depends on the radiator area (A_R), radiator temperature (T_R), and the environmental view factor (F). The governing equations for this energy balance are defined below:

$$\dot{q}_{in} = \dot{q}_{out} \tag{1.1}$$

$$\dot{q}_{in} = \dot{q}_{solar} + \dot{q}_{albedo} + \dot{q}_{planet} + \dot{q}_{S/C} \tag{1.2}$$

$$\dot{q}_{out} = \sigma F \varepsilon (T_R^4 - T_s^4) \tag{1.3}$$

$$\dot{q}_{R\ HRC} = \sigma F \varepsilon (T_R^4 - T_s^4) - (\dot{q}_{solar} + \dot{q}_{albedo} + \dot{q}_{planet} + \dot{q}_{S/C}) \tag{1.4}$$

$$\sigma A_R F \varepsilon (T_R^4 - T_s^4) = A_R (\dot{q}_{solar} + \dot{q}_{Albedo} + \dot{q}_{planet} + \dot{q}_{S/C}) + q_{eq} \tag{1.5}$$

The Earth rotates on its axis relative to the Sun every 24.0 hours of mean solar time, with an inclination of 23.5 degrees from the plane of its orbit around the Sun. In addition, Earth revolves in orbit around the Sun in 365 days, 6 hours and 9 minutes with reference to the stars, at a speed ranging from 29.29 to 30.29 km/s [2]. From liftoff through final orbit insertion and throughout the spacecraft's operational period, the spacecraft undergoes various thermal cycles. The side exposed to the Sun experiences high temperatures, while the opposite side facing the cold expanse of space encounters extremely low temperatures. As the spacecraft moves along its orbit, the sun-facing side changes periodically. This thermal variation must be accounted for during the thermal design phase to select appropriate materials and equipment for effective thermal regulation.

Satellite thermal design is both complex and iterative, involving a blend of design selection and analysis of the chosen design. Design selection involves specifying materials, geometries, structural types, equipment allocation, and appropriate thermal control systems based on the spacecraft's mission criteria. The design scenarios for spacecraft are influenced by factors such as orbital heating, internal heat dissipation from components, equipment temperature requirements, and the satellite configuration.

In orbit, thermal surfaces are exposed by charged particles, ultraviolet (UV) radiation, high vacuum conditions, and the deposition of contamination films that settle on nearly all spacecraft surfaces. The thermo-optical characteristics of thermal surfaces at the start of a satellite's life, before any degradation has occurred, are referred to as "Beginning of Life (BOL)," while the term "End of Life (EOL)" denotes the opposite, representing conditions after degradation and prolonged use. Table 1.1 illustrates changes in thermo-optical properties for several materials.

Table 1.1: *Thermo-Optical Properties of Different Materials (Adapted from [3])*

Components	Solar Absorptivity (BOL)	Solar Absorptivity (EOL)	Emissivity
OSR	0.11	0.266	0.84
External MLI	0.35	0.5	0.61
External Black MLI	0.93	0.93	0.84

The GEO spacecraft strategically positions high heat-dissipating equipment on its north and south panels [4]. These panels demonstrate the highest radiator efficiency due to their angle with the solar vector, which does not exceed 23.5° as illustrated in Figure 1.4. The reduced variability of solar radiation on these surfaces throughout the orbit enables the design of a more stable radiator. As the Earth rotates on its axis, the angle between the sun vector and each of the other four panels varies from 0° to 90°. Therefore, to accommodate heat-dissipating equipment on these four surfaces, bent heat pipes may be required to transfer heat to the north and south panels. However, such solutions encounter several challenges: the heat pipes must be gently curved to prevent any fractures, and the assembly of such layouts proves to be quite complex as illustrated in Figure 1.5. For these reasons, it is standard practice to mount the highest heat-dissipating equipment on the north and south faces.

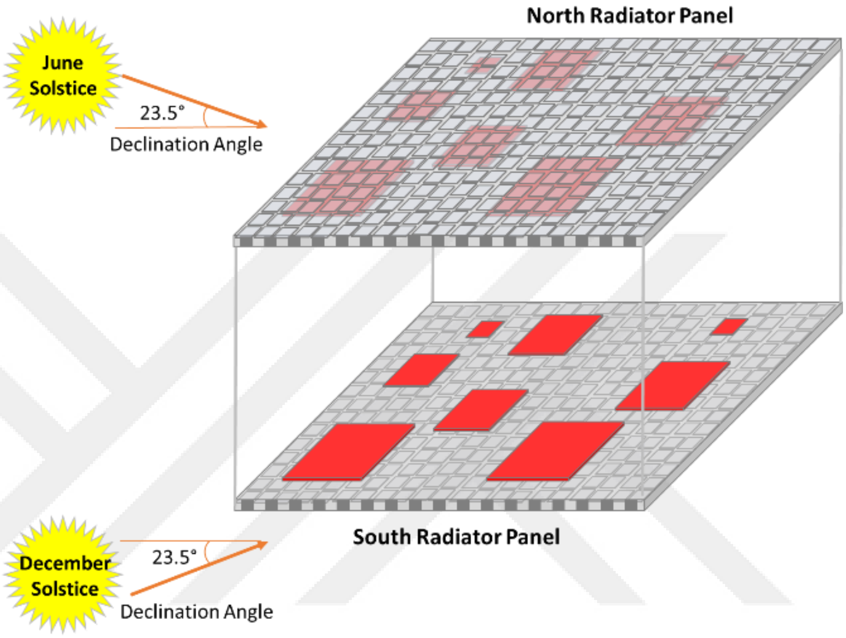

Figure 1.4: *Solar Illumination on the North and South Faces of a GEO Satellite*

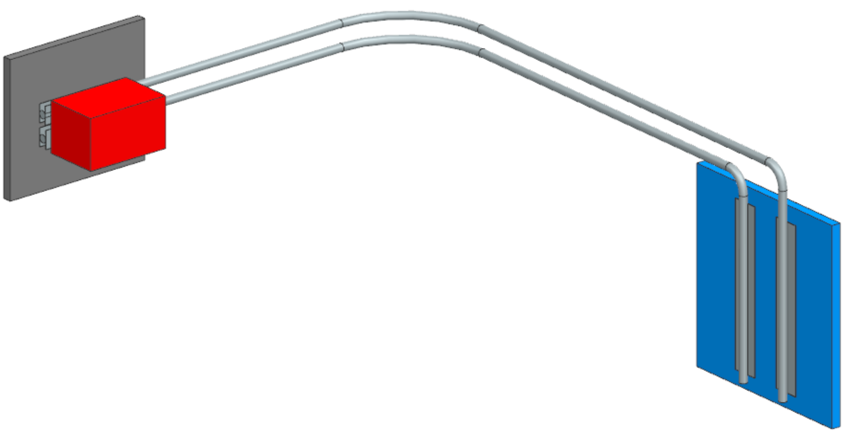

Figure 1.5: *Bent Heat Pipe Profile*

Spacecraft thermal engineers primarily concentrate on scenarios known as "sizing cases," which represent the worst-case conditions concerning both hot and cold temperatures for the spacecraft. Worst-case hot scenarios are used to size radiator dimensions, while worst-case cold scenarios are used to size heater power.

In a worst hot case scenario for GEO spacecraft, all equipment operates at its maximum possible heat dissipation. The angle between the solar vector and radiator can reach a maximum of 23.5°, resulting in the highest solar heat flux. During the June solstice, the angle between the sun vector and the north radiator is 23.5°, while during the December solstice, the angle between the sun vector and the south radiator is also 23.5°. The end-of-life thermo-optical properties of the radiator's external surfaces result in heightened absorption of solar flux relative to their initial condition. Therefore, for the sizing of the north radiator, June solstice orbit parameters are applied, while December solstice orbit parameters are used for the sizing of the south radiator, considering end-of-life thermo-optical properties.

In a worst cold case scenario for GEO spacecraft, all equipment operates at its minimum possible heat dissipation. Near the Vernal and Autumnal Equinoxes, eclipses can occur with a maximum duration of approximately 72 minutes in geostationary orbit. Satellites experience a lack of solar fluxes during these periods due to the Earth obstructing the Sun as illustrated in Figure 1.6. Therefore, to determine the maximum power needed for heaters, equinox orbit parameters are utilized. Due to the absence of solar flux, the absorbed solar flux is zero during the eclipse. Consequently, the choice between end-of-life and beginning-of-life thermo-optical parameters for the radiator's external surfaces does not affect the results. The spacecraft will experience lower temperatures due to the beginning-of-life (BOL) thermo-optical properties at the onset of the eclipse. Therefore, the spacecraft is likely to reach its minimum temperature during the eclipse period. As a result, BOL thermo-optical properties are used for the worst-case cold analysis.

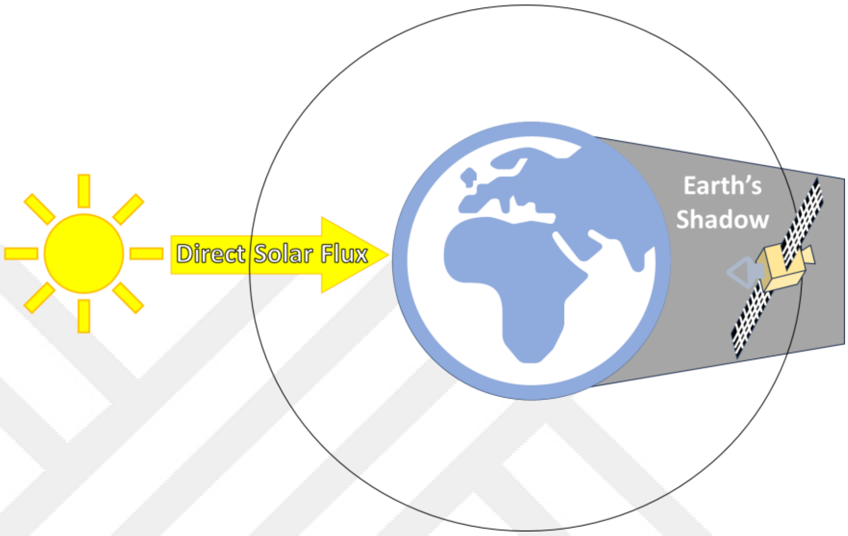

Figure 1.6: *Equinox Eclipse Condition in Geostationary Orbit*

Thermal design and analysis processes aim to satisfy the thermal requirements of spacecraft, such as maximum and minimum temperature limits, allowed temperature gradients, and required temperature stabilities. Some examples of thermal requirements for the operational conditions of typical spacecraft equipment are provided in Table 1.2.

Table 1.2: *Thermal Requirements Example (Adapted from [5])*

Equipment	**Temperature Ranges**	
	Min Temperature	Max Temperature
Electronics	-10 °C	+50 °C
Batteries	0	+20 °C
Solar Arrays	-100 °C	+120 °C
Antenna	-65 °C	+95 °C
Hydrazine Tank	+10 °C	+50 °C
Infrared Detectors	-223 °C	+100 °C
Inactive Structure	-100 °C	+100 °C
	Temperature Gradients	
Optoelectronics	$\Delta T < 5$ °C	
High Resolution Cameras	$\Delta T < 0.1$ °C	
Detectors	$\Delta T < 0.01$ °C	
	Temperature Stabilities	
Electronics	$dT/dt < 5$ °C / hour	
Detectors During Observation Periods	$dT < 0.1$ °C	

The minimum and maximum design temperature limits for equipment are determined based on information provided by the equipment manufacturer while also considering the temperature margin philosophy. This philosophy is standardized by the National Aeronautics and Space Administration (NASA) and the European Space Agency (ESA), as illustrated in Figure 1.7 and Figure 1.8. The thermal design margin (uncertainty) for internal units is specified as ± 5 °C in passive thermal control systems and ± 2.5 °C in active thermal control systems. Conversely, for external units, the thermal design margin (uncertainty) is defined as ± 10 °C in passive thermal control systems and ± 2.5 °C in active thermal control systems [6].

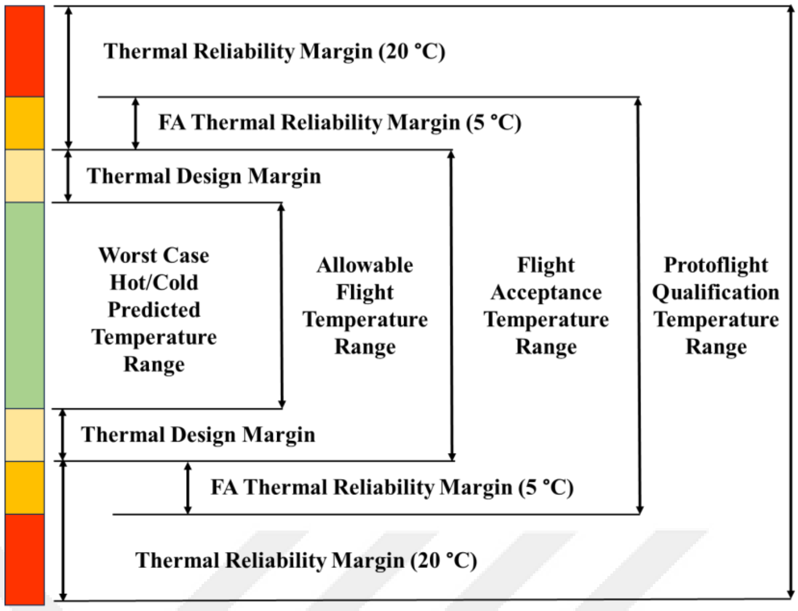

Figure 1.7: *NASA Temperature Margin Philosophy (Adapted from [7])*

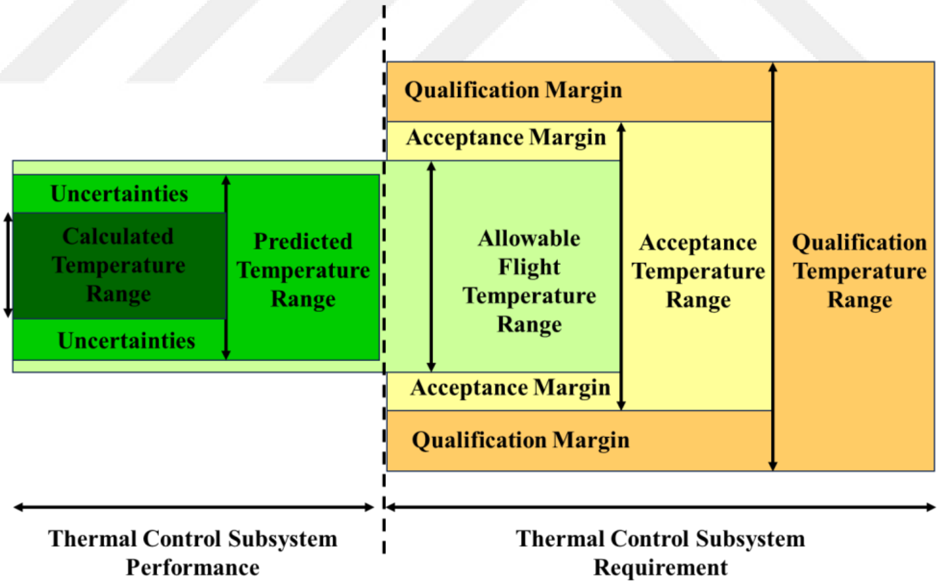

Figure 1.8: *ESA Temperature Margin Philosophy (Adapted from [6])*

Alongside the temperature margin philosophy, the sizing of radiators and heater power includes margins that reflect the program’s risk tolerance, the potential consequences of exceeding predicted temperatures, and the need to balance conservatism, cost, and design complexity.

The thermal design of a spacecraft is both complex and iterative. It involves developing a thermal design and then analyzing the selected approach. Figure 1.9 provides a clear illustration of the thermal design method. This method identifies the design parameters of the thermal control subsystem that meet the thermal requirements of the spacecraft equipment. The parameters include the dimensions, placement, materials, and quantities of multi-layer insulation blankets, heaters, and heat pipes, as well as the specifications for radiator configuration and equipment layout. Additionally, the thermal analysis conducted during this process provides predictions of the flight temperatures of the spacecraft's subsystems.

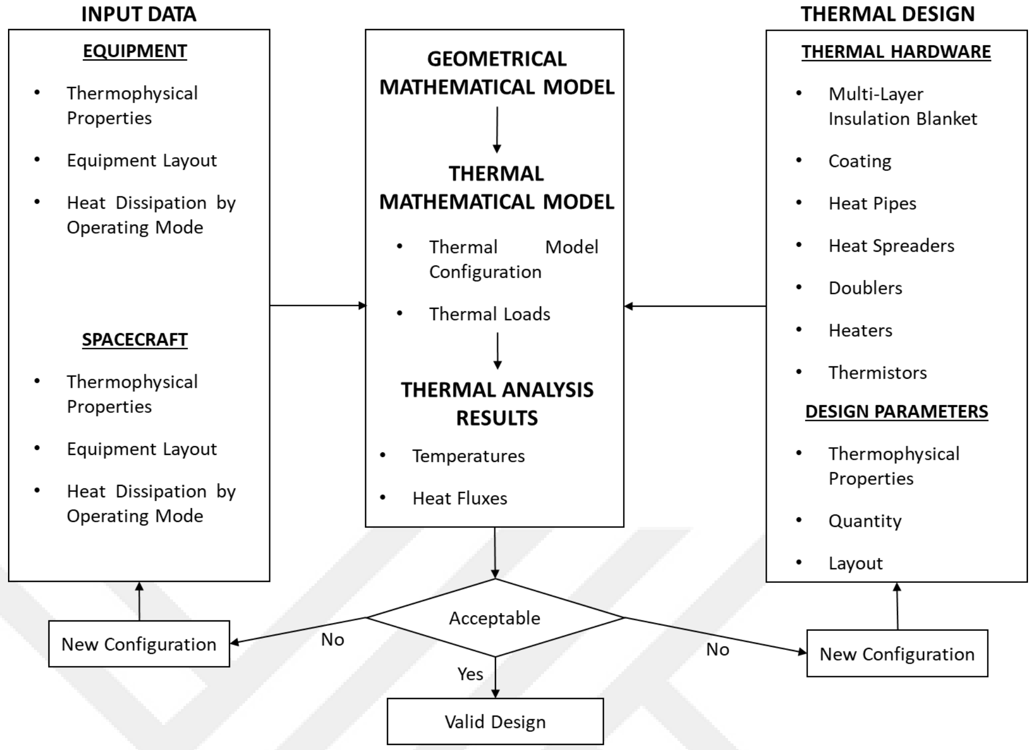

Figure 1.9: *Thermal Control Subsystem Design Flowchart*

Thermal control subsystem design can directly impact the structural design, while the need for heaters influences power management, electronics, harnesses, and onboard data processing system designs within the spacecraft. In addition, designing the equipment layout from a thermal perspective can affect the electrical and electronic system architecture by increasing the distances between interconnected components, potentially resulting in efficiency losses. Consequently, the design of the thermal control subsystem is an intricate and iterative process that requires close integration with multiple spacecraft subsystems.

Typically, during the initial stages of the development phase, a GEO spacecraft is divided into sections based on its panels for thermal design and analysis—such as the north payload panel, north service panel, south payload panel, south service panel, and others. This segmentation enables a focused approach to the thermal design of each panel, which helps expedite the development process. The thermal mathematical models (TMM) of each segment are referred to as "local models." As the thermal design matures, these local models are combined to form the "global model." The development process then continues using the global thermal model. Initially, hand calculations based on the energy balance equation are performed to establish a baseline for thermal design and analysis. Subsequently, commercial software tools for design and thermal analysis—based on finite element or finite difference methods—are employed. Various software packages are commonly used in the space sector for this purpose, including Systems Improved Numerical Differencing Analyzer / Fluid Integrator (SINDA/FLUINT), Thermal Synthesizer System Space 3D (TSS Space 3D), European Space Agency Thermal Analysis Network Thermal Modelling Suite (ESATAN TMS), Simcenter 3D Space Systems Thermal (SST), ANSYS, and COMSOL Multiphysics. A comparison of these software packages, as presented in Table 1.3, was conducted by Atar and Aktaş [8].

Table 1.3: *Comparison of Thermal Simulation Software (Adapted from [8])*

Capabilities	SINDA / FLUINT	TSS Space 3D	ESATAN TMS	SIMCENTER 3D SST	COMSOL	ANSYS
Geometrical Mathematical Model Generator	AutoCAD	Space 3D	CAD Bench	NX	Design Module	Space Claim
Mesh Operations	✗	✓	✓	✓	✓	✓
Surface Boundary Conditions	✓	✗	✓	✓	✓	✓
Radiation Analyzer	RadCAD	Radk	ESARAD	Built-in	Built-in	Built-in
Thermal Analyzer	SINDA	SINDA	ESATAN	Built-in	Built-in	Built-in
Coupled Thermo-Fluid	✓	✓	✓	✓	✓	✓
Coupled Thermo-Mechanic	✗	✗	✗	✓	✓	✓

This study employs NX Space Systems Thermal, and two-dimensional quadrilateral finite elements are preferred for the thermal analysis. The software utilizes a Galerkin-based finite element method to spatially discretize the governing heat conduction equation, as shown in Equation (1.6).

$$\int_{\Omega} \xi_j \left[\frac{\partial}{\partial x}\left(k_x \frac{\partial T^e}{\partial x}\right) + \frac{\partial}{\partial y}\left(k_y \frac{\partial T^e}{\partial y}\right) + \frac{\partial}{\partial z}\left(k_z \frac{\partial T^e}{\partial z}\right) + q_v - \rho c \frac{\partial T^e}{\partial t}\right] d\Omega = 0 \quad (1.6)$$

where:

• k is the thermal conductivity, where subscripts x, y, and z are the anisotropic specifications in space directions.

• q_v is the heat generation per unit volume.

• ρ is the material density.

• c is the specific heat capacity.

• Ω is the solid domain.

• ξ_j is the shape function.

The temperature distribution within each element is approximated using the element shape function ξ_j, as defined in Equation (1.7).

$$T^e(x, y, z, t) = \sum_{j=1}^{m} \xi_j(x, y, z) T_j^e(t) \quad (1.7)$$

Where:

• m is the number of nodes in an element.

• $T_j(t)$ is the time-dependent temperature of nodes.

Applying the Gauss theorem and boundary conditions, where only Neumann boundary conditions are evaluated at Ω_N, the conduction equation becomes (where i and j denote the local node indices of the finite element):

$$-\int_{\Omega}\left[k_x\frac{\partial\xi_j}{\partial x}\frac{\partial\xi_i}{\partial x}T_i^e(t)+k_y\frac{\partial\xi_j}{\partial y}\frac{\partial\xi_i}{\partial y}T_i^e(t)\right.$$
$$\left.+k_z\frac{\partial\xi_j}{\partial z}\frac{\partial\xi_i}{\partial z}T_i^e(t)\right]d\Omega+\int_{\Omega}\left[\xi_j q_v-\xi_j\rho c\frac{\partial\xi_i}{\partial t}T_i^e(t)\right]d\Omega-\int_{\Omega_N}\xi_j q_v\,d\Omega_N=0 \tag{1.8}$$

The previous equation can be expressed in a matrix form:

$$[C_{ij}]\left\{\frac{\partial T_i^e}{\partial t}\right\}+[K_{ij}]\{T_i^e\}=\{f_j\} \tag{1.9}$$

Where the global mass matrix is:

$$[C_{ij}]=\int_{\Omega}\rho c\xi_i\xi_j\,d\Omega \tag{1.10}$$

The element stiffness matrix is defined as:

$$[K_{ij}]=\int_{\Omega}\left[k_x\frac{\partial\xi_j}{\partial x}\frac{\partial\xi_i}{\partial x}+k_y\frac{\partial\xi_j}{\partial y}\frac{\partial\xi_i}{\partial y}+k_z\frac{\partial\xi_j}{\partial z}\frac{\partial\xi_i}{\partial z}\right]d\Omega \tag{1.11}$$

The nodal loads vector is:

$$\{f_j\}=\int_{\Omega}\xi_j q_v\,d\Omega-\int_{\Omega_N}\xi_j q_v\,d\Omega \tag{1.12}$$

The thermal solver defines integration points and shape functions for various element types, enabling the discretization of a continuous domain using finite elements. Numerical integration at these points is used to evaluate element temperatures, while shape functions approximate the thermal response. Table 1.4 presents examples of shape functions and their graphical representations for supported 2D elements.

Table 1.4: *Shape Function and Graphical Representations (Adapted from [9])*

Element Type	Graphical Representation	Shape Function
Linear Quadrilateral	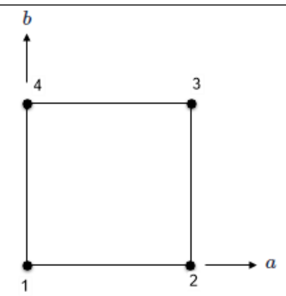	$\xi_1 = (1-a)(1-b)$ $\xi_2 = a(1-b)$ $\xi_3 = ab$ $\xi_4 = (1-a)b$
Parabolic Quadrilateral	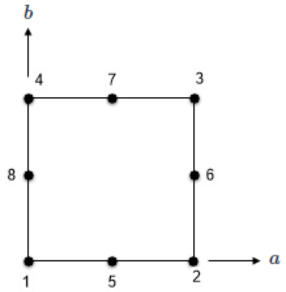	$\xi_1 = (1-a)(1-b)(1-2a-2b)$ $\xi_2 = a(1-b)(2a-2b-1)$ $\xi_3 = ab(2a+2b-3)$ $\xi_4 = (1-a)b(-2a+2b-1)$ $\xi_5 = 4a(1-a)(1-b)$ $\xi_6 = 4ab(1-b)$ $\xi_7 = 4ab(1-a)$ $\xi_8 = 4b(1-a)(1-b)$

Radiative heat transfer between elements i and j is described by:

$$Q_{ij} = \sigma\epsilon_i A_i VF_{G_{ij}}\left(T_i^4 - T_j^4\right) = -\sigma\epsilon_j A_j VF_{G_{ji}}\left(T_j^4 - T_i^4\right) \qquad (1.13)$$

where:

- Q_{ij} is the net radiative heat load from element i to element j.
- σ is Stefan-Boltzmann's constant.
- T_i, T_j are the absolute temperatures of elements i and j.
- ϵ_i, ϵ_j are the emissivities of elements i and j.
- A_i, A_j are the surface areas of elements i and j.

- VF_{Gij} is the gray body view factor from i to j, which is the fraction of the emitted or reflected radiant heat load leaving the surface i and absorbed by j after multiple diffuse reflections from all the elements.

As with the black body view factor, the gray body view factor has the reciprocity property:

$$VF_{G_{ij}} A_i = VF_{G_{ji}} A_j \tag{1.14}$$

As illustrated in Figure 1.10, if no shadowing surfaces exist between elements i and j, the elements are not subdivided. In such cases, a specialized algorithm for unshadowed view factor computation is employed to directly calculate the view factor VF_{ij} between them.

$$VF_{ij} = \frac{1}{2\pi A_i} \int_{C_i} \int_{C_j} lnS(C_i, C_j)\, dC_i\, dC_j \tag{1.15}$$

where:

- C_i and C_j are the paths around the perimeters of elements i and j.
- S (C_i, Cj) is the length of a line between two points on the perimeters of elements i and j.

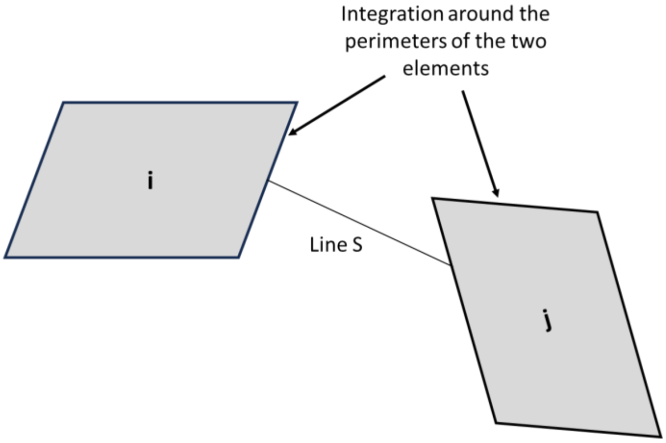

Figure 1.10: *Integration Path Between Elements i and j (Adapted from [9])*

Thermal vacuum chambers (TVCs), which are used for spacecraft thermal testing, are large tanks in which the pressure is reduced to simulate the space environment that the spacecraft will encounter during its mission. Within these chambers, several key measures are implemented to replicate orbital conditions. First, a vacuum is created by reducing the pressure to near-space levels, thereby eliminating convective heat transfer. Second, thermal shrouds are used to provide precise temperature control. Cold black shrouds, cooled with liquid nitrogen or gaseous helium, simulate deep-space conditions, while heated shrouds can replicate infrared radiation from Earth or other spacecraft components. Third, solar simulation is achieved using infrared (IR) or xenon arc lamps, with collimators ensuring the radiation is nearly parallel, as it would be in orbit. These combined measures ensure that heat fluxes are carefully regulated and that shroud temperatures closely match the thermal conditions of space, enabling accurate thermal model correlation and reliable performance assessment.

TMM is utilized to analyze the spacecraft's thermal behavior in orbit. However, before its application, the TMM must be correlated with test data obtained from TVC testing under the specified test scenario. This test scenario consists of several stages, as illustrated in Figure 1.11, including thermal cycles and thermal balance conditions. Thermal cycles are utilized to assess equipment performance at qualification or acceptance temperature levels, whereas thermal balance stages establish steady-state conditions for correlating the TMM. At each stage of the test scenario, the TVC is adjusted accordingly, with modifications to shroud temperatures and heat fluxes implemented to simulate the required conditions. Results from the TVC tests are then compared with TMM predictions obtained under boundary conditions identical to those in the TVC. The TMM parameters, including thermo-optical properties, absorptivity, emissivity, and thermal conductance, are subsequently adjusted according to the results of the thermal balance test stages to ensure alignment between model predictions and empirical results. Subsequently, orbital thermal analyses are repeated using the updated spacecraft parameters to verify compliance with design requirements prior to launch, with any necessary modifications implemented accordingly.

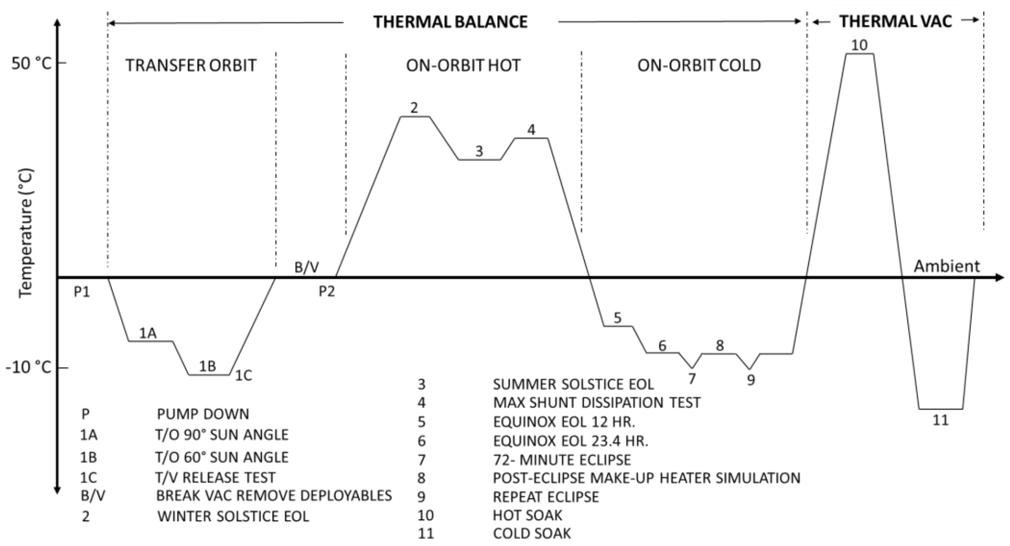

Figure 1.11: *Thermal Vacuum Test Profile (Adapted from [10])*

The thermal control subsystem of a spacecraft encompasses three fundamental functions: thermal design, analysis, and testing. These processes are closely interconnected, and the design and analysis steps are typically repeated in an iterative manner until the specified thermal requirements are met. All these efforts aim to ensure that the spacecraft can operate at the required performance level under harsh space conditions.

1.1.1 Spacecraft Radiator Applications

Radiators are an essential component of spacecraft thermal design. They serve to dissipate the waste heat generated by onboard equipment into space through radiative heat transfer. The thermal performance of radiators depends on factors such as their surface area, operating temperature, and thermo-optical properties of the outer facesheet (FS) exposed to space. In addition to their heat rejection capabilities, radiators also serve as housings for equipment and are often pieces of the main structural framework of the spacecraft. Therefore, besides meeting thermal requirements, radiators must also fulfill structural criteria such as stiffness, hardness, toughness, ductility, and fatigue strength. These properties ensure that radiators can withstand the static, dynamic, and thermal stresses encountered during launch, deployment, and operational phases. The geometry and configuration of radiators should be compatible with the overall spacecraft design, which varies in shape and size depending on mission objectives, launcher envelope and equipment requirements.

The spacecraft radiator panels can comprise internal and external facesheets, honeycomb structures, adhesive materials, heat pipes, and specialized coatings. Radiators are expected to be lightweight while meeting mechanical and thermal requirements. Therefore, honeycomb structures are typically used between two facesheets due to their high strength to weight ratio and high stiffness. Aluminum alloys are commonly used for facesheets and honeycomb cores due to their favorable properties, including high strength-to-weight and stiffness-to-density ratios, excellent workability, ease of machining, non-magnetic nature, cost-effectiveness, high ductility, corrosion resistance, and availability in various forms [11]. Heat pipes or other heat spreaders are used to distribute heat across the radiator, ensuring efficient utilization of the radiator area and preventing the formation of hot spots.

Radiators can be classified into passive structure radiators, deployable radiators, body-mounted radiators, and structural panels with heat pipes. Each type has its advantages and disadvantages when compared to the others, and the selection among them is based on mission requirements.

1.1.1.1 Passive Structure Radiators

Passive structure radiators are the simplest type of spacecraft radiator. They consist of aluminum facesheets, honeycomb structures, coatings, and adhesives, as illustrated in Figure 1.12. These structures serve as both a radiator and a structural component of the spacecraft's wall. Heat is conducted from the inner facesheet that accommodates equipment to the coated outer facesheet through honeycomb material. Therefore, the transverse heat conduction pathway is crucial for dissipating waste heat into the environment. Thermal doublers can also be used between the equipment and the inner facesheet to spread heat in the in-plane direction and reduce hot spots. Additionally, increasing the thickness of the facesheets can enhance conduction in the in-plane direction. Furthermore, incorporating heat spreaders provides an effective means to transfer heat from the equipment not only in the in-plane direction, but also transversely through the panel structure, thereby facilitating more uniform heat distribution and enhancing the overall thermal performance of the system.

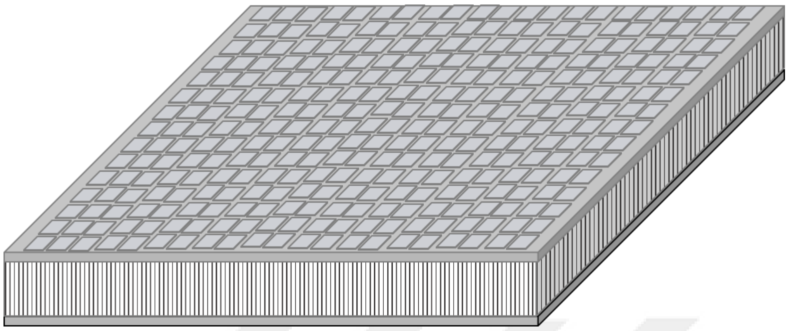

Figure 1.12: *Passive Structure Radiator*

1.1.1.1.1 Thermal Doublers

Doublers are auxiliary metallic structures, typically fabricated from high-thermal-conductivity materials such as aluminum or copper, and are employed to enhance in-plane heat conduction between a localized heat source and the primary radiator surface. Functioning as thickened sub-regions of the main mounting interface, doublers reduce thermal resistance by increasing the cross-sectional area available for conduction and by locally lowering the temperature gradient. They are strategically integrated beneath or adjacent to high-power components to improve lateral heat conduction. This configuration allows for efficient thermal coupling between neighboring units, such as active and redundant avionics, and promotes uniform heat spreading into the radiator substrate, as illustrated in Figure 1.13. The design of doublers typically optimizes both thickness and footprint to balance mass constraints with thermal performance, making them a mechanically simple yet effective solution for thermal integration challenges in spacecraft.

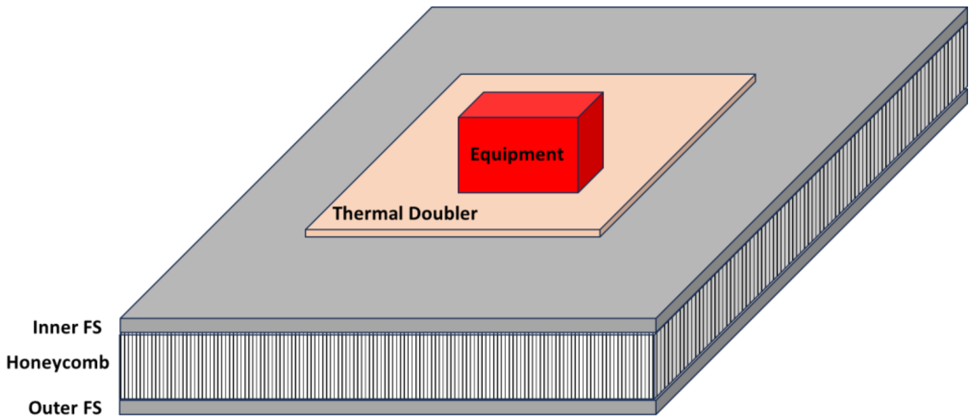

Figure 1.13: *Radiator Panel with Integrated Thermal Doubler*

1.1.1.1.2 Heat Spreaders

Heat spreaders (HSs) are large-area, high-thermal-conductivity components integrated into the thermal path between heat sources and radiative surfaces. Their primary function is to promote a uniform temperature distribution, thereby enhancing the thermal performance of the radiator. These structures are typically constructed from materials such as aluminum alloys (e.g., AL 6061-T6 or AL 2024-T3) or highly thermally conductive carbon-based materials (e.g., annealed pyrolytic graphite or advanced carbon–carbon composites). Heat spreaders increase the effective footprint of a thermal interface by conducting heat away from concentrated sources and distributing it over a broader radiative area. In spacecraft applications, they are often embedded into honeycomb-core panels, as illustrated in Figure 1.14, or attached to the radiator's inner face to mitigate temperature gradients, thereby preventing hot spots and improving overall heat rejection. The thermal performance of spreaders is highly dependent on their in-plane thermal conductivity and thickness; a thicker spreader can significantly reduce lateral temperature differentials due to increased conduction capacity. In many designs, a balance must be struck between the added mass of thicker plates and the thermal benefits they provide, particularly under high power density or multi-source configurations.

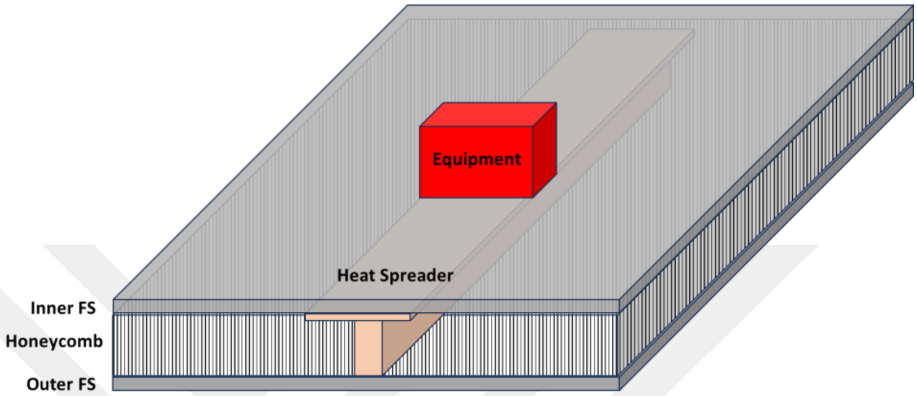

Figure 1.14: *Radiator Panel with Embedded HS*

Heat spreaders, particularly those made from highly thermally conductive carbon-based materials, offer an effective alternative to heat pipes in space applications. Unlike heat pipes, which rely on phase change and capillary action to transfer heat, heat spreaders use high-conductivity materials to distribute thermal energy evenly. This makes them suitable for compact, orientation-insensitive, and simplified designs. They also avoid the dry-out issues associated with heat pipes, providing enhanced reliability. For heat transport over short distances, heat spreaders can match the performance of heat pipes while reducing both complexity and cost. Ralphs et al. [12], at the NASA Thermal & Fluids Analysis Workshop (TFAWS) 2023, demonstrated through thermal analysis that radiators embedded with pyrolytic graphite sheets achieved thermal performance comparable to those with embedded heat pipes for lengths up to 20 inches (approximately 50 cm), while heat pipes provided superior performance at greater lengths.

1.1.1.2 Deployable Radiators

As spacecraft power levels increase and overall sizes decrease, additional radiator area is needed to effectively reject waste heat. However, the limited allowable radiator area on spacecraft often necessitates the use of deployable radiators to expand the available surface for heat rejection. These deployable radiators utilize specialized mechanisms for stowing and deployment. In addition to the hold and release mechanism, high-thermal-conductivity hardware is required to transfer waste heat from the spacecraft to the secondary radiator structure. An example of a deployable radiator and its components is shown in Figure 1.15. Because of the moving parts and complex operational requirements, deployable radiator systems are generally not considered a primary thermal solution for spacecraft.

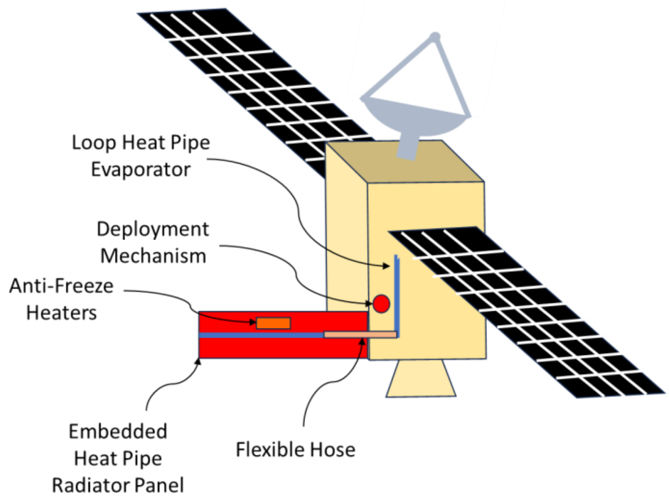

Figure 1.15: *Deployable Radiator Components (Adapted from [13])*

1.1.1.3 Body-Mounted Radiators

Body-mounted radiators, as depicted in Figure 1.16, are not part of the spacecraft's primary structure but are instead attached externally to the main body. Certain equipment is highly sensitive to temperature fluctuations and must operate within narrow thermal limits to ensure optimal performance, necessitating dedicated radiators. Additionally, placement constraints may also require separate radiators. As a result, body-mounted radiators are employed for such equipment. Being thermally detached from the main spacecraft body, these radiators can be customized to meet specific equipment thermal requirements, often exhibiting different thermal behavior than the rest of the spacecraft. However, due to constraints imposed by the spacecraft or equipment, they may need to be positioned at a considerable distance from the components requiring thermal regulation. In these cases, heat transport mechanisms like heat pipes or capillary pumped loops are used to transfer heat from the equipment to these radiators. Depending on the radiator's location and the distance between the radiator and the equipment, the heat transport mechanism can become complex in structure.

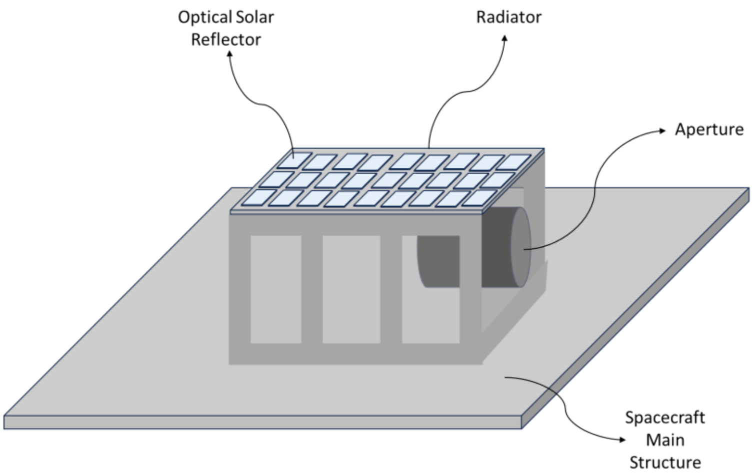

Figure 1.16: *Body Mounted Radiator (Adapted from [14])*

1.1.1.4 Structural Panels with Heat Pipes

Passive structural panels for high heat-dissipating equipment utilize heat pipes to distribute heat throughout a sufficiently extensive radiator area, as the thermal conductivity of facesheets alone is frequently inadequate. Therefore, the use of heat pipes reduces the temperature gradient across the radiator area and increases radiator efficiency. As a result of that, higher heat rejection capability is achieved, making it easier to keep the equipment temperature within the allowable flight range. Heat pipe layouts are adjusted to have direct or indirect contact areas with equipment and to transport excessive heat to colder locations on the panel. To maximize surface contact with the heat source, heat pipes typically feature flanges.

Structural panels with heat pipes, as shown in Figure 1.17, can be categorized into two groups according to their assembly type: embedded heat pipe radiator panels and surface mounted heat pipe radiator panels. Each type has advantages and disadvantages.

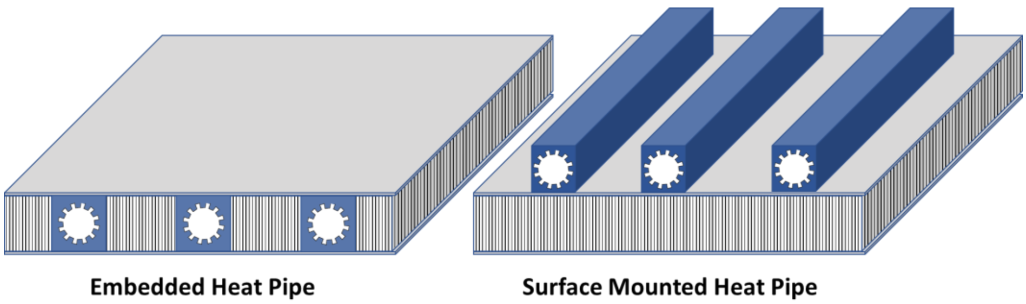

Figure 1.17: *Typical HPs and Radiator Panel Configurations*

Surface mounted heat pipe radiator panels are easier to assemble and in case of any problem before launch, they can be replaced. However, these heat pipes are placed on the inner facesheet of the radiator panel and occupy space intended for assembling equipment, harnesses, and other structural joints. Conversely, embedded heat pipes between the inner and outer facesheets, along with the honeycomb structure, provide flexibility for equipment installation. In addition, these heat pipes are in contact with the outer facesheet, enhancing not only in-plane but also transverse heat transfer. However, their assembly is more complex than surface mounting and requires precise alignment to avoid damage during assembly.

The quantity, placement, and spacing of heat pipes in structural panels are essential for optimal thermal performance. One-dimensional temperature distribution of a structural panel with embedded heat pipes is illustrated in a graph in Figure 1.18. Due to their lower thermal resistance compared to the facesheets and honeycomb, a uniform temperature is achieved along the longitudinal axis of the heat pipes, with temperature differences occurring between the heat pipe and its sides. Additionally, in regions where heat pipes are embedded between the inner and outer facesheets, there is no significant temperature difference between facesheets. In contrast, areas that contain only honeycomb structures exhibit a temperature difference between the facesheets. As a result of the higher outer facesheet temperature achieved by embedded heat pipes, these regions can reject more heat compared to areas containing only honeycomb, enhancing the overall thermal performance of the radiator.

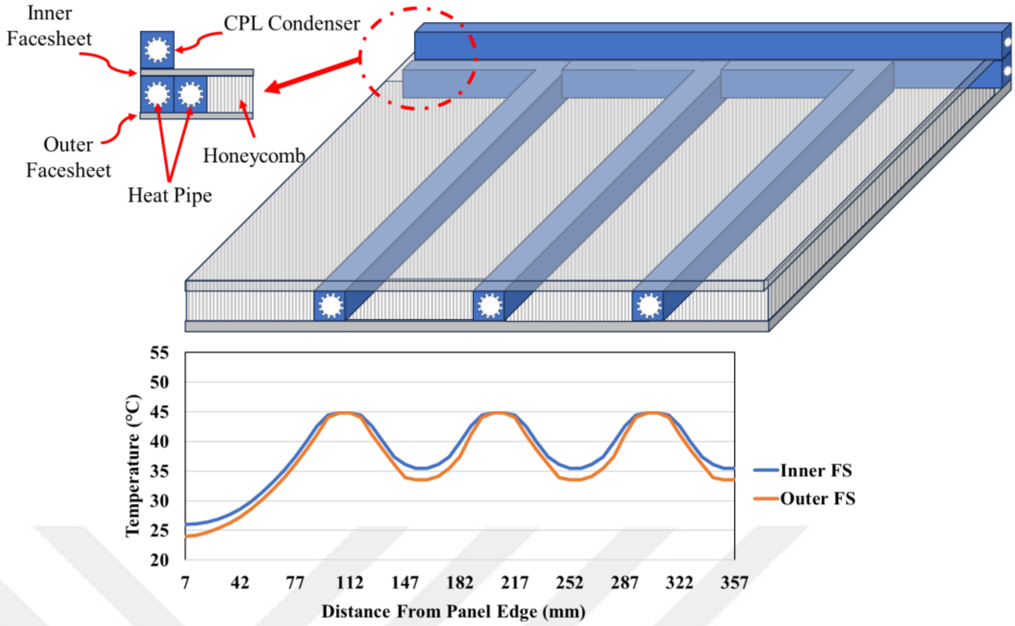

Figure 1.18: *Temperature Profile of Radiator with Embedded HP (Adapted from [15])*

The design parameters of the radiators must be selected in accordance with system requirements in order to utilize the radiator panel efficiently and dissipate the excess heat into space. Otherwise, surplus mass may result from oversizing the panel or choosing the facesheets, the honeycomb structure, and heat pipe parameters incorrectly, which is not desirable for spacecraft.

1.1.1.4.1 Heat Pipes

Heat pipes efficiently transport waste heat from a heat source to a heat sink without the need for external power or control. Their two-phase thermal characteristics make them particularly suitable for long-distance heat transfer with minimal temperature drop, as well as for creating nearly isothermal surfaces that stabilize temperature [16]. Due to the utilization of latent heat during phase change, heat pipes exhibit an effective thermal conductivity that is substantially higher than that of conventional solid conductors such as copper, as noted by Consolo and Boettcher [17]. The thermal performance of a heat pipe depends on its design and operating parameters. Alijani et al. [18] further demonstrated that the groove geometry and filling ratio strongly affect the thermal performance of heat pipes.

Heat pipes are used to prevent hot spots caused by high heat-dissipating equipment, enable heat transfer through radiators, and maintain uniform panel temperatures. These systems typically consist of a wick structure, a working fluid, and a container, which includes a fill tube and an end cap. Flanges may also be incorporated to increase the contact area, as shown in Figure 1.19.

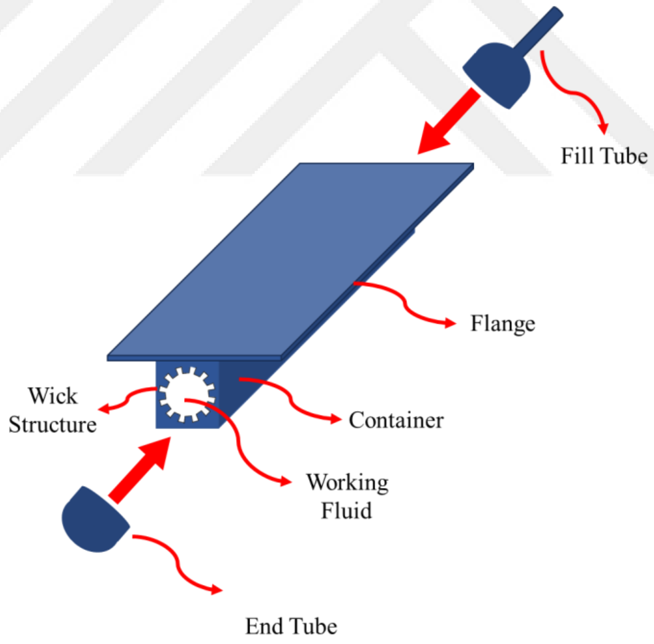

Figure 1.19: *Flanged Axially Grooved HP*

One endpoint of the heat pipe container is equipped with an end cap, while the opposite endpoint has a sealed fill tube, together forming a closed system. The wick structure, located inside the heat pipe container, can be designed in various configurations, including mesh, groove, and sintered powder, each offering specific advantages and limitations. The axially grooved wick structure is commonly used in space applications due to its efficient heat transport over long distances. Capillary pumping, provided by the wick, moves liquid from the condenser to the evaporator, keeping the wick filled with liquid. In the evaporator region, the liquid phase undergoes vaporization due to heat loads, and the vapor is then transported to the condenser zone through a pressure differential. The working principle of the heat pipe is illustrated in Figure 1.20.

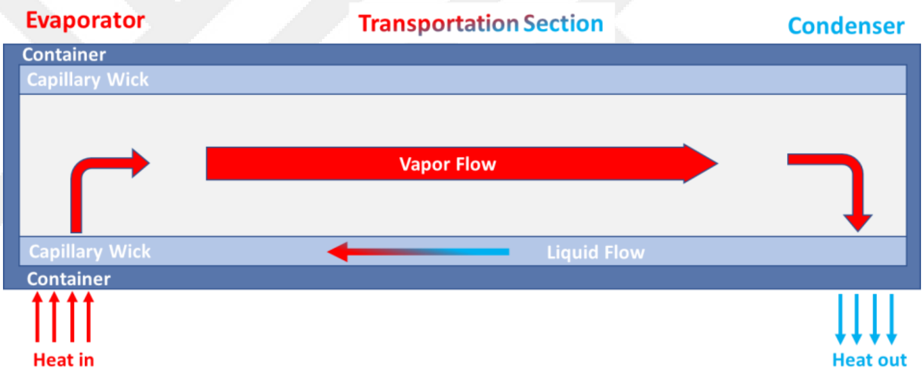

Figure 1.20: *Working Principle of HP*

The heat transfer capability of a heat pipe is constrained by factors such as capillary action, sonic limits, condenser performance, boiling dynamics, and viscous resistance. The performance of a heat pipe is defined by these limitations. When these limits are exceeded, the heat pipe may experience a reduction in efficiency or even failure. For example, exceeding the capillary limit can result in the wick's inability to return liquid to the evaporator, while surpassing the sonic limit can lead to pressure instability. Similarly, the condenser limit may cause insufficient heat dissipation, and boiling or viscous limits may reduce the overall heat transfer capacity. Entrapment of vapor can result in incomplete phase changes, reducing the heat pipe's ability to function effectively.

1.2 Engineering Optimization

Optimization is a branch of mathematics focused on determining the conditions that yield extreme values of functions under specific constraints. Essentially, it aims to maximize or minimize an objective in order to identify the optimal solution to a given problem. Optimization is fundamental to any problem involving decision-making, as it requires selecting from various alternatives. It is critical in solving real-world issues across multiple disciplines, including mathematics, economics, science, engineering, medicine, and artificial intelligence. In optimization algorithms, these problems are represented using mathematical functions.

Establishing the ideal optimization strategy requires a comprehensive and accurate problem classification. This classification can be performed according to the criteria outlined in Table 1.5.

Table 1.5: *Classification of Optimization Problems (Adapted from [19])*

Base of Classification	Category	Specifications
Number of Design Variables	Single Variable	The vector of design variables includes only one variable
	Multi Variable	The vector of design variables includes more than one variable.
Number of objective functions	Single Objective	There is one criterion expressed as an objective function
	Multi Objective	There are many criteria that are considered together to determine an optimum solution
Presence of constraints	Unconstrained	A minimum or maximum of objective function without any limitation is attempted.
	Constrained	Some constraints define the set of feasible solutions.
Features of constraints and objective function	Linear Programming	Objective functions and constraints are linear.
	Nonlinear Programming	Some of the objective functions and constraints can be nonlinear. Quadratic programming and geometric programming problems are two specific kinds of nonlinear optimization problems.
Nature of design variables	Static	Design variables are independent. They are not functions of other parameters
	Dynamic	Design variables are functions of other parameters, e.g., time.
Nature of design variables and design input data	Deterministic	All design variables or preassigned parameters such as loads acting on a structure are assumed to be deterministic
	Probabilistic	All or some of design variables or preassigned parameters are described by random or probabilistic variables within a given range.
Nature of objective functions and design constraints	Crisp	The constraints and objective functions are expressed by non-fuzzy and unambiguous expressions or responses.
	Fuzzy	Some of the constraints and objective functions are described by fuzzy expressions or responses.

Optimization methods have been utilized since the era of Galileo and Newton, as evidenced by historical records. In recent decades, extensive research has focused on the development of many different optimization approaches, which can be broadly classified as either search-based or calculus-based. In particular, advancements in computing technology have led to the development of numerous modern optimization techniques, including genetic algorithms (GAs), simulated annealing (SA), particle swarm optimization (PSO), ant colony optimization (ACO), harmony search algorithm (HSA), firefly algorithm (FFA), cuckoo search (CS), bat algorithm (BA), Big Bang Big Crunch (BB-BC), charged system search (CSS), tabu search (TS), and krill herd (KH) algorithm. These modern techniques are predominantly applied to engineering optimization problems that are extremely nonlinear and involve a combination of discrete and continuous design variables subject to multiple constraints. Optimization strategies should be selected based on the characteristics of the problem. The classification proposed by Sahab [19], as illustrated in Figure 1.21, can be utilized for this purpose.

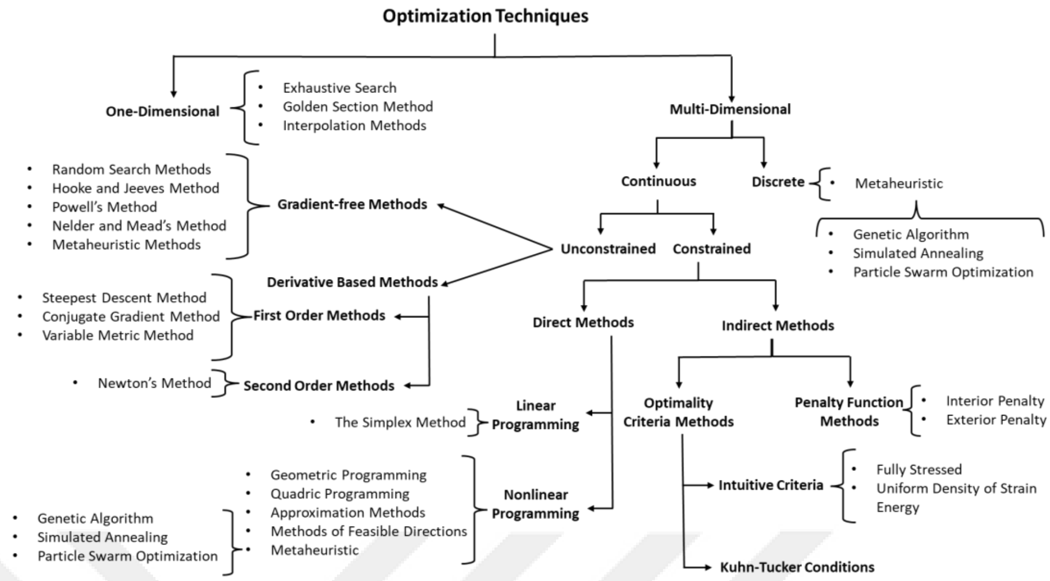

Figure 1.21: *Classification of Numerical Optimization Techniques (Adapted from [19])*

In engineering optimization problems, design objectives, such as cost, weight, rigidity, and thermal performance, are utilized to assess the quality of a design. Conventional calculus-based techniques, while effective for solving basic problems by iteratively refining the solution around an initial point, have difficulties when it comes to solving complex engineering problems with constraints or nonlinear programming. These methods face significant limitations when applied to complex engineering problems, including difficulties in calculating derivatives, sensitivity to initial conditions, and high memory requirements. Metaheuristic algorithms have been increasingly employed in recent years to address these complex engineering challenges. Metaheuristic techniques, such as GA, SA, and TS, provide robust methods for finding satisfactory solutions, though they may not always yield the optimal one. Hence, they are beneficial tools for preliminary design concepts in engineering applications due to their quick adaptability and responsiveness. These approaches are predominantly based on intuition, and the majority of them are inspired by physical laws, biological evolution, and swarm behaviors.

In general, metaheuristic algorithms can be divided into two categories: population-based metaheuristic algorithms and single-solution algorithms, as seen in Figure 1.22. Single-solution-based metaheuristic algorithms use a single candidate solution and improve it through local search. Nevertheless, single-solution-based metaheuristics may produce solutions that become trapped in local optima. Popular examples of single-solution-based metaheuristics are TS and SA. In the search procedure, population-based metaheuristics employ a multitude of candidate solutions. The most feasible option can be selected from these potential alternatives based on the objective function or performance index. These metaheuristics preserve population diversity and prevent solutions from becoming stuck in local optima. ACO, GA, and PSO are well-known examples of population-based metaheuristic algorithms.

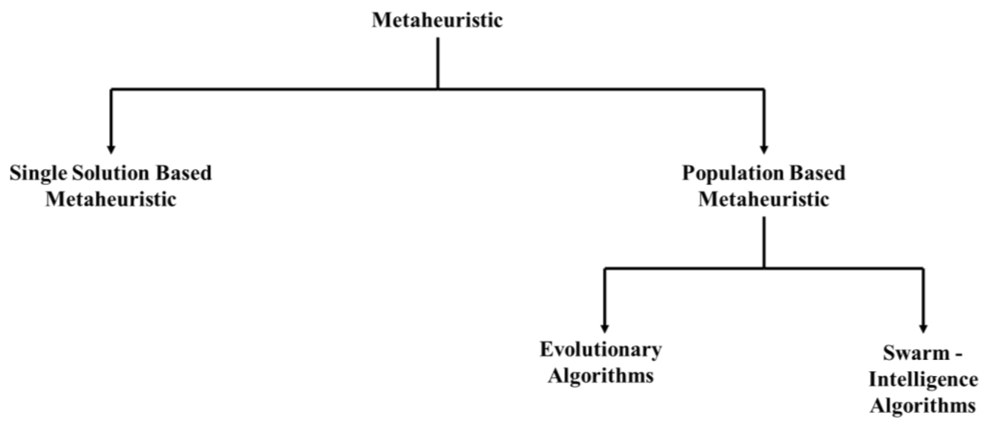

Figure 1.22: *Classification of Metaheuristic Algorithms (Adapted from [32])*

1.2.1 Definition of Genetic Algorithm

The GA is widely recognized as one of the most prominent techniques among metaheuristic algorithms. The term "genetic algorithm" was first used by Bagley [20], and his pioneering work on the subject was published in 1967. However, the first use of GAs as an optimization method occured in the 1970s. The initial significant contributions to GAs were made by Holland [21] and De Jong [22] in 1975. Grefenstette [23], Baker [24], and Goldberg [25] greatly accelerated the progress of GAs during the 1980s. Nowadays, GAs have been increasingly employed in optimization problems as a result of their numerous benefits. They do not require an initial estimate to begin searching for the best solution and use randomized searches, eliminating the need for gradient computations. Furthermore, GAs can be applied to problems involving discrete, integer, continuous, or hybrid types of variables.

GAs produce a population consisting of encoded candidate solutions and iteratively direct this population towards the optimum solution. A randomly generated initial population, whose members satisfy the constraints, is generated at the beginning of the process. Subsequently, the fitness of each member in the population is assessed, and genetic operators, namely selection, crossover, and mutation, are employed to generate the next generations. Furthermore, specific strategies like elitism may be employed if required. Penalty functions are commonly employed to adjust the fitness values of candidate solutions based on predefined criteria. Penalty functions are designed to either directly eliminate individuals or reduce the possibility of producing new offspring from these individuals [26]. The newly generated individuals replace those in the current generation and are sorted within the population based on their fitness values.

The iterative process continues until the termination criteria are satisfied. The utilization of GA is illustrated in Figure 1.23 through a flowchart.

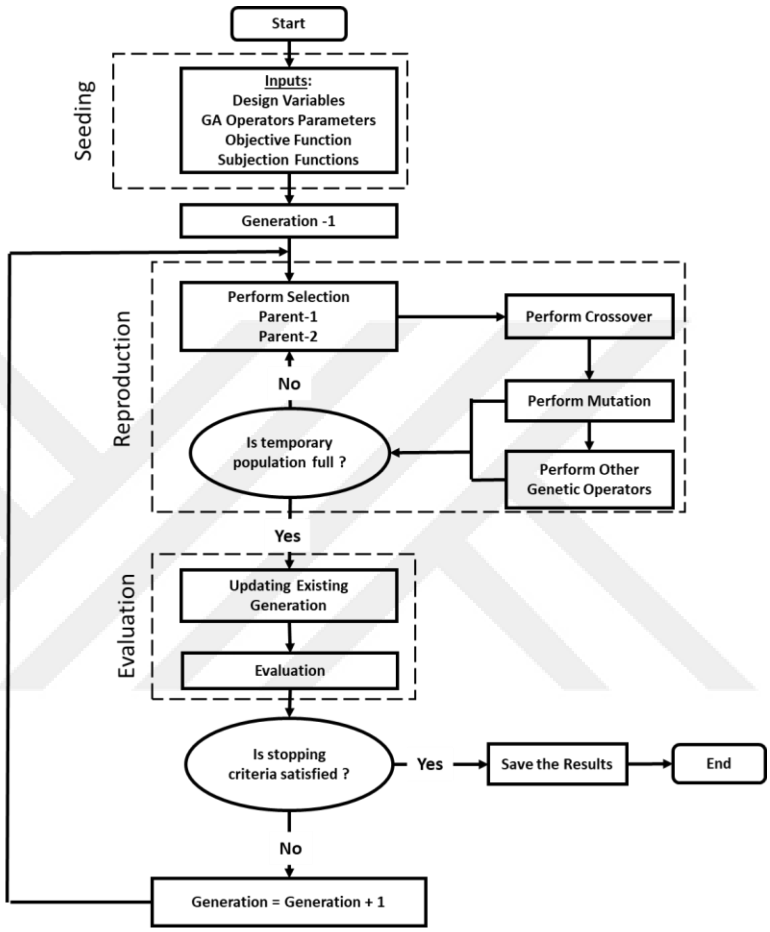

Figure 1.23: *Flowchart of Genetic Algorithm*

GAs employ operators such as encoding, decoding, selection, crossover, and mutation to maintain diversity and achieve the best possible outcomes. These operators are based on biological and sociological principles. As illustrated in Figure 1.24, they include various encoding methods, selection strategies, crossover techniques, and mutation processes. Additionally, the integration of methods such as elitism can enhance the performance of the algorithm.

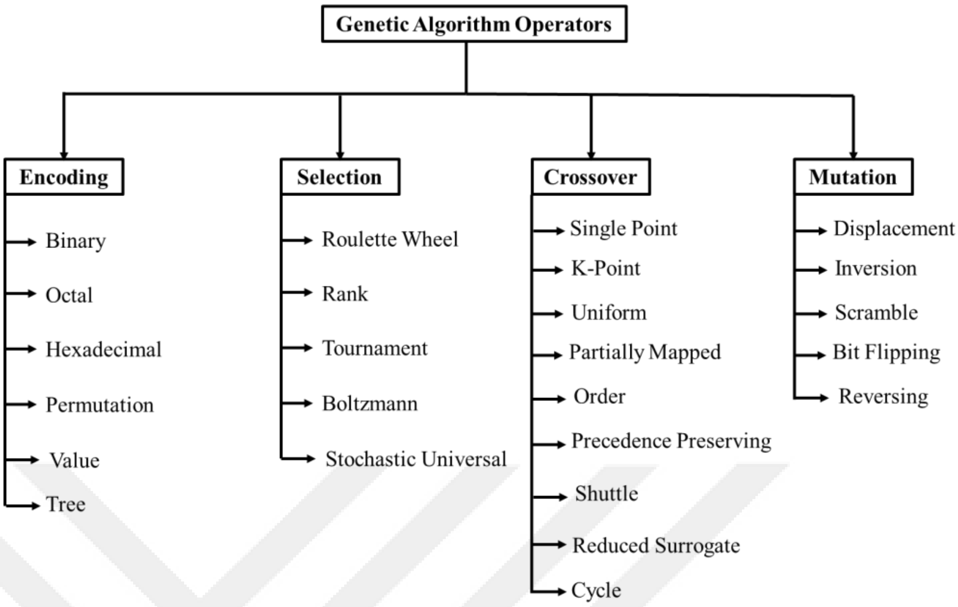

Figure 1.24: *Operators of Genetic Algorithm (Adapted from [32])*

Before starting the optimization process, the core parameters of the GA must be defined. These parameters include the mutation and crossover probabilities, population size, generation gap, and stopping criteria. There are no standardized parameters for GAs. Therefore, they must be properly tuned to identify optimal solutions. The parameters of a GA are carefully defined based on the characteristics of the optimization problem at hand. Utilizing improper GA parameters could affect the algorithm's ability to identify the optimal solution or require an inordinate number of computational resources and time to achieve it. To assess the effects of these characteristics and choose more appropriate ones, it is necessary to run the GA with multiple configurations.

2. LITERATURE REVIEW

2.1 Thermal Modelling of Spacecraft Radiators

In heat transfer applications, fin efficiency is a key parameter for improving the thermal performance of radiators by maximizing the effectiveness of the surface area used for heat dissipation. In thermal engineering, fin efficiency (η) is defined as the ratio of the actual heat transferred from the radiator to the maximum potential heat transfer, which is assumed to occur when the entire radiator surface is at the base temperature. This ratio helps assess the effectiveness of the radiator in utilizing its surface area for heat dissipation.

Numerous studies have explored the impact of various factors on fin efficiency, including operating conditions, material properties, surface coatings, and fin geometry. Thermal conductivity, thickness, and temperature gradients along the fin are essential variables that are incorporated into the analytical assessment of fin efficiency. A significant number of researchers have employed the fin efficiency approach in their investigations to achieve optimal spacecraft radiator design solutions. In 1984, Chang [27] developed a computer model to analyze embedded heat pipe radiators, exploring the relationship between fin efficiency and heat pipe spacing. The effects of different combinations of design variables are examined and illustrated through graphical representations for trade-off analysis. However, not all design variables are investigated concurrently during the optimization process. Therefore, although this study provides valuable insights into the combined effects of certain design variables, its scope is limited. A more comprehensive approach, in which all design parameters are investigated simultaneously, is necessary to identify potentially superior solutions.

Mertesdorf [28] conducted a study in 1986 on radiator weight optimization for high-power spacecraft, investigating the effects of heat pipe spacing and heat exchanger temperature drop on fin efficiency and weight. The study assumes uniform heat dissipation from heat pipes via specialized exchangers but omits the honeycomb structure, leaving the facesheet with attached heat pipes directly exposed to the harsh deep-space environment. This omission overlooks micrometeoroid impact risks and the structural requirements of space missions, resulting in a simplified design without a honeycomb core or second facesheet. Consequently, the optimization is carried out with a reduced set of design variables.

Kelly and Reisenweber [15] focused on the thermal performance of embedded heat pipe spacecraft radiator panels in 1993, comparing different heat pipe types and depicting temperature changes based on heat pipe spacing through graphical representations. The model was designed to interface with a capillary pumped loop (CPL), assuming uniform heat distribution from the CPL to the heat pipes, with dissipation at the vapor core. While the results showed that embedded heat pipes were more mass- and area-efficient than surface-mounted designs, the analysis did not explore variations in radiator aspect ratio and was limited to a narrow geometric domain. In addition, the effects of different honeycomb core structures were not investigated, as only a single honeycomb configuration was considered.

Curran and Lam [29] explored weight optimization for honeycomb radiators with embedded heat pipes in 1996, examining radiator parameters like heat pipe spacing, facesheet thickness, radiative surface properties, and panel thermal conductivities using individual graphs. However, the study does not account for out-of-plane temperature gradients. While the graphical results provide useful guidance for engineering applications, the analysis treats design variables independently, without examining their coupled interactions.

In 2006, Roy and Avanic [30] investigated the optimization of space radiators with energy storage, specifically analyzing embedded heat pipe radiator panels with phase change material (PCM) for transient heat loads scenarios. Although the use of PCM effectively buffers temperature fluctuations and contributes to maintaining a stable radiator temperature, it partially replaces the honeycomb core, resulting in an increase in radiator mass. The study focuses on the thermal modeling and integration of PCM into the radiator structure but does not investigate conventional radiator design parameters such as facesheet thickness, fin geometry, or alternative core configurations. Furthermore, the optimization is limited to the PCM-based configuration without comparing its performance against conventional radiator designs.

Finally, in 2016, Kim et al. [31] studied the optimization of space radiator designs for thermal performance and mass reduction. The study examined design parameters such as heat pipe spacing, facesheet thickness, and honeycomb core density individually, validating results with a fourth-order finite difference method. It assumed a constant heat pipe temperature and complete heat transfer from components to the pipes, with conduction through the outer facesheet and honeycomb core. However, equipment layout effects were not considered, even though thinner inner facesheets made of aluminum 2024 were investigated, which cannot distribute heat uniformly in-plane or effectively share heat loads among the heat pipes. In addition, variables were not studied in combination, which limits insight into potential parameter interactions.

In conclusion, the fin efficiency approach is widely adopted as an analytical method in radiator design studies. In contrast to these previous works, the present study examines radiator design variables concurrently using a genetic algorithm to identify a more optimal starting point for radiator design. Earlier studies generally assumed that the heat loads from equipment were homogeneously distributed, even when thinner inner facesheets were used. In the current study, homogeneous heat distribution is promoted by employing a thicker, high-conductivity inner facesheet. Furthermore, because equipment layout has a significant influence on in-plane heat distribution, the layout design is also evaluated alongside the radiator design to achieve a more uniform thermal distribution across the panel.

2.2 Genetic Algorithms for Optimization-Based Engineering Design

GAs have been increasingly popular for solving complex real-world problems across various fields. A review study on GAs in 2020 highlighted that, up until that point, approximately 2,764,792 research papers had been published on the topic, based on sources such as Google Scholar, PubMed, and manual searches [32]. This underscores the increasing acknowledgment of GAs as a potent instrument for dealing with complicated problems. Engineering issues, which are frequently characterized by a high degree of nonlinearity and constraints, provide substantial challenges for traditional optimization methods. GAs have demonstrated significant effectiveness in engineering problems due to their robustness and ability to handle complex, multi-dimensional search spaces. In engineering, where minimizing cost and/or weight while maintaining performance is essential, GAs are particularly valuable for their ability to generate not only a single optimal solution but also a diverse set of feasible alternatives. This capability allows engineers to thoroughly evaluate a wide range of alternatives, supporting more informed decision-making and enhanced design optimization. The design variables considered may include shape, quantity, topology, geometry, and the physical properties of components.

GAs are invaluable for conceptual and preliminary engineering design studies and are widely employed by engineers for thermal optimization problems. In 2004, Codreanu et al. [33] analyzed the use of GAs to optimize the thermal performance of heat exchangers, focusing on minimizing temperature distribution and maximizing heat transfer efficiency in semiconductor cooling systems. However, the study employed a single set of GA parameters, without exploring how variations in population size, crossover rate, or mutation rate might influence optimization outcomes. Moreover, the analysis focused on a specific micro-channel heat exchanger configuration, without exploring broader geometric or operational variations that could affect the generality of the findings.

In 2009, Hengeveld et al. [34] investigated the optimal placement of electronic components with the objective of minimizing heat flux non-uniformities. As an alternative to using high thermal conductivity systems in radiator panels, such as embedded heat pipes, integrated pumped fluid loops, or high conductivity face sheets like annealed pyrolytic graphite (APG), the study proposed optimizing component placement to minimize thermal gradients. Although the results showed that optimal layouts could reduce heat flux non-uniformities, the method assumed identical component sizes and did not include actual spatial overlap constraints. Each component was represented as an idealized circular “thermal influence zone,” and variations in radiator or equipment geometry were not considered, which limited applicability to more complex spacecraft designs.

Moving forward to 2019, Akpınar [35] investigated the thermal insulation performance of a cylindrical structure and determined the thermal boundary layer thickness for laminar airflow using GA. However, the study did not explore the effects of varying GA parameters, and key enhancement strategies such as elitism were not implemented to preserve high-quality solutions across generations. Additionally, the algorithm termination was based solely on a predefined maximum number of iterations, without consideration of convergence criteria, making it difficult to assess the trend or stability of solution quality. Furthermore, the optimization results were not validated, limiting confidence in the proposed approach.

Most recently, in 2021, Mekki et al. [36] conducted a study on the topology optimization of heat exchanger fins for aerospace applications, utilizing GA. The study examined the sensitivity of the GA to parameters such as mutation rate and population size. However, since the initial population was generated exclusively by mutating a single baseline geometry, this approach may introduce bias and reduce diversity in the design space, potentially limiting the exploration of topologically distinct solutions. Furthermore, the analysis focused on a specific fin geometry and did not examine broader variations in heat exchanger configurations, which could restrict the general applicability of the findings.

In conclusion, these examples highlight the versatility and effectiveness of genetic algorithms in addressing a wide range of thermal optimization challenges across various engineering fields. In contrast to previous works, the present study investigates the influence of key GA parameters, namely population size, mutation rate, and crossover rate, to identify the most suitable configuration for the problem at hand. The initial population is generated randomly, thereby avoiding bias in the search space. Furthermore, both a minimum iteration count and convergence criteria are applied simultaneously, enabling more reliable and controlled termination of the algorithm.

2.3 Objective of Thesis

Utilizing conventional methods for designing embedded heat spreader GEO radiators and equipment layout can be inefficient in achieving optimal designs. These methods often require numerous iterations of finite element method (FEM) or finite difference method (FDM) thermal analysis, typically adjusting only one design parameter per iteration, which makes the process time-consuming. Additionally, this approach limits the ability to observe the simultaneous effects of multiple parameters, leading to lengthy processes and large data sets that must be evaluated and compared. The objective of this work is to apply a GA to assist in the design of embedded heat spreader GEO radiator panels and their integrated equipment layouts, with the goal of ensuring sufficient heat rejection capability, minimizing mass, and reducing non-uniform temperature distribution across the radiator. This study simultaneously evaluates design parameters while considering constraints such as allowable spacecraft dimensions, non-overlapping placement of equipment, and the requirement to keep all equipment within the defined radiator area. As a result, this approach enhances thermal design methodologies and offers valuable insights for optimizing embedded heat spreader radiator configurations and equipment layout.

2.4 Outline of Thesis

In line with the above-mentioned thesis aims to:

• **In Chapter I:** The introduction provides an overview of the thermal design of GEO spacecraft radiators, with a focus on engineering optimization, particularly GA, and concludes with a summary of the thesis contributions and structure.

• **In Chapter II:** The literature review chapter discusses previous studies on the use of fin efficiency in radiator design and the application of GA to engineering problems.

• **In Chapter III:** The methodology chapter presents the thermal design of embedded heat spreader radiators, including radiator sizing, dimensioning, and the fin efficiency approach. The working mechanism of the GA and its operators is introduced. Finally, a detailed explanation is provided on the use of GA for optimizing embedded heat spreader GEO radiators and equipment layout, with the goal of minimizing mass and ensuring adequate thermal performance within spacecraft constraints.

• **In Chapter IV:** The discussion chapter presents two case studies involving different numbers of distinct equipment to demonstrate the flexibility and applicability of the optimization methodology. These cases highlight the method's capability to handle both simpler and more complex configurations, showcasing its broader scope. The results are followed by comprehensive verification through FEM-based thermal analysis.

• **In Chapter V:** The conclusion chapter emphasizes the effectiveness of applying GA to the design of embedded heat spreader GEO radiators and equipment layouts. It provides a summary of the benefits and applicability of the proposed methodology in spacecraft projects, highlighting its practical value in the design process.

3. METHODOLOGY

3.1 Thermal Design of Embedded Heat Spreader GEO Radiators

The design of the embedded heat spreader GEO radiator is specifically engineered to dissipate heat from equipment, thereby ensuring optimal thermal management. The radiators are composed of internal and external facesheets, honeycomb structures, heat spreader components, and specialized coatings. Specialized adhesives are used to securely bond all components, ensuring both structural integrity and optimal performance.

The radiator composition and size are designed with consideration for the worst hot-case scenario. To account for maximum orbital heating, the north and south radiator panels of the examined GEO spacecraft are analyzed separately, each considering a maximum sun incidence angle (θ_s) of 23.5°. Additionally, it is assumed that all equipment operates at its maximum possible heat dissipation. The rationale behind using this scenario is that if the radiator can provide an efficient thermal environment for the equipment under these extreme conditions, it will be capable of functioning adequately under any other conditions.

The equipment is usually placed on the inner facesheet of the radiator to be shielded from the harsh conditions of space. Honeycomb structures are deliberately positioned between the inner and outer facesheets to achieve a lightweight design while meeting structural requirements. The embedded heat spreaders, situated between the inner and outer facesheets and within the honeycomb structure, are essential for transferring heat from the heat source to the heat sink. In the GEO radiator, equipment is intentionally placed above the heat spreaders whenever possible, as seen in Figure 3.1. This configuration enhances thermal conductivity between the heat spreader and the equipment.

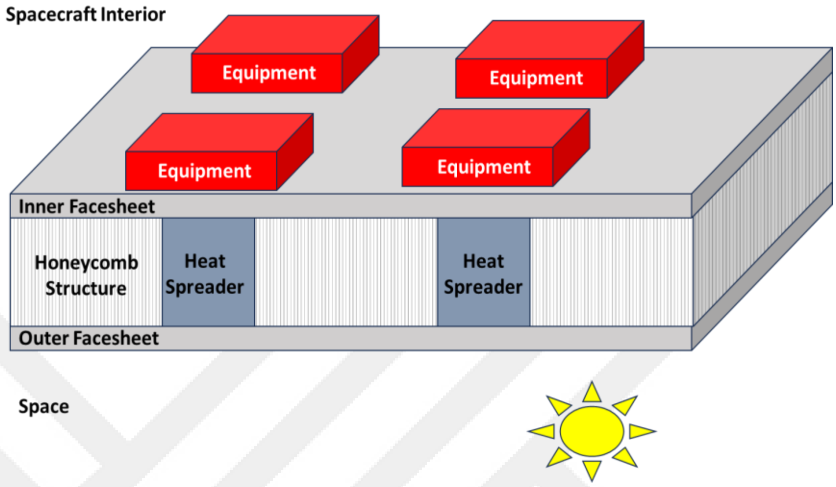

Figure 3.1: *Equipment Placement on Embedded HS GEO Radiator Panel*

Figure 3.2 illustrates the thermal resistance network of the embedded heat spreader GEO radiator. This schematic representation captures the key thermal pathways involved in the heat transfer process. It includes the radiative thermal resistance between the inner facesheet and the internal surfaces of the spacecraft, which are coupled through a defined view factor. Conductive thermal resistance is represented between the equipment and the inner facesheet, reflecting the direct mechanical interface. In-plane conduction through the honeycomb core and the facesheets is also modeled, accounting for lateral heat spreading. Additionally, the diagram includes transverse conductive resistance from the inner facesheet to the outer facesheet via the honeycomb structure and embedded heat spreader, which captures vertical heat transport. Finally, radiative thermal resistance from the outer facesheet to deep space is included, representing the final heat rejection step. Together, these elements form a comprehensive model of the thermal behavior of the radiator system.

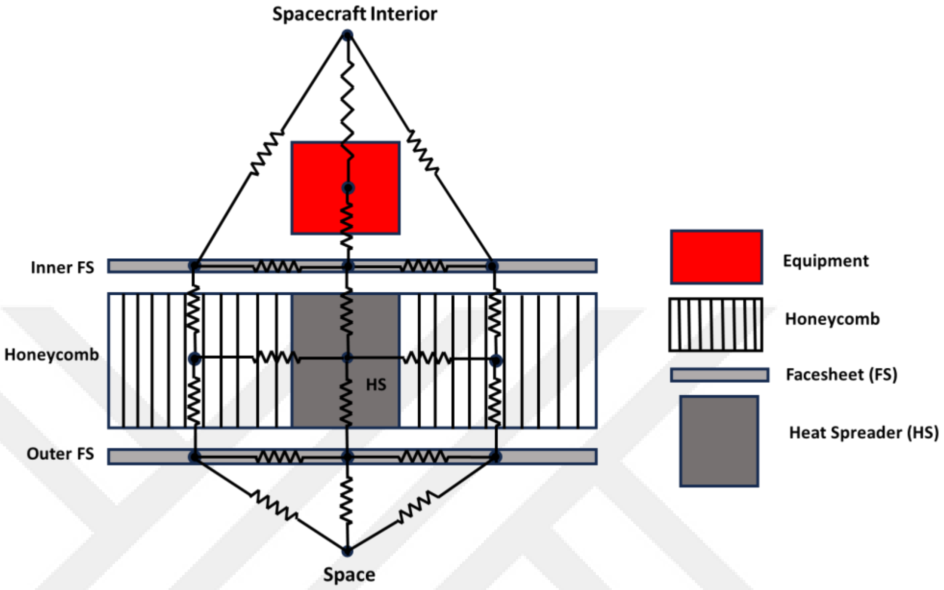

Figure 3.2: *Thermal Resistance Diagram of Embedded HS GEO Radiator*

3.1.1 Radiator Sizing and Dimensioning

Before starting the design of the radiator, the maximum allowable inner facesheet temperature ($T_{Inner\ FS_i}$) is calculated for each equipment (i=1,…,n) based on the equipment temperature limit (T_{Limit_i}), heat transfer coefficient of thermal filler (h_{TF_i}) between the equipment baseplate and inner facesheet, the equipment heat load (q_i) and contact area (L_iW_i) as depicted in Equation (3.1).

$$T_{Inner\ FS_i} = T_{Limit_i} - \frac{q_i}{L_iW_ih_{TF_i}} \tag{3.1}$$

Calculated maximum allowable inner facesheet temperatures for each equipment are compared, and the minimum of these maximum allowable temperature values is selected as the target temperature of the inner facesheet $\left(T_{Inner\ FS_i}\right)$ as depicted in Equation (3.2). The achieved target temperature of the inner facesheet of the radiator ensures compatibility with the thermal needs of all equipment.

$$\min\left(T_{Inner\ FS_i}, \dots, T_{Inner\ FS_n}\right) = T_{Inner\ FS} \tag{3.2}$$

The next step is to calculate the temperature of the outer facesheet ($T_{Outer\ FS}$), which is necessary for determining the required radiator area using radiative heat transfer equations. This temperature is determined using the temperature of the inner facesheet ($T_{Inner\ FS}$), the total thermal resistance (Ω) between the inner and outer facesheets, and the total heat load of the equipment ($q_{internal}$), as depicted in Equation (3.3).

$$T_{Outer\ FS} = T_{Inner\ FS} - (\Omega\ q_{internal}) \tag{3.3}$$

The next step involves defining the thermal balance, accounting for all heat fluxes impacting the radiator face, to calculate the net heat rejection capability of the radiator ($\dot{q}_{R\ HRC}$) using Equations (3.4). In contrast to the Low Earth Orbit (LEO) and the Medium Earth Orbit (MEO) spacecraft, the Albedo ($\dot{q}_{albedo}$) and Earth infrared ($\dot{q}_{planet}$) heat fluxes are considered negligible for GEO spacecraft due to their low proportional effect compared to solar ($\dot{q}_{solar}$) heat fluxes. Radiative heat flux from spacecraft appendages and interior surfaces of the spacecraft ($\dot{q}_{S/C}$) is also neglected. Therefore, Equation (3.4) is simplified to Equation (3.5).

$$\dot{q}_{R\ HRC} = \sigma\epsilon F\left(T^4_{Outer\ FS} - T^4_{Space}\right) - \left(\dot{q}_{solar} + \dot{q}_{albedo} + \dot{q}_{planet} + \dot{q}_{S/C}\right) \tag{3.4}$$

$$\dot{q}_{R\,HRC} = \sigma\epsilon F\left(T_{Outer\,FS}^4 - T_{Space}^4\right) - (\,\dot{q}_{solar}) \tag{3.5}$$

In Equation (3.6), the radiator area (A_R) must meet the heat rejection requirements of equipment by matching the radiator heat rejection capability ($\dot{q}_{R\,HRC}$).

$$\sum_{Eq_1}^{Eq_n} q_i = \dot{q}_{R\,HRC} A_R \tag{3.6}$$

Equation (3.7) illustrates that the radiator area (A_R) is determined by multiplying the width of the radiator (W_R) and the length of the radiator (L_R). The aspect ratio (AR) is defined as the ratio of the width of the radiator to its length, as depicted in Equation (3.8).

$$A_R = W_R L_R \tag{3.7}$$

$$AR = \frac{W_R}{L_R} \tag{3.8}$$

3.1.2 Fin Efficiency Approach and Equations

The temperature distribution across radiators varies due to the location of equipment on the radiator panel and the associated thermal resistances. Despite the utilization of heat spreaders to enhance thermal conductivity, temperature variations remain. Therefore, although relying solely on the average temperature of a radiator to determine its heat rejection capability is practical, it lacks precision. In order to overcome this issue, thermal designers employ the fin efficiency approach, which simplifies heat transfer by treating it as one-dimensional. This method enhances the accuracy of heat rejection predictions by considering the non-uniform temperature distribution in radiator systems.

In order to begin the process of thermal design of the embedded heat spreader GEO radiator and be to find candidate thermal solution sets, it is necessary to establish specific assumptions and accept certain conditions. Some of these are general guidelines for the thermal design of spacecraft, while others simplify the calculations. The assumptions that have been adopted for this study are provided in the following key points [27, 28, 29, 31].

- The fin root temperature (T_{FR}), which is the average temperature of the heat spreader, is assumed to remain constant along the heat spreader's longitudinal projection. This assumption is applied in the early stage of radiator design, when equipment layout data is unavailable. It enables the investigation of radiator thermal performance using a one-dimensional (1D) thermal resistance approach.
- The radiative heat transfer between the inner facesheet of the radiator, equipment and interior surfaces of the spacecraft is neglected. This is a result of the inability to estimate the temperature of the spacecraft's interior surfaces and calculate the view factors.
- In the transverse direction, heat is conducted from the inner facesheet to the outer facesheet through the heat spreaders. The transverse thermal conductivity of the honeycomb structure is neglected due to the significantly lower thermal resistance of the heat spreaders compared to the honeycomb structure.
- The environmental view factor of the outer facesheet coating is considered to be 1. To simulate the worst-case hot scenario, the thermo-optical properties of the coating at the end of its life are used. The coated surface is modeled as a grey body, with the assumption of uniform emittance that is independent of temperature.

- The thermal conductivity of the radiator component materials is assumed to remain constant and not vary as a function of temperature.
- The adhesives used in the radiator have high thermal conductivity and very low thickness, resulting in negligible thermal resistance and mass. Therefore, they are disregarded in the calculations.
- In the early stage of radiator design, a 10 mm thickness for the inner facesheet is utilized to reduce the impact of equipment layout on thermal performance and to achieve a more uniform temperature distribution across the inner surface.
- Heat spreaders interface with the inner and outer facesheets through specialized, high-thermal-conductivity adhesives applied along the longitudinal axis.

In conclusion, considering all the assumptions mentioned above, the thermal resistance network is simplified as shown in Figure 3.3. The heat generated by the equipment is first transferred to the inner facesheet of the radiator through a conductive thermal resistance. This resistance depends on the type of thermal interface between the equipment baseplate and the inner facesheet, such as thermal filler materials, dry contact, or other interface solutions. From there, the heat flows transversely through the heat spreaders to the outer facesheet. This path involves transverse conductive resistance, which accounts for the heat transfer between the heat spreader and the facesheets, considering the adhesive layers that bond the heat spreader to the facesheets. Once it reaches the outer facesheet, the heat spreads laterally across the panel via in-plane conductive resistance, which includes conduction through the facesheet and half the thickness of the honeycomb core. Finally, the heat is radiated into space via a radiative thermal resistance from the outer facesheet to the space environment. This simplified thermal network effectively captures the dominant resistances in the heat transfer path and supports accurate thermal modeling of the radiator's performance during the optimization and design phases.

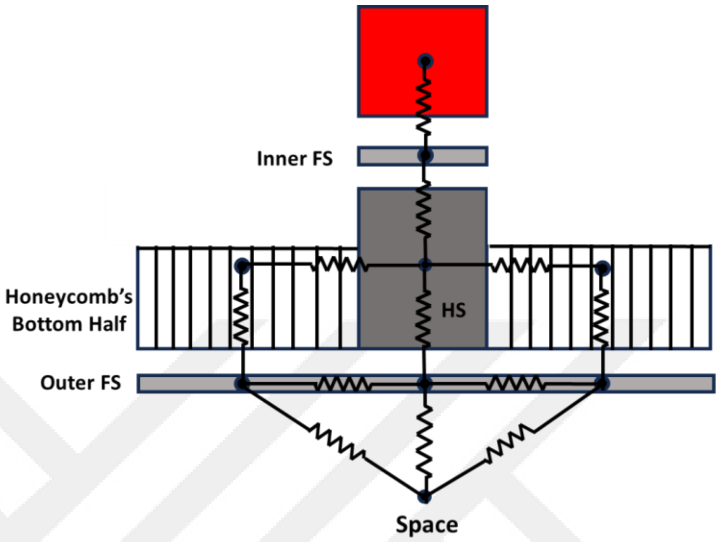

Figure 3.3: *Simplified Thermal Resistance Diagram of Embedded HS GEO Radiator*

In the preliminary design phase, since the equipment locations have not yet been determined, the radiator's physical configuration is assumed to be symmetric, as shown in Figure 3.4, to enable a comprehensive evaluation of the entire radiator area. This approach facilitates the assessment of the radiator's overall heat rejection capability by analyzing a representative specific portion (ℓ). This portion consists of a single heat spreader ($2L_p$) and two side fins ($2L_F$). The heat rejection capability of this small section is obtained using fin efficiency calculations, and the heat rejection capability of the complete panel can be computed by multiplying the number of heat spreaders (N) by the heat rejection capability of the small section.

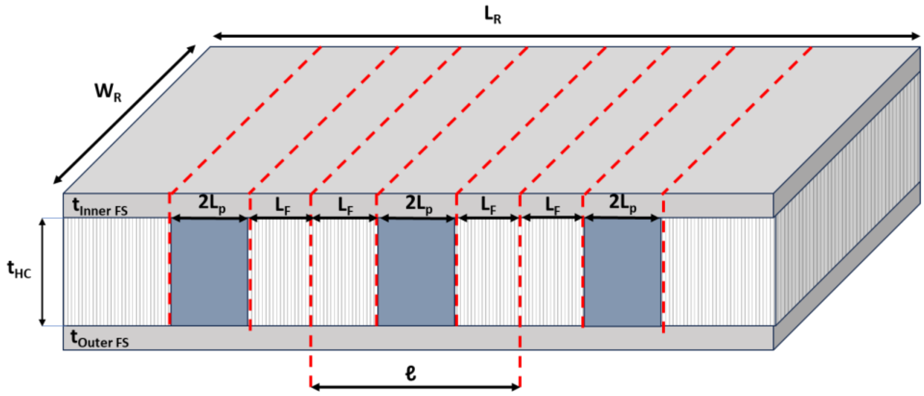

Figure 3.4: *Schematic Diagram of a Radiator with Embedded HS*

In the fin efficiency approach, the total heat load is evenly distributed across small portions (ℓ) in symmetric radiator layouts. The temperature gradient from the heat spreaders to the fin tip leads to variations in heat rejection capability due to the temperature dependence of radiative heat transfer. To account for these variations, which significantly influence thermal performance, the fin efficiency parameter (η) is employed. The derivation of this parameter (η) involves solving differential equations that combine radiation and conduction factors along the fin, as depicted in the x-direction in Figure 3.5, and utilizes dimensionless parameters (θ and λ) within these equations.

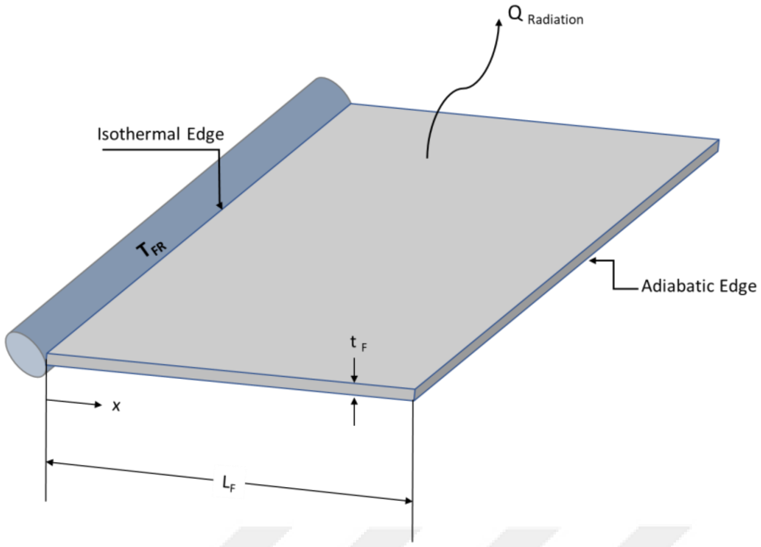

Figure 3.5: *HS and Fin in Radiator*

The dimensionless fin conductance parameter (λ) is defined as the ratio between the radiation conductance and conduction conductance, as illustrated in Equation (3.9). In this equation, σ denotes the Stefan-Boltzmann constant (5.87×10^{-8} W/m^2K^4); ε_R represents the emissivity of the radiator's outer surface, which is used for radiative heat transfer to space. T_{FR} signifies the fin root temperature (K), accepted as the average temperature of the heat spreader and assumed to remain constant along its length [27]. L_F indicates the length of the fin (m), while k_F t_F represents the one-dimensional equivalent conductance (W/K).

$$\lambda = \frac{\sigma \varepsilon_R T_{FR}^3 L_F^2}{k_F t_F} \tag{3.9}$$

The calculation of the one-dimensional equivalent conductance along the fin includes the conductance of the facesheet and half of the honeycomb, as shown in Equation (3.10) [31]. In this equation, k_{FS} and k_{HC_w} denote the thermal conductivity of the facesheet (W/mK) and the thermal conductivity of the honeycomb (W/mK) along the fin direction, respectively. t_{FS} and t_{HC} represent the thickness of facesheet (m) and the thickness of honeycomb (m), respectively.

$$k_F t_F = k_{FS} t_{FS} + k_{HC_w} (t_{HC}/2) \tag{3.10}$$

For calculating the in-plane thermal conductivity of honeycomb, Equation (3.11) is used. In this equation, k_{HC} indicates thermal conductivity of honeycomb material (W/mK). δ_{HC} and S denote thickness of the honeycomb ribbon (m) and cell size of the honeycomb (m), respectively. These parameters are illustrated in Figure 3.6.

$$k_{HC_w} = \frac{k_{HC}\delta_{HC}}{S} \tag{3.11}$$

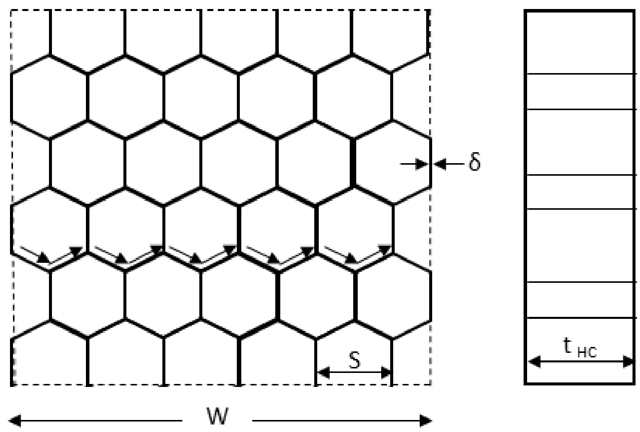

Figure 3.6: *Honeycomb Structure and Heat Transfer Pathways*

The dimensionless parameter θ is defined as the ratio of the equivalent heat sink temperature to the fin root temperature, as illustrated in Equation (3.12). In this equation,

T_s and T_{FR} represent the equivalent heat sink temperature (K) and fin root temperature (K), respectively.

$$\theta^4 = \frac{T_s^4}{T_{FR}^4} \tag{3.12}$$

The radiator's outer surface is subjected to various heat fluxes in orbit, including solar radiation, Earth infrared radiation, and albedo. Additionally, there is infrared heat flux from external components (i) like star trackers, antennas, and solar arrays that are positioned outside the spacecraft and have a direct line of sight to the radiator surface (F_{R-i}). In order to simplify the calculations for fin efficiency equations, an equivalent heat sink temperature (T_s) is utilized. This temperature is determined using Equation (3.13), which takes into consideration the impact of the various heat fluxes discussed earlier [27, 29]. In this equation, $\cancel{S}$ and E_{EIR} represent the solar constant (W/m^2) and Earth infrared emission (W/m^2), respectively. The parameters α_s, r_A and F represent the radiator's solar absorptivity, reflectance for albedo, and view factor, respectively.

$$T_s^4 = \frac{(\alpha_s \cancel{S} \sin\theta_s + \alpha_s r_A \cancel{S} F_A + \varepsilon_R F_{EIR} E_{EIR} + \sum_i F_{R-i} \varepsilon_R \sigma T_i^4)}{\sigma \varepsilon_R} \tag{3.13}$$

The solar radiative effect is significantly stronger than other heat sources; therefore, the influence of these other sources is disregarded. As a result, Equation (3.13) is simplified to Equation (3.14) for the calculation of the equivalent heat sink temperature (T_s) [29].

$$T_s = \left(\frac{\alpha_s \cancel{S} \sin\theta_s}{\sigma \varepsilon_R}\right)^{1/4} \tag{3.14}$$

Chang's study [27] methodically investigates the effectiveness of longitudinal radiating fins with various profile forms and aims to develop analytical correlations that can be more effectively utilized in computer-assisted thermal analysis and design. His research focuses on enhancing the thermal performance and design efficiency of radiators by examining different fin geometries. The study provides provides correlated Equation (3.16) and Equation (3.19) for a flat structure with a uniform cross-section, notably relevant to the calculation of fin efficiency in embedded heat spreader radiators.

The parameter δ represents the fin thickness ratio, defined as the ratio of the fin tip thickness (t_T) to the fin base thickness (t_B), as expressed in Equation (3.15). The general fin geometry, which represents constant outer facesheet thickness and constant honeycomb core thickness, is illustrated in Figure 3.7. In the present study, a flat fin structure with uniform thickness along the panel is considered; therefore, δ is equal to 1.

$$\delta = \frac{t_T}{t_B} \tag{3.15}$$

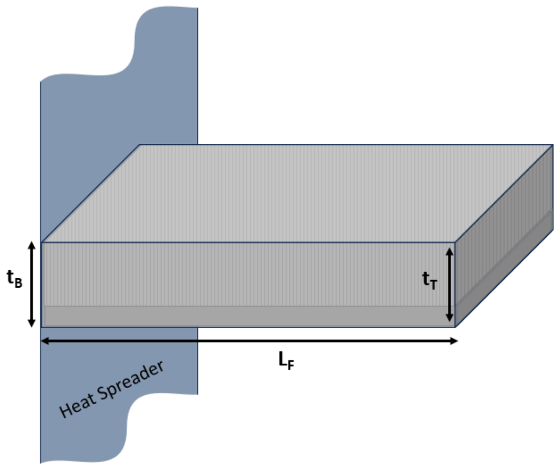

Figure 3.7: *Longitudinal Radiating Fin of Flat Shape*

Fin Efficiency (η) for $0.01 \leq \lambda \leq 0.2$:

$$\eta = (1 - A_1\lambda + A_2\lambda^2)(1 - \theta^4) \tag{3.16}$$

Equation (3.17) and Equation (3.18) present the expressions for the coefficients A_1 and A_2 respectively, which are functions of the fin thickness ratio (δ).

$$A_1 = 10^{(0.2480 - 0.151\delta)} \tag{3.17}$$

$$A_2 = 10^{(0.4674 - 0.2634\delta)} \tag{3.18}$$

Fin Efficiency (η) for $0.2 \leq \lambda \leq 2.0$:

$$\eta = (-B_1 \log \lambda + B_2)(1 - \theta^4) \tag{3.19}$$

Equation (3.20) and Equation (3.21) present the expressions for the coefficients B_1 and B_2 respectively, which are functions of the fin thickness ratio (δ).

$$B_1 = 0.0129\delta + 0.3920 \tag{3.20}$$

$$B_2 = 0.0403\delta + 0.4918 \tag{3.21}$$

Equation (3.22) is used for determining the net heat rejection capacity of a single fin ($q_{F_{HRC}}$), taking into account the fin efficiency (η). This single fin includes half the width of the heat spreader (L_p) and one side fin (L_F). To simplify the calculation, Equation (3.22) is transformed into Equation (3.23).

$$q_{F_{HRC}} = W_R\left(L_p\varepsilon_R\sigma(T_{FR}^4 - T_s^4) + \eta L_F\varepsilon\sigma T_{FR}^4\right) \tag{3.22}$$

$$q_{F_{HRC}} = W_R\varepsilon_R\sigma T_R^4\left(L_p(1 - \theta^4) + \eta L_F\right) \tag{3.23}$$

As the final step, Equation (3.24) calculates the radiator's net heat rejection capacity. Here, N represents the number of heat spreaders. This equation illustrates that the radiator's total net heat rejection capacity is determined by multiplying the net heat rejection capacity of a single fin section (L_F+L_P) by 2 and N, due to the radiator's symmetric design, where each heat spreader is flanked by two identical fins.

$$q_{R\,HRC} = 2W_R N \varepsilon_R \sigma T_R^4 \left(L_p(1-\theta^4) + \eta L_F\right) \tag{3.24}$$

3.2 Genetic Algorithm

GAs are numerical optimization techniques inspired by the natural laws of evolution. The fundamental goal in evolutionary genetics is to preserve advantageous genes while eliminating disadvantageous ones. Individuals with greater fitness have a higher likelihood of transmitting their genetic material to future generations. In the long term, organisms with the optimum combination of genes become dominant in their community. Occasionally, in the ongoing process of evolution, spontaneous mutations might take place in genes. When these modifications result in advantages in the competition for survival, new individuals in the population predominantly inherit them from previous generations. Meanwhile, natural selection eliminates unsuccessful genotypes.

The mathematical formulation of a general constrained, mixed-discrete optimization problem for a GA is as follows:

$$Find\ x = \{x_1, x_2, \dots, x_n\}^T = \{x^D, x^C\}^T$$

which minimize or maximize $f(x)$

subject to certain set of constraints:

$$g_j(x) \leq 0 \quad j = 1, \dots, p$$

$$h_k(x) = 0 \quad k = 1, \ldots, m$$

$$x_i^l \leq x_i \leq x_i^u \; i = 1, \ldots, n$$

The solution vector, denoted as x, consists of n independent design variables. The feasible subset of discrete variables is $x^D \epsilon R^D$, while the feasible subset of continuous variables is $x^C \epsilon R^C$. $g_j(x)$ and $h_k(x)$ are the inequality and the equality constraints, respectively. The objective function is f(x). Furthermore, x_i^l and x_i^u are the lower and upper bounds respectively for different design variables.

3.2.1 Operators of the Genetic Algorithm

3.2.1.1 Population Size

The population size is an essential component that needs to be defined in GAs. It consists of candidate solutions for the problem. These candidate solutions are represented by chromosomes, and the population renews itself in each generation through the application of GA operators.

In order to obtain satisfactory solutions, it is important to provide the algorithm with an appropriate number of chromosomes. Genetic drift and selection pressure are key factors that help to determine the required population size. Researchers frequently argue that a small population size can cause the algorithm to produce inadequate solutions because of a lack of diversity, whereas a large population size can lead to excessive computation time because of an unnecessarily wide search space [22, 37, 38, 39]. Lobo and Goldberg developed a graph that illustrates the effects of population size on GAs, as shown in

Figure 3.8 [40]. Studies and observations indicate that a population size ranging from 40 to 200 is often effective for addressing most problems [41].

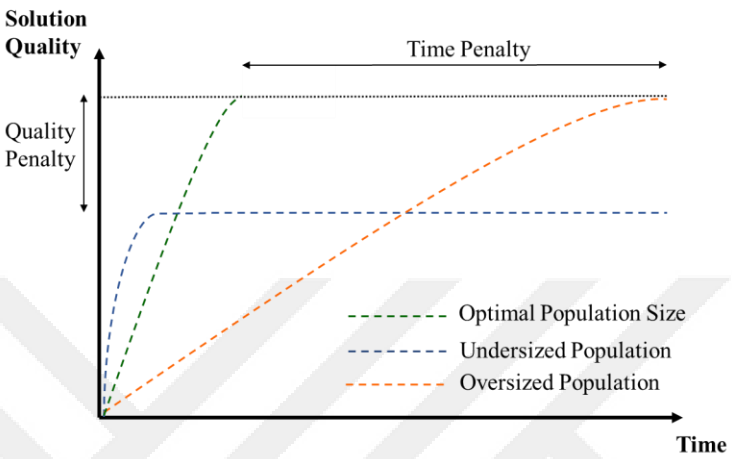

Figure 3.8: *Population Sizing in Genetic Algorithms (Adapted from [40])*

The size of the population directly impacts the quantity of search points for each generation. The parameters of a GA should not be considered as independent variables and must be collectively determined, as they have a combined effect on the effectiveness of the GA. In populations with 20 to 40 chromosomes, achieving good GA performance is linked to either a high crossover rate paired with a low mutation rate, or a low crossover rate paired with a high mutation rate. For populations consisting of 30 to 90 chromosomes, it appears that the ideal crossover rate decreases as the population size increases [23]. Moreover, the optimal population size is affected by chromosome length as well [42]. Therefore, chromosome length should also be considered when determining the optimal population size.

3.2.1.2 Encoding and Decoding

Design variables can be categorized as discrete, continuous, or a combination of both. Discrete design variables have uneven spacing between consecutive values, whereas continuous design variables have even spacing, referred to as resolution. Encoding these variables is the first step in applying GAs. Design variables are encoded as genes, which combine to form chromosomes that represent potential solutions to the optimization problem. Consequently, design variables are not directly input into the GA but are represented by encoded chromosomes. This allows GAs to work with design spaces that include a mix of continuous, discrete, and integer variables. The physical values of the design variables are derived by decoding the genes within the chromosomes. These values are then utilized in relevant functions, and the compliance with the problem's constraints is checked.

The encoding strategy plays a fundamental role in GAs, as it determines how data is represented and structured for processing. Encoding techniques are categorized according to the characteristics of the problem domain and its associated variables. The commonly recognized encoding systems include binary, octal, hexadecimal, permutation, value-based, and tree, as illustrated in Table 3.1.

Table 3.1: *Comparison of Common GA Encoding Schemes (Adapted from [32])*

Encoding Schemes	Pros	Cons
Binary	Easy implementation Faster execution	Inversion operator unavailable
Octal	Easy implementation	Inversion operator unavailable
Hexadecimal	Easy implementation	Inversion operator unavailable
Permutation	Inversion operator available	Binary operators unavailable
Value	No value conversion required	Requires specific crossover and mutation
Tree	Easy application of operator	Tree design complexity

Binary encoding is the most commonly used encoding scheme, where design variables are represented as binary strings. Design variables are encoded as fixed-length binary strings, known as genes, using the binary alphabet (0, 1), as illustrated in Figure 3.9. The genes are subsequently concatenated to form an elongated sequence, referred to as a chromosome. Each bit in binary encoding affects a specific design variable, therefore determining the characteristics of the solution. This implies that each chromosome encodes a distinct combination of design variables, leading to a unique solution. This encoding scheme enables the effective application of crossover and mutation operators. Nevertheless, converting data into binary form requires additional effort, and the accuracy of the binary conversion is critical, as it directly impacts the results and processes of the GA.

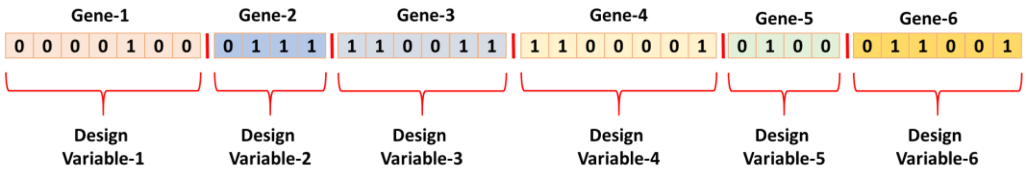

Figure 3.9: *Chromosome Structure – 34-Bit String with 6 Genes*

3.2.1.2.1 Binary Representation of Discrete Design Variables in GAs

The length of the binary digit gene string for discrete design variables is denoted by λ, where 2^{λ} is the total number of viable discrete subset variables. For example, when there are 32 distinct values, the value of λ is 5. Consequently, the gene representing a discrete design variable is encoded as a binary string with a length of 5. If the number of discrete values does not correspond to any power of 2 (2^{λ}), alternative methods such as the penalty approach or redundant distribution method can be employed for the decoding of the gene [43]. Alternatively, the number of viable discrete values can be adjusted to match 2^{λ} instead of applying these approaches. Once the value of λ_i for each design variable is established, the overall length Λ of the chromosome, which has n design variables, is calculated by using Equation (3.25).

$$\Lambda = \sum_{i=1}^{n} \lambda_i \tag{3.25}$$

The mapping relationships between unsigned decimal integers and discrete values are used to construct a two-stage mapping process that obtains the physical values of discrete design variables. In the first stage, the binary digit substring, called a gene, is converted into an unsigned decimal integer, denoted as I. In the second stage, the physical value of the design variable is determined through a direct and unique mapping from the set of integers (I) to discrete values. The two-stage mapping technique is demonstrated using three-bit strings as an example, as shown in Table 3.2. A three-bit string can be decoded into an unsigned decimal integer ranging from 0 to 7. This unsigned decimal integer can then be associated with any of the 8 distinct values in the set. For example, the gene string representing the discrete design variable, such as 101, can be decoded into the unsigned decimal integer 5, as shown in Equation (3.26). The unsigned decimal integer 5 corresponds to the discrete value of D_6 when matched across the table.

$$I = 1 \times 2^2 + 0 \times 2^1 + 1 \times 2^0 = 5 \tag{3.26}$$

Table 3.2: *Decoding Discrete Variables with Two-Stage Three-Bit Mapping*

Binary Digit String	**Unsigned Decimal Integers**	**Discrete Values**
000	0	D_1
001	1	D_2
010	2	D_3
011	3	D_4
100	4	D_5
101	5	D_6
110	6	D_7
111	7	D_8

3.2.1.2.2 Binary Representation of Continuous Design Variables in GAs

A continuous variable can be treated as a discrete variable with small increments, referred to as resolution. These resolutions are chosen to closely approximate the typical increments of continuous variables.

The length of the continuous design variable gene string can be calculated by Equation (3.27). Here, the symbol ε denotes the resolution, whereas x^u and x^l represent the upper and lower bounds on x in its side restrictions, respectively. For instance, if $\varepsilon=0.1$, $x^u=20.0$, and $x^l=45.0$, then λ, which represents the length of the binary gene string for the feasible subsets of continuous variables, is greater than or equal to 8.

$$\lambda \geq log_2 \frac{x^u - x^l}{\varepsilon} \tag{3.27}$$

The physical value of the continuous variable is determined using the unsigned decimal integer (I), along with the resolution (ε) and the upper or lower bounds, as shown in Equation (3.28). For example, given $\epsilon = 0.001$, $x^l = 5.000$, and $x^u = 9.096$, the required gene length λ is at least 12. Thus, 12-bit fixed-length chromosomes can be used for this continuous design variable. For instance, the bit string 100000000011 is decoded into the unsigned decimal integer I = 2051, which corresponds to a design variable value of x = 7.051.

$$x = x^l + I \times \epsilon \tag{3.28}$$

3.2.1.3 Generation Gap and Elitism

Traditional GAs employ generational replacement, which means that the complete population is replaced in each generation. The complete renewal of a population may result in the loss of advantageous chromosomes. As a consequence, these chromosomes may not appear in the next generation, and additional generations may be required to rediscover them. This leads to a high number of function evaluations, causing increased computational time and convergence challenges. To deal with these inefficiencies, a GA employs a special strategy known as elitism. Elitism encourages the GA to preserve the high-quality individuals in a certain generation and transmit them forward without any modifications to the subsequent generation.

The elitist strategy, first proposed by De Jong [22], is commonly employed to prevent any possible performance degradation between successive generations. The primary approach to executing elitism involves directly transferring one or more of the highest-performing chromosomes from the parent generation into the next generation. This strategy offers a faster approach to achieving the optimal individual when compared to alternative strategies. Another strategy is combining the parent and child populations into a single mating pool, ensuring that the mating population is always at least as strong as the previous one. However, the population size increases as the number of generations progresses in this strategy. Consequently, a substantial number of evaluations is needed.

To implement elitism, the fitness values of all chromosomes in the population must first be evaluated. In each generation, the chromosomes are then ranked from best to worst based on their normalized fitness scores, allowing the top-performing individuals to be preserved and carried over to the next generation without modification. The top-performing chromosomes are selected according to the elitism parameter, called generation gap, and carried directly into the next generation. This ensures that the best performance always survives intact, and any regression in performance will be prevented from one generation to the next. Without such a strategy, the best individuals might disappear due to sampling error, crossover, or mutation. The generation gap (G), which controls the percentage of the population replaced in each generation, is defined by Equation (3.29). Here, N_p refers to the population size, and M represents immigrations, the number of individuals that will be renewed. For example, if the generation gap is 80%, then 80% of the population is renewed, while 20% of the new population is replaced with the elite individuals from the current population.

$$G = \frac{M}{N_p} \times 100 \tag{3.29}$$

3.2.1.4 Selection in Genetic Algorithms

Selection is an essential step in GAs, determining whether a particular chromosome will participate in the reproduction process. In natural environments, species that are weak or unfit undergo extinction due to natural selection, while stronger individuals have increased chances of passing on their genes to successive generations. Over time, species possessing beneficial genetic combinations become predominant within their populations, as failed variations are gradually eliminated by natural selection. Similarly, the selection operator in evolutionary algorithms functions in an approach similar to natural selection in nature. It guides the search towards fitter individuals, replicating the concept of survival of the fittest.

The chromosomes chosen for crossover are determined by the fitness level of each individual. GAs employ several selection methods that utilize fitness values in different manners. Commonly employed techniques for selecting chromosomes to undergo crossover include roulette wheel selection, Boltzmann selection, ranking, and tournament selection [44]. Table 3.3 presents the advantages and disadvantages of these common methods.

Table 3.3: *Comparison of Different Selection Techniques (Adapted from [32])*

Selection Techniques	**Pros**	**Cons**
Roulette Wheel	Easy Implementation Simple Free from Bias	Premature Converge Risk Sensitive to Variance in Fitness Function
Rank	Preserve Diversity Free from Bias	Slow Convergence Sorting Required High Computational Cost
Tournament	Preserve Diversity Parallel Implementation No Sorting Requirement	Diversity Loss at Large Tournament Size
Boltzmann	Global Optimum Achieved	High Computational Cost
Stochastic Universal Sampling	Fast Method Free from Bias	Premature Convergence

A widely adopted and straightforward selection method is roulette wheel selection, often referred to as proportional selection. This technique employs relative fitness values to determine selection probabilities, reducing the likelihood of selecting low-fitness individuals while increasing the probability of choosing those with high fitness. Relative fitness is defined as the ratio of an individual's normalized fitness value to the sum of all normalized fitness values in the population. Every individual in the population is allocated a proportional section on a roulette wheel, as depicted in Figure 3.10. The size of each section is determined by the individual's relative fitness value. This ensures that each individual has a chance of being selected in proportion to its fitness.

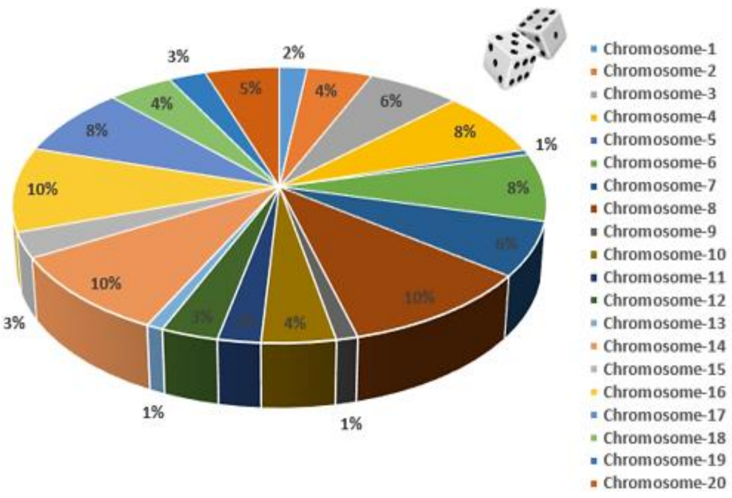

Figure 3.10: *Roulette Wheel for Fitness-Based Population Selection*

The roulette wheel can be built following the steps below for a population size of n:

- Calculate the fitness, evaluation (v_i) for each chromosome (i=1, ..., n)
- Calculate the total fitness of the population
  - $F = \sum_{i=1}^{n} evaluation(v_i)$
- The Probability of selection for each chromosome (i=1, …, n)
  - $p_i = \frac{evaluation(v_i)}{F}$
- Calculate the cumulative probability for each chromosome (i=1, …, n)
  - $q_i = \sum_{j=1}^{n} p_j$

The number of roulette wheel spins is determined by the mechanism used to generate the next population. The required number of spins can vary for each generation. A parent is selected with each spin of the roulette wheel, depending on which section of the wheel the pointer lands in. After two individuals are selected as parents, new offspring are produced using a crossover operator. The selection process includes the following steps:

- Generate a random floating-point number, r, in the interval [0,1]
- If $r < q_1$, then select the first chromosome v_1,
- Otherwise, select the i-th chromosome ($2 \leq i \leq n$) such that $q_{i-1} \leq r \leq q_i$.

Chromosomes with higher relative fitness values may be selected more than once as parents for crossover, while those with lower relative fitness values are chosen less often. This means that new offspring will primarily be created from the best chromosomes, allowing their genes to be passed on to future generations. In contrast, weaker chromosomes are less likely to be selected and will have a lower probability of passing their genes to subsequent generations. This selection process continues until the stopping criteria are satisfied, at which point the GA terminates.

3.2.1.5 Crossover in Genetic Algorithms

The crossover operator is the primary recombination mechanism in GAs. It is used to generate new chromosomes, called offspring, by combining the genetic information of two chromosomes, referred to as parents. The parents are selected from among the existing chromosomes in the population, with a preference for higher fitness, so that the offspring are expected to inherit advantageous genes that make the parents fitter. By iteratively applying the crossover operator, beneficial genes from strong chromosomes are expected to appear more frequently in the population, eventually leading to convergence to an overall optimal solution [45].

The crossover process enables the exchange of segments of the internal representations of parent individuals within the population pool, with the objective of improving the fitness of the resulting offspring in the subsequent generation. This process is analogous to the transmission of genetic material in biological reproduction, which occurs through Deoxyribonucleic Acid (DNA) and Ribonucleic Acid (RNA) strands. Various crossover operators can be chosen depending on the chromosome encoding scheme and the specific requirements of the optimization problem. Commonly used crossover operators include single-point, two-point, k-point, uniform, partially matched, mixed (shuffle), reduced surrogate, and various combinations of these. Each of these techniques has its own advantages and disadvantages, as outlined in Table 3.4.

Table 3.4: *Comparison of Different Crossover Techniques (Adapted from [32])*

Crossover Techniques	**Pros**	**Cons**
Single Point	Easy Implementation Simple	Less Diversity
Two and K-Point	Easy Implementation	Less Diversity Effective for Small Subsets
Reduced Surrogate	Effective in Small-Scale Problems	Premature Convergence
Uniform	Unbiased Exploration Applicable on Large Subsets Improved Recombination	Less Diversity
Precedence Preservative	Improved Offspring Generation	Risk of Redundant Offspring
Order Crossover	Improved Exploration	Information Loss from Parent
Cycle Crossover	Unbiased Exploration	Premature Convergence

Mixed two-point crossover is especially effective at producing higher quality solutions [46] and is therefore typically preferred for engineering optimization problems. This crossover technique involves randomly selecting two crossover points (loci) within the chromosomes for each crossover operation. The segments between these points are then exchanged between the parent chromosomes to produce two new offspring. Figure 3.11 illustrates the exchange of genetic information between the selected crossover points.

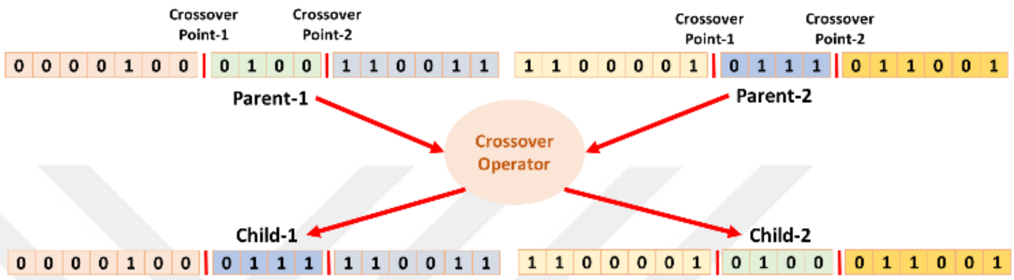

Figure 3.11: *Mixed Two-Point Crossover Operator*

The crossover rate, denoted as p_c, determines the probability of executing crossover and significantly influences the effectiveness of the search for optimal solutions. The crossover rate is usually set to a high value, typically ranging from 0.7 to 1.0 [47]. A higher crossover rate introduces new structures into the population more rapidly. However, if the crossover rate is too high, high-quality structures may be lost before selection can enhance them. Conversely, if the crossover rate is too low, the search may stagnate because of insufficient exploration.

The following steps are involved in the mixed two-point crossover operation:

- Generate a random floating-point number, r, for each crossover, within the interval [0, 1].
- If $r < p_c$, then select the parents, $x = (x_1, x_2, \ldots, x_\ell)$ and $y = (y_1, y_2, \ldots, y_\ell)$, where x and y represent the chromosomes with genes x_1 to x_ℓ and y_1 to y_ℓ, respectively.

- Generate two distinct random integers, P_1 and P_2, as crossover points (loci) for each crossover, within the interval [1, ℓ-1], where ℓ represents the length of the chromosome.
- Apply crossover to parents (x and y) to create offspring (x' and y'). The offspring are generated as follows:
  - $x' = (x_1, \ldots, x_{P_1}, y_{P_1+1}, \ldots, y_{P_2}, x_{P_2+1}, \ldots, x_\ell)$
  - $y' = (y_1, \ldots, y_{P_1}, x_{P_1+1}, \ldots, x_{P_2}, y_{P_2+1}, \ldots, y_\ell)$

3.2.1.6 Mutation in Genetic Algorithms

Mutation is a secondary search operator that increases population variability, thereby preventing premature convergence to suboptimal solutions. When selection and crossover operations are applied repeatedly without introducing additional variation, the genetic diversity of the population tends to decline. This reduction in diversity results in the generation of increasingly similar chromosomes, which can hinder the discovery of other potentially advantageous chromosomes that differ from those currently present. To address this issue, the mutation operator is implemented, helping to maintain diversity and reduce the likelihood of producing identical or highly similar offspring. Mutation introduces random alterations to genetic material, allowing these changes to be passed on to future generations. This reintroduction of genetic diversity helps the search process escape local optima and ensures the algorithm does not become trapped in local minima [45].

The mutation operator involves randomly altering parts of an individual to generate a new individual. Common mutation operators include displacement, inversion, scramble, bit flipping, and reversal. Table 3.5 summarizes their key characteristics, including the pros, cons, and typical applications of each.

Table 3.5: *Comparison of Different Mutation Techniques (Adapted from [21, 25])*

Mutation Techniques	**Pros**	**Cons**
Displacement	Local Change Maintains Structure	Limited Exploration Suboptimal Convergence
Inversion	Improved Diversity Improved Exploration	Risk of Disrupting Good Solutions
Scramble	Maintain Diversity Preserve Gene Values	Risk of disruption
Bit Flipping	Simple Easy Implementation	Poor Convergence
Reversing	Supports Local Exploration	Limited Exploration

Bit flipping is a bitwise operator frequently used in mutation techniques to increase population diversity in optimization problems. While mutating a single site may have limited effectiveness, applying mutations at multiple sites can improve the evolutionary efficiency of the algorithm. Each bit position of the newly generated chromosomes after crossover is subject to random alteration, based on a predetermined mutation probability (p_m). As a result, approximately p_m * population size (N) * length of the chromosome (L) mutations occur per generation. For binary encodings, the mutation operator flips each bit from 1 to 0 or vice versa on an individual basis, as illustrated in Figure 3.12.

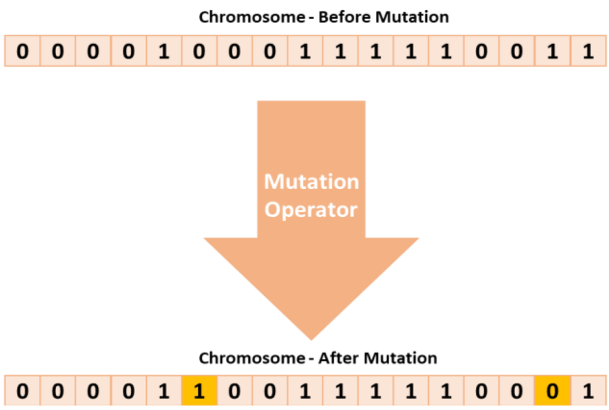

Figure 3.12: *Bitwise Mutation Operator*

Many researchers have investigated the effect of mutation probability in GAs. Grefenstette [23] concluded that mutation probabilities above 0.05 are generally detrimental to the optimal performance of GAs. Smith and Fogarty [48] demonstrated that varying mutation probabilities can significantly improve GA performance, while Hesser and Männer [49] found that the mutation probability should decrease during convergence, supporting Smith and Fogarty's findings. According to Bäck [50], the mutation rate, or the probability of altering gene properties, is typically very small and depends on chromosome length and population size, as illustrated in Equation (3.30). Consequently, chromosomes exposed to mutation are generally not significantly different from the originals.

A low mutation probability may result in the algorithm becoming trapped in local optima, whereas a high mutation probability could hinder the propagation of advantageous schemata, effectively reducing the algorithm to a random search method. Higher mutation rates tend to benefit offline performance, while lower rates are preferable for online performance. Low mutation rates result in less time spent creating the initial generation but require more generations for the GA to converge due to reduced initial diversity. Conversely, very high mutation rates may prolong the generation of new individuals without significantly enhancing convergence, as there is a limit to the beneficial diversity that mutation can introduce.

$$\frac{1}{population\ size} < p_m < \frac{1}{choromosome\ length} \tag{3.30}$$

The bitwise mutation operation applied to each bit of the chromosome follows these steps:

- Generate a random floating-point number, r, within the interval [0,1].
- If $r < p_m$, mutate the bit by flipping its value: change 0 to 1, or 1 to 0.

3.2.1.7 Fitness Evaluation in Genetic Algorithms

Fitness functions are fundamental components of GAs. In GAs, the fitness value represents the performance level of each chromosome and is subsequently used to determine their ranking. The ranking system governs the distribution of reproductive opportunities, meaning that individuals with higher fitness values have a greater probability of being selected as parents. Consequently, fitness serves as a measure of quality that the algorithm aims to maximize.

The objective function can be directly used as a fitness function, or alternative fitness functions can be formulated to compute the fitness values of individual chromosomes in the population. A fitness function evaluates and assigns a numerical score to each encoded solution, also known as a chromosome, based on its quality or performance. When maximizing a numerical function f(x) using a GA, the performance value u(x) of a chromosome x is typically defined as u(x) = f(x) or u(x) = f(x) – f(min), where f(min) represents the minimum value that f(x) can take within the specified search area. In contrast, when minimizing a numerical function f(x) using a GA, the performance value u(x) of a chromosome x is defined by u(x)=f(max)−f(x), where f(max) represents the maximum value that f(x) can take within the specified search area. f(max) must be sufficiently large to avoid negative fitness values. This approach ensures that lower values of f(x) correspond to higher fitness values in minimization problems.

As a first step, the initial population is generated, and the fitness of this population is calculated. During the selection process, chromosomes are chosen based on their fitness values for further processing to generate new populations. If f_i is the fitness measure of the i-th member, it can be assigned a probability of $f_i/(\sum_i^m f_i)$, where m is the population size. A new population pool of the same size as the original is created, with the goal of achieving a higher average fitness value. The creation of new generations and the evaluation of fitness values continue until the stopping criteria are met.

3.2.1.8 Stopping Criteria in Genetic Algorithms

GAs are terminated using predefined stopping criteria to prevent indefinite searching for an optimal solution. Once these criteria are met, the optimization process stops, and the solution sets from the last generation are accepted as optimal solutions, considering their ranking based on fitness values. To avoid non-optimal results, stopping conditions must be carefully defined, along with other GA parameters. Improper stopping conditions can lead to premature convergence, getting stuck in a local optimum, or failing to converge at all. The population size, together with the stopping criteria, significantly influences the algorithm’s runtime. A larger population requires a greater number of evaluations, leading to an increased number of function executions. Consequently, larger populations need more time to satisfy the stopping criteria and terminate the algorithm.

The algorithm continues producing successive generations until the predetermined termination criteria are met. There are various methods for determining when to terminate a GA. One common approach is to specify a fixed number of generations; after each new generation is created, the generation count is incremented, and the algorithm stops when this predefined number is reached. Another method uses convergence criteria, assessing the algorithm's progression toward a stable solution set. This is done by comparing the fitness values of the top-performing solutions in the current generation with those in the previous one. If the difference falls below a predefined relative error threshold, a counter is incremented and the next generation is produced; otherwise, the counter is reset. Convergence is assumed when the relative error between successive generations remains below the specified threshold for a defined number of generations. To apply this method, the number of top solutions to compare, the acceptable relative error, and the required number of stable generations must be specified. This approach assumes that no significantly better solutions remain to be found, thereby justifying termination of the search. Either of these stopping criteria can be used individually or in combination, with the algorithm terminating only when both conditions are satisfied.

Many researchers have studied the optimal stopping criteria for GAs. De Jong [22] established that a chromosome is considered converged when 95% of the population shares the same value, indicating that most or all chromosomes are identical or very similar at convergence. Hesser and Manner [49] demonstrated that the mutation probability should be decreased during convergence, which aligns with the findings of Fogarty [51]. Additionally, Goldberg [25] proposed that convergence can be identified by observing the diversity of the population. When the diversity drops below a certain threshold, the algorithm can be stopped to avoid unnecessary computations. More recent studies, such as those by Rudolph [52] and Michalewicz [53], have explored adaptive methods for determining stopping conditions. These methods dynamically adjust parameters like mutation rates and selection pressure based on the algorithm's performance and convergence state. Smith and Fogarty [48] also emphasized the importance of adaptive mechanisms in GAs, suggesting that adaptive mutation rates can enhance the algorithm's ability to escape local optima and achieve better overall solutions. By integrating these insights, researchers aim to develop more effective stopping criteria, balancing computational efficiency with solution quality. This ensures that GAs do not terminate prematurely, nor do they continue running indefinitely without meaningful improvements.

3.3 Application of GA in Radiator and Equipment Layout Optimization

GA is employed to optimize both the radiator configuration and the equipment layout, respectively. The optimization process involves a series of equations related to the objective function, constraint functions, fitness evaluation, boundary definitions, and solution ranking. Additionally, the GA operators—selection, crossover, and mutation—are mathematically defined and applied in each iteration to evolve the population toward better solutions. Throughout this process, multiple input and output files are read and written during each optimization cycle. To efficiently manage and automate these tasks, a set of Python scripts has been developed. This code, named the Developed Radiator Optimization Code (DROC), executes the genetic algorithm, handles file operations, and ensures seamless integration of all components within the optimization workflow.

Within the DROC, the genetic algorithm employs roulette wheel selection, two-point crossover, and bit-wise mutation, with elitism integrated to preserve the best-performing individuals across generations. The design variables for both the radiator and the equipment layout are encoded as binary strings, with examples shown in Figure 3.13 and Figure 3.14, respectively. These binary representations are decoded and used in the relevant evaluation functions during optimization. The length of each gene, the number of genes, and the overall chromosome length may vary, depending on the design variables and the corresponding design space being optimized.

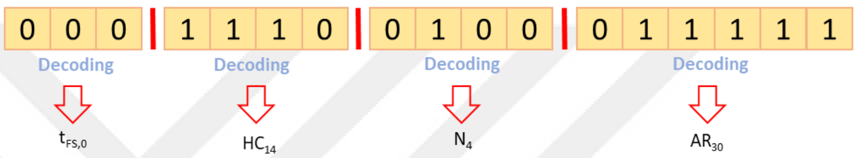

Figure 3.13: *Chromosome Representation of Radiator Design Variables*

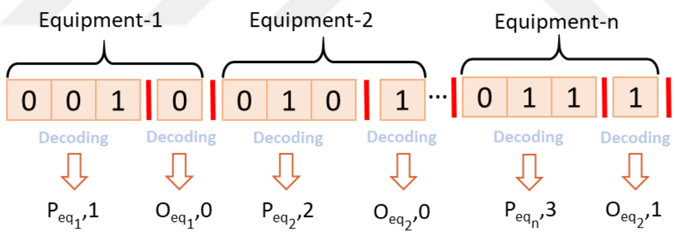

Figure 3.14: *Chromosome Representation of Equipment Layout Variables*

3.3.1 Problem Statement for Optimizing Embedded HS GEO Radiators

The application of GA to optimize embedded heat spreader GEO radiators requires a substantial number of computations. In each generation of the GA, the fin efficiency equations—which are integrated into the constraint related to the required heat rejection capacity—are solved alongside the objective function that evaluates radiator mass for fitness calculation. Additionally, it is essential to ensure that each individual in the population satisfies all specified design limits and constraints. These include geometric restrictions such as radiator dimensions to comply with launcher envelope and integration requirements, the maximum heat transport capacity of heat spreader, and the radiator's ability to reject sufficient heat to maintain equipment within its allowable temperature range.

Each individual in the population represents the solution set, which contains design variables of the radiator. In this phase of the optimization, the design variables include, the thickness of facesheet (t_{FS}), honeycomb properties, (density (ρ_{HC}), cell size (S) and ribbon thickness (δ_{HC})), quantity of heat spreader (N) and the aspect ratio of the radiator panel (AR), as illustrated in Figure 3.15. Optimization aims to achieve an efficient radiator configuration by determining the optimal combination of these design variables.

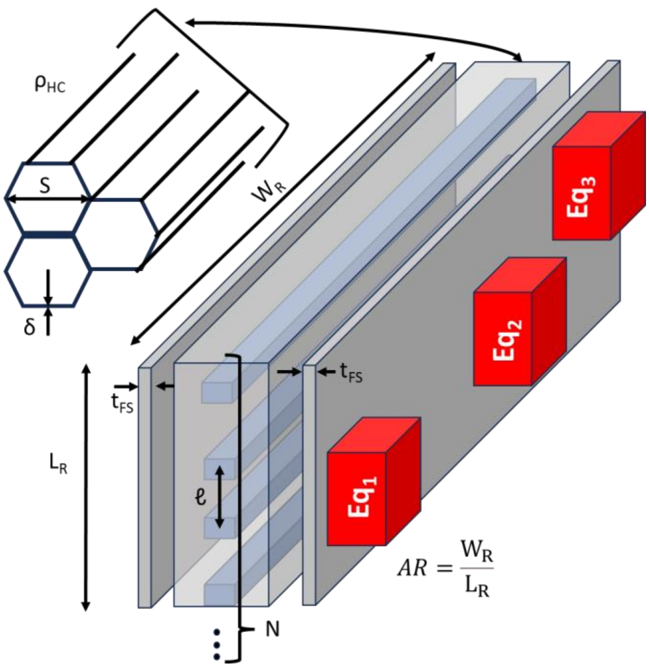

Figure 3.15: *Design Parameters of Embedded HS Radiators*

Mathematical formulation of the optimization problem for an embedded heat spreader GEO radiator, addressed using a GA, is presented below:

Find $x = (AR, S, \delta_{HC}, \rho_{HC}, N, t_{FS})$ which minimizes:

$$f_1(x) = m_{HC} + m_{Inner\ FS} + m_{Outer\ FS} + m_{HS} \tag{3.31}$$

Subject to:

$$g_1(x) = 2W_R N \varepsilon_R \sigma T_{FR}^4 \left(L_p(1-\theta^4) + \eta L_F\right) \geq q_{eq} \tag{3.32}$$

$$g_2(x) = \frac{q_{eq}}{N} \leq Transversal\ Heat\ Transfer\ Limit \tag{3.33}$$

$$g_3(x) = 0.2 \leq \lambda \leq 2.0 \tag{3.34}$$

$$W^L \leq W_R \leq W^U \tag{3.35}$$

$$L^L \leq L_R \leq L^U \tag{3.36}$$

$$t^L \leq t_{FS} \leq t^U \tag{3.37}$$

$$\eta^L \leq \eta \tag{3.38}$$

Where:

$$q_{eq} = \sum_{Eq_1}^{Eq_n} q_i \tag{3.39}$$

$$W_R = (A_R AR)^{0.5} \tag{3.40}$$

$$L_R = \left(\frac{A_R}{AR}\right)^{0.5} \tag{3.41}$$

$$L_F = \left(\frac{\left(\frac{A_R}{AR}\right)^{0.5}}{N} - 2L_p \right) \Big/ 2 \quad (3.42)$$

$$\lambda = \frac{\sigma \varepsilon T_{FR}^3 L_F^2}{k_F t_F} \quad (3.43)$$

$$if \quad 0.01 \le \lambda \le 0.2\,; \quad \eta = (1 - 1.25\lambda + 1.6\lambda^2)(1 - \theta^4) \quad (3.44)$$

$$else \quad 0.2 \le \lambda \le 2.0; \quad \eta = (0.5321 - 0.4049 \times \log_{10} \lambda)(1 - \theta^4) \quad (3.45)$$

$$k_F t_F = k_{FS} t_{FS} + \left(\frac{k_{HC} \delta_{HC}}{\mathrm{S}} \right) (t_{HC}/2) \quad (3.46)$$

$$\theta^4 = \frac{T_s^4}{T_{FR}^4} \quad (3.47)$$

$$T_s^4 = \frac{\alpha_s \cancel{S} \sin \theta_s}{\sigma \varepsilon_R} \quad (3.48)$$

$$T_{Inner\ FS_i} = T_{Limit_i} - \frac{q_i}{L_i W_i H_{TF_i}} \quad (3.49)$$

$$\min\left(T_{Inner\ FS_i}, \dots, T_{Inner\ FS_n}\right) = T_{Inner\ FS} \quad (3.50)$$

$$T_{FR} = T_{Inner\ FS} - \left(\Omega \, \frac{q_{eq}}{N} \right) \quad (3.51)$$

$$\mathrm{m}_{Inner\ FS} + m_{Outer\ FS} = 2 t_{FS} A_R \rho_{FS} \quad (3.52)$$

$$m_{HP} = N(A_R AR)^{0.5} \dot{m}_{HP} + W_R L_{flange} t_{flange}\, \rho_{HP} \quad (3.53)$$

$$m_{HC} = t_{HC}\left(A_R - (2NL_P)\right)\rho_{HC} \quad (3.54)$$

The parameters selected for optimizing the radiator are represented by x. These parameters are chosen from a defined subset of continuous and discrete values. In the above formulations, $f(x)$ denotes the objective function that calculates the total mass of the radiator, accounting for the masses of inner ($m_{Inner\ FS}$) and outer ($m_{Outer\ FS}$) facesheets, honeycomb (m_{HC}) and heat spreaders (m_{Hs}).

The purpose of the constraint function $g_1(x)$ is to ensure that the radiator maintains equipment temperatures within their design limits by providing adequate heat rejection. This constraint calculates the heat rejection capacity of the radiator by incorporating fin efficiency into the analysis. The value of $g_1(x)$ is intended to represent the total heat load of the equipment. However, in equations used to calculate fin effectiveness, the radiator temperature is estimated based on certain assumptions. When this constraint is satisfied, the value of $g_1(x)$ is expected to be equal to or slightly greater than the actual total heat load.

The purpose of constraint function $g_2(x)$ is to ensure that the transversal heat transfer limit complies with the specified heat transfer limit for each heat spreader. Additionally, this constraint is intended to account for the heat transfer capability limits of embedded thermal hardware, such as phase change materials and heat pipes, in radiator designs considered in future studies.

The purpose of the constraint function $g_3(x)$ is to ensure that the conductance parameter (λ) used in the fin efficiency calculations remains within the valid correlation range, thereby guaranteeing the accurate application of the corresponding fin efficiency equations.

The parameters of the radiator are constrained by lower (x^L) and upper (x^U) bounds. These constraints may arise from various considerations, including manufacturing feasibility, launcher size limitations, and structural requirements. For example, dimensional constraints can be imposed on the radiator's width (W_R) and length (L_R). Structural constraints related to stiffness can be associated with the thickness of the facesheet (t_{FS}). Additionally, a target fin efficiency (η^L) may be specified as a design requirement. Therefore, in addition to satisfying the constraint functions, all parameter values must remain within these defined bounds.

In conclusion, the GA is designed to minimize the objective function, mass of the radiator, while ensuring that the specified constraint functions and boundary limits are satisfied.

3.3.2 Problem Statement for Optimizing Equipment Layout

The application of GA to optimize the equipment layout on the radiator requires a significant amount of computation. In each generation, the GA evaluates candidate solutions using equations that ensure dimensional compatibility between the equipment and the radiator. These equations, along with the objective function—which assesses heat spreading and promotes uniform heat distribution across the radiator surface—are incorporated into the fitness evaluation. Furthermore, constraints are applied to limit the maximum heat transfer through the heat spreaders and to ensure that the equipment remains within the radiator area without overlapping.

Each individual in the population represents a candidate solution, consisting of the design variables associated with the equipment layout. In this phase of the optimization, the design variables include the orientation of each equipment item (O_{eq_i}), indicating whether the equipment is placed vertically or horizontally, and the position of each equipment item (P_{eq_i}), which specifies the index of the first heat spreader it contacts. These design variables are illustrated in Figure 3.16. The optimization aims to achieve uniform heat dissipation along the radiator surface and prevent localized hot spots by identifying the optimal combination of orientation and position for each equipment.

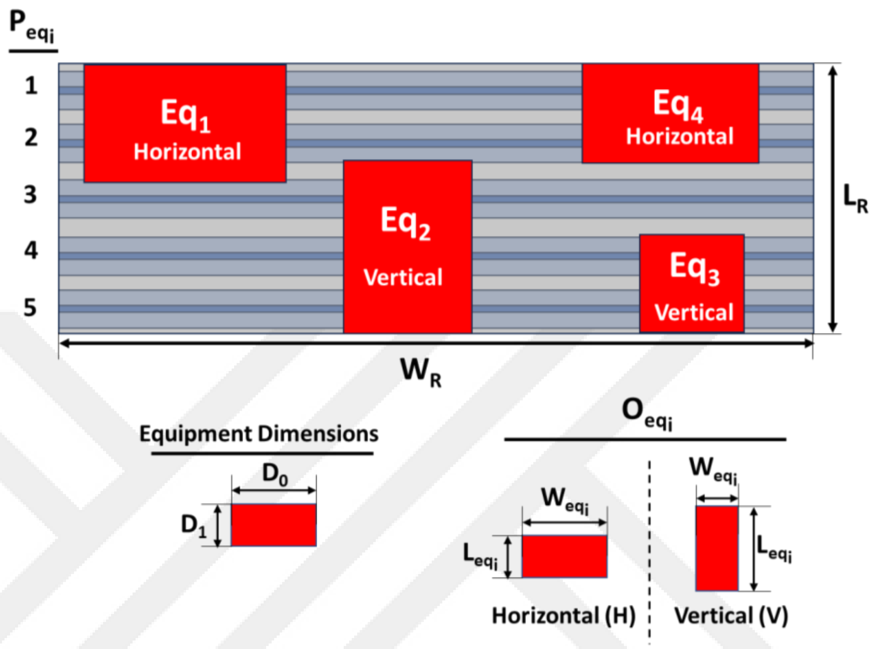

Figure 3.16: *Design Variables of Equipment Layout*

The equipment layout, comprising n pieces of equipment, for optimization using a GA, can be mathematically expressed as follows:

Find $x = (P_{eq_1}, O_{eq_1}, P_{eq_2}, O_{eq_2} \dots P_{eq_n}, O_{eq_n})$ which minimizes:

$$f_2(x) = \sqrt{\frac{1}{N}\sum_{i=1}^{N}(q_{HS_i} - \bar{q})^2} \tag{3.55}$$

Subject to the following conditions for n pieces of equipment:

$$W_R \geq W_{eq_i} \tag{3.56}$$

$$L_R \geq L_{eq_i} \tag{3.57}$$

$$If\ \{Eq_i, Eq_j, \dots, Eq_k\} \cap HS_m, \qquad m = 1,2,\dots,N \qquad :$$

$$g_4(x) = W_R \geq (W_{eq_i} + W_{eq_j} + \dots + W_{eq_k}), \quad i,j,..,k \in \{1,2,\dots,n\} \tag{3.58}$$

$$g_5(x) = L_{eq_i} \leq L_R - (N - P_{eq_i} + 1)\ell, \qquad \mathrm{i} = 1,2,\dots,\mathrm{n} \tag{3.59}$$

$$g_6(x) = \emptyset_{HS_m}^{eq_i} \frac{q_{eq_i}}{N_{eq_i}} + \emptyset_{HS_m}^{eq_j} \frac{q_{eq_j}}{N_{eq_j}} + \dots + \emptyset_{HS_m}^{eq_k} \frac{q_{eq_k}}{N_{eq_k}} \leq HTCL_{HS} \tag{3.60}$$

Where:

$$(W_{eq_i}, L_{eq_i}) = \begin{cases} (D_0, D_1), & O_{eq_i} = H \\ (D_1, D_0), & O_{eq_i} = V \end{cases} \tag{3.61}$$

$$\bar{q} = \frac{1}{N}\sum_{i=1}^{N} q_{HS_i} \tag{3.62}$$

The parameters selected for optimizing the equipment layout are represented by x. These are chosen from a defined feasible subset of discrete values. In the above formulations, $f_2(x)$ denotes the objective function that calculates the standard deviation (Std Dev) of the heat loads on the heat spreaders.

The dimensions of the equipment must fit within the available area of the radiator. To ensure proper fit, the length of the equipment (L_{eq_i}) is compared with the length of the radiator (L_R), while the width of the equipment (W_{eq_i}) is compared with the width of the radiator (W_R). The equipment length and width are defined based on its orientation on the radiator, either vertical or horizontal.

The purpose of the constraint function $g_4(x)$ is to ensure that no equipment overlaps within the radiator layout. To enforce this, equipment located on the same heat spreader is grouped together, and the widths of this equipment are summed. The total width is then checked to ensure it does not exceed the width of the radiator, thereby preventing any overlap in the layout. Additionally, during this calculation, 'stay-away' zones—resulting from harnesses and mounting requirements—are incorporated into the dimensions of the relevant equipment to account for these additional constraints.

The purpose of the constraint function $g_5(x)$ is to ensure that the vertical length of any equipment remains within the radiator area after it is positioned on a heat spreader. To evaluate this, the equipment position (P_{eq_i}), which indicates the index of the first heat spreader with which the equipment is in contact, is used. This index is subtracted from the total number of heat spreaders to determine the number of heat spreaders available in the vertical direction after placement. The result is then multiplied by the specific portion length, ℓ, (which accounts for the combined width of two fins and one heat spreader) to calculate the remaining vertical space. The vertical length of the equipment must not exceed this available length to satisfy the constraint.

The purpose of the constraint function $g_6(x)$ is to ensure that the heat spreaders can efficiently transfer the heat loads from the equipment while complying with the specified transverse heat transfer limits. The heat load of each equipment item is distributed among the heat spreaders it contacts, based on the number of heat spreaders it overlaps, $\emptyset_{HS_m}^{eq_i}$. For each heat spreaders, the total heat load is calculated by summing the contributions from all associated equipment. This total must not exceed the maximum heat transfer limit of the heat spreader to satisfy the constraint.

In conclusion, the GA is designed to minimize the objective function, the standard deviation of the heat loads on the heat spreaders, while ensuring that the specified constraint functions and boundary limits are satisfied.

3.3.3 Workflow of the Developed Radiator Optimization Code

DROC includes a series of iterative processes to attain the optimal solution. The initial phase of optimization aims to identify a lightweight radiator layout with sufficient heat rejection capacity. Upon completion of this phase, the radiator design parameters are selected from the viable candidate solution sets generated. These radiator parameters are then used as inputs for the subsequent optimization phase. In this next phase, the objective is to determine an equipment layout that achieves maximal uniformity in heat dissipation across the radiator surface. DROC continues performing optimizations in sequence until the stopping criteria are met for each phase.

Throughout each phase, GA operators are employed to generate subsequent generations. Before introducing new individuals into the population, their compliance with all constraints is evaluated. Only those that satisfy all constraints are incorporated into the population. As a result, DROC comprises numerous steps, and its flowchart is illustrated in Figure 3.17.

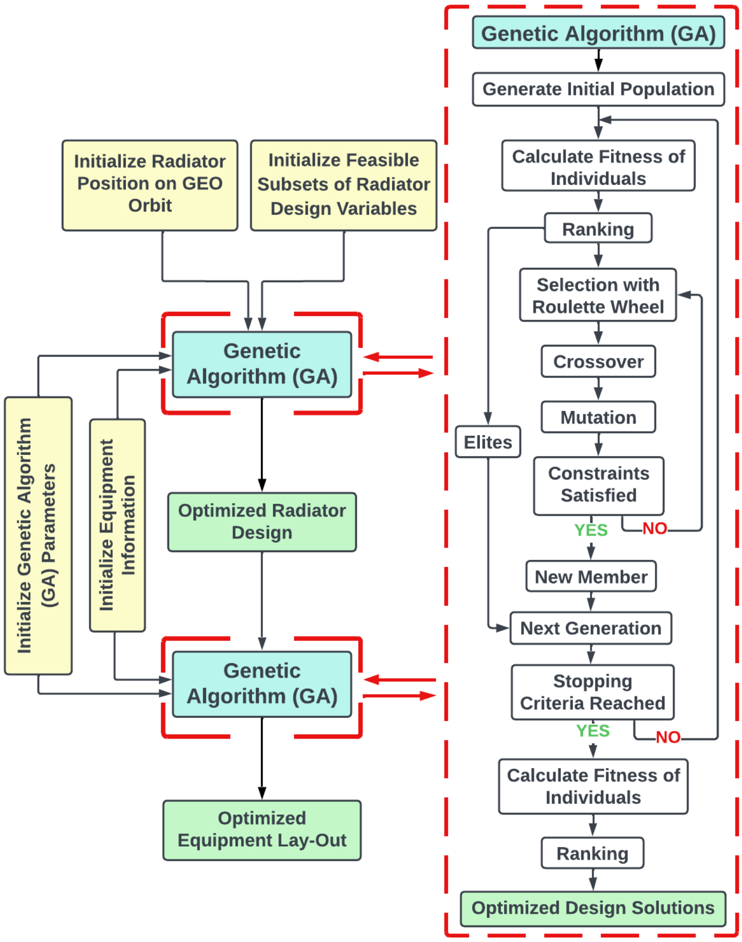

Figure 3.17: *Flowchart of the Developed Radiator Optimization Code*

To initiate DROC, input parameters must first be defined. One of the key inputs is the subset of the radiator's design variables, which includes the thickness of the facesheets, the type of honeycomb core structure, the number of heat spreaders, and the aspect ratio of the radiator panel. Another essential input to DROC is the selection of various sets of GA parameters, such as crossover probability, mutation probability, population size, and stopping criteria.

The stopping mechanism is based on two conditions. The first requires the algorithm to run for a minimum number of iterations before termination is permitted. The second condition monitors convergence by analyzing the average fitness of a defined number of top-performing chromosomes across successive generations. If the relative difference between these averages falls below a predefined threshold over a specified number of generations, it indicates that further improvement is unlikely, and the optimization process is terminated. Employing multiple sets of GA parameters helps mitigate the risk of poor search performance that may result from relying on a single parameter configuration.

In addition to these inputs, equipment-related data serve as a primary driver in the design of both the radiator and the equipment layout. Equipment data include the baseplate area, heat dissipation rate, maximum allowable temperature, radiator orientation, and the thermal conductance between the radiator and each equipment item. Based on this information, the required radiator size and expected facesheet temperatures are determined.

Lastly, material properties, key assumptions, and design constraints—such as geometric limitations of the radiator and the maximum heat transfer capacity of the heat spreaders—are specified prior to executing DROC. The inputs and outputs of DROC are depicted in Figure 3.18.

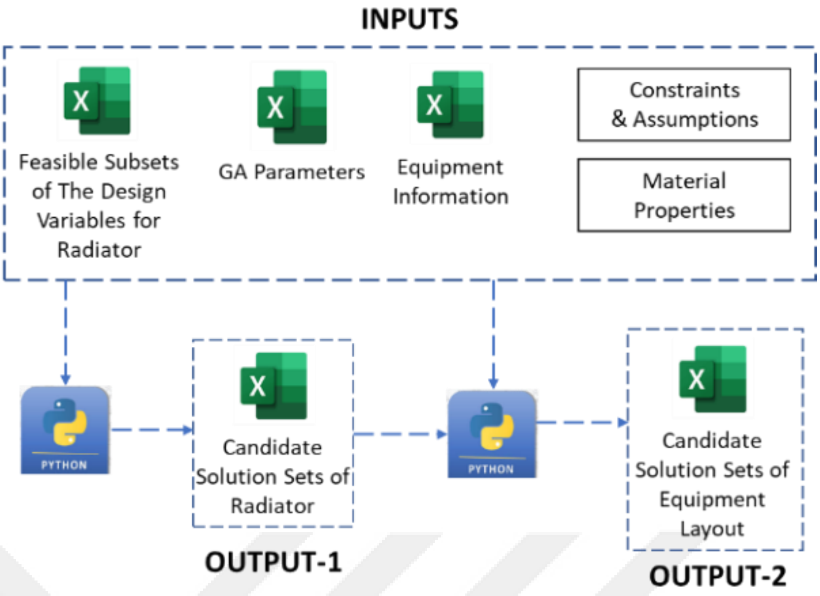

Figure 3.18: *Inputs and Outputs of the Developed Radiator Optimization Code*

Design variables are represented using a binary system and arranged in a specific sequence to form chromosomes. This encoding facilitates the application of GA operators to the chromosomes. After GA operations, the chromosomes are decoded to retrieve the original design variables, which are then used in the relevant equations.

At the beginning of the GA, an initial population is generated randomly according to the defined population size. Subsequently, the GA operations—selection, crossover, and mutation—are executed iteratively to produce new generations and guide the population toward the optimal range until the specified stopping criteria are met. The selection process utilizes the roulette wheel approach, while the two-point crossover method is employed. Elitism is implemented by selecting a specified number of the highest-performing chromosomes to be directly passed on to the next generation without any modifications. The remaining portion of the population is composed of newly generated chromosomes produced by the GA operators.

To obtain the final set of potential solutions for the radiator, the GA must terminate according to predefined stopping criteria. These criteria are essential, as they directly influence both computational time and the quality of the radiator configurations. The stopping criteria in this study consist of a predefined maximum number of iterations and a convergence criterion that evaluates the performance of two consecutive generations.

As the final step of radiator optimization in DROC, the last generation is exported in Microsoft Excel format. This file contains candidate solution sets for the radiator configuration, sorted by fitness value, which in this study is based on weight. Consequently, the top candidate in the list corresponds to the configuration with the lowest weight. An example of the DROC output is presented in Table 3.6.

Table 3.6: *Example of Sorted Candidate Solution Sets Based on Mass*

Chromosome	**t_{FS} (mm)**	**S (mm)**	**δ (μm)**	**ρ_{HC} $\left(\frac{kg}{m^3}\right)$**	**N**	**AR**	**m_R (kg)**
01000000100101011000	0.305	3.8	21.1	35	5	5.4	12.48
10000000100100101010	0.508	3.8	21.1	35	5	4.8	13.61
10100000100100001011	0.635	3.8	21.1	35	5	4.4	14.48
00100000100111000100	0.254	3.8	21.1	35	5	6.7	14.74
00000010100110000101	0.203	3.8	30.2	51	5	5.9	15.25
01100000101101100010	0.406	3.8	21.1	35	6	5.5	15.26
10001010101101010010	0.508	4.5	28.6	48	6	5.3	16.16
00111010100110010010	0.254	5.2	82.6	111	5	6.1	16.46
00011100111100000000	0.203	6.1	36.3	61	8	4.3	16.49
10111110100100011100	0.635	6.1	48.4	76	5	4.6	16.94
01101000110110001001	0.406	4.5	20.0	33	7	6.0	17.09
00101100101101001101	0.254	4.5	42.9	67	6	5.2	17.25
10111000100011110100	0.635	5.2	68.8	94	5	4.1	17.29
11100010100101101010	1.016	3.8	30.2	51	5	5.6	17.56
⋮	⋮	⋮	⋮	⋮	⋮	⋮	⋮
11110000111011101111	1.016	4.5	71.4	107	8	4.0	26.45

After selecting the optimal configuration for the embedded heat spreader radiator from the first output file, a second output file is generated. This file contains candidate solution sets, with each set specifying the design parameters for equipment layout based on the selected radiator configuration. Examples of these groups of alternative solutions, as illustrated in Table 3.7, provide the designer with options for selecting the final design.

Table 3.7: *Sorted Candidate Equipment Layouts by HS Heat Load Std. Dev.*

Chromosome	Eq_1		Eq_2		Eq_3		Eq_4		Std Dev (W)
	P	O	P	O	P	O	P	O	
00111001000000101101	4	1	3	0	1	1	7	1	31.11
00000010010101101101	1	0	5	1	6	1	7	1	31.64
00000010010101101100	1	0	5	1	6	1	7	0	31.64
00000001000101101101	1	0	3	0	6	1	7	1	34.09
01001001000000100001	5	1	3	0	1	1	1	1	34.23
00111001000000001101	4	1	3	0	1	0	7	1	34.88
00111001000000100001	4	1	3	0	1	1	1	1	34.95
⋮	⋮	⋮	⋮	⋮	⋮	⋮	⋮	⋮	⋮
00000001000000000000	1	0	3	0	1	0	1	0	95.46

GA performance in DROC is highly dependent on its parameters, such as population size, crossover rate, mutation rate, generation gap, selection strategy, and convergence criteria. It is important to properly define these parameters before the optimization process begins. Fine-tuning these parameters through multiple trials and result comparisons is essential for optimizing the GA. This process aims to achieve the best possible outcomes by balancing solution quality, convergence speed, and computational efficiency, ultimately leading to the identification of optimal candidate solutions.

4. RESULTS AND DISCUSSION

4.1 Finite Element-Based Thermal Modelling

Simcenter Space Systems Thermal (Release Name:2021.2, Version:1996), a thermal analysis software based on the FEM, is utilized for the thermal modeling and verification of the case studies. Integrated with the NX CAD platform, the software enables a streamlined and efficient transition between geometric modeling, meshing, and thermal analysis. It supports detailed thermal modeling features, including conduction, radiation (using both view factor and ray-tracing methods), and internal or external heating sources such as orbital environment effects, making it well-suited for spacecraft thermal simulations. In this study, thermal analysis is performed under steady-state conditions.

4.1.1 Geometric Modelling

The design solution obtained from the GA is used for geometric modeling. Dimensions and equipment layout are arranged according to this solution. All components of the radiator—including facesheets, heat spreaders, and equipment—are generated individually in NX, as shown in Figure 4.1.

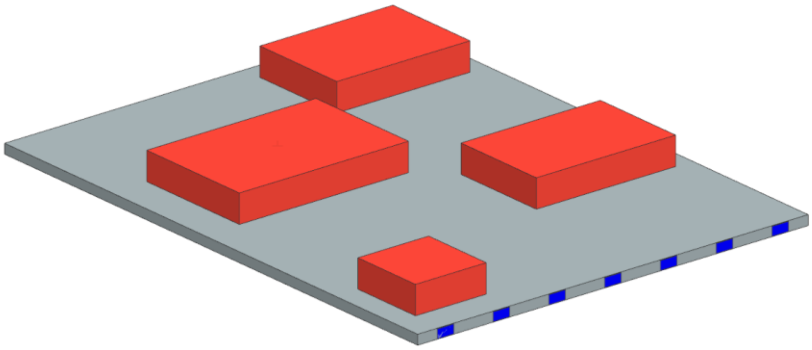

Figure 4.1: *Geometric Model of Radiator and Equipment*

4.1.2 Meshing

The geometric models of the radiator components and equipment are meshed individually. While the baseplate of the equipment is modeled using a single finite element, the other components are discretized with multiple elements. Since the geometries are not complex, 2D QUAD4 thin shell elements are used for mesh generation, as illustrated in Figure 4.2. This element type is well-suited for thin-walled structures and provides an efficient balance between accuracy and computational cost.

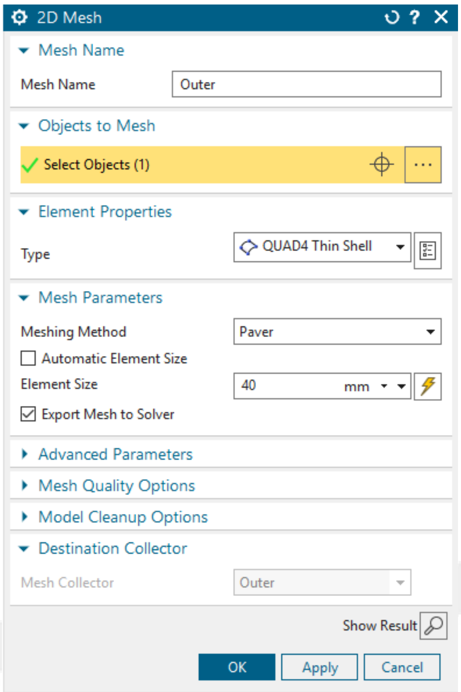

Figure 4.2: *2D Mesh Creation*

The assembly-level finite element model is illustrated in Figure 4.3.

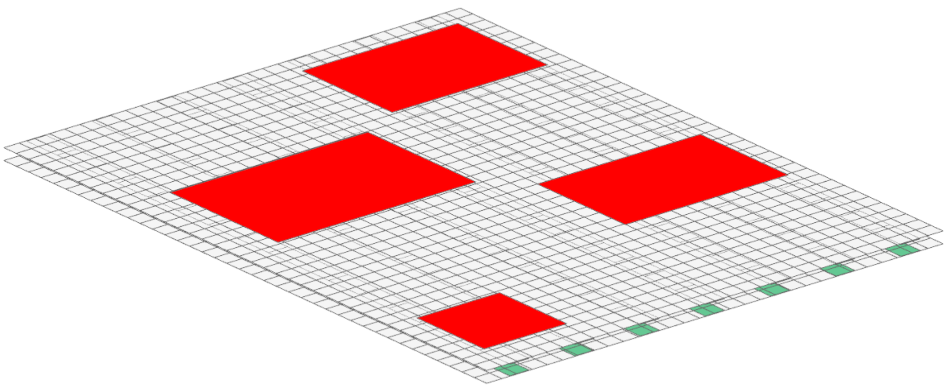

Figure 4.3: *Assembly-Level Finite Element Model of Radiator and Equipment*

Sub-level finite element model is illustrated in Figure 4.4.

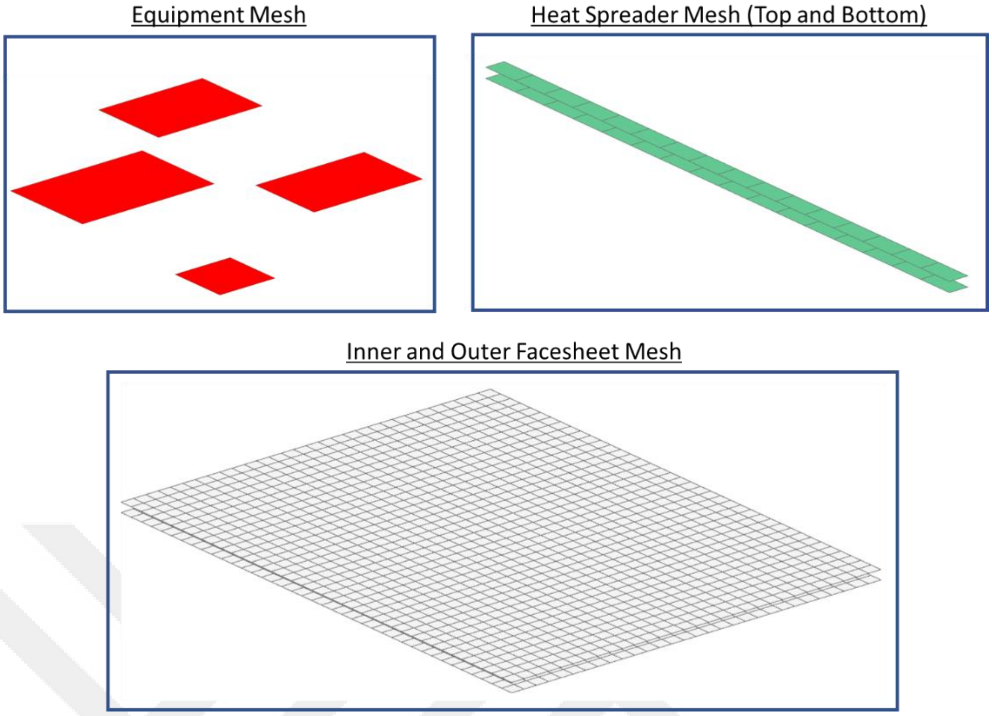

Figure 4.4: *Sub-Level Finite Element Model of Radiator and Equipment*

The mesh collector assigned to the 2D elements specifies the element type and includes the necessary thermal and physical properties for analysis, as illustrated in Figure 4.5. These properties include the material definition, which provides thermal conductivity; the element thickness, which defines the physical dimension; and the thermo-optical characteristics, such as the solar absorptivity and infrared emissivity of the element surfaces.

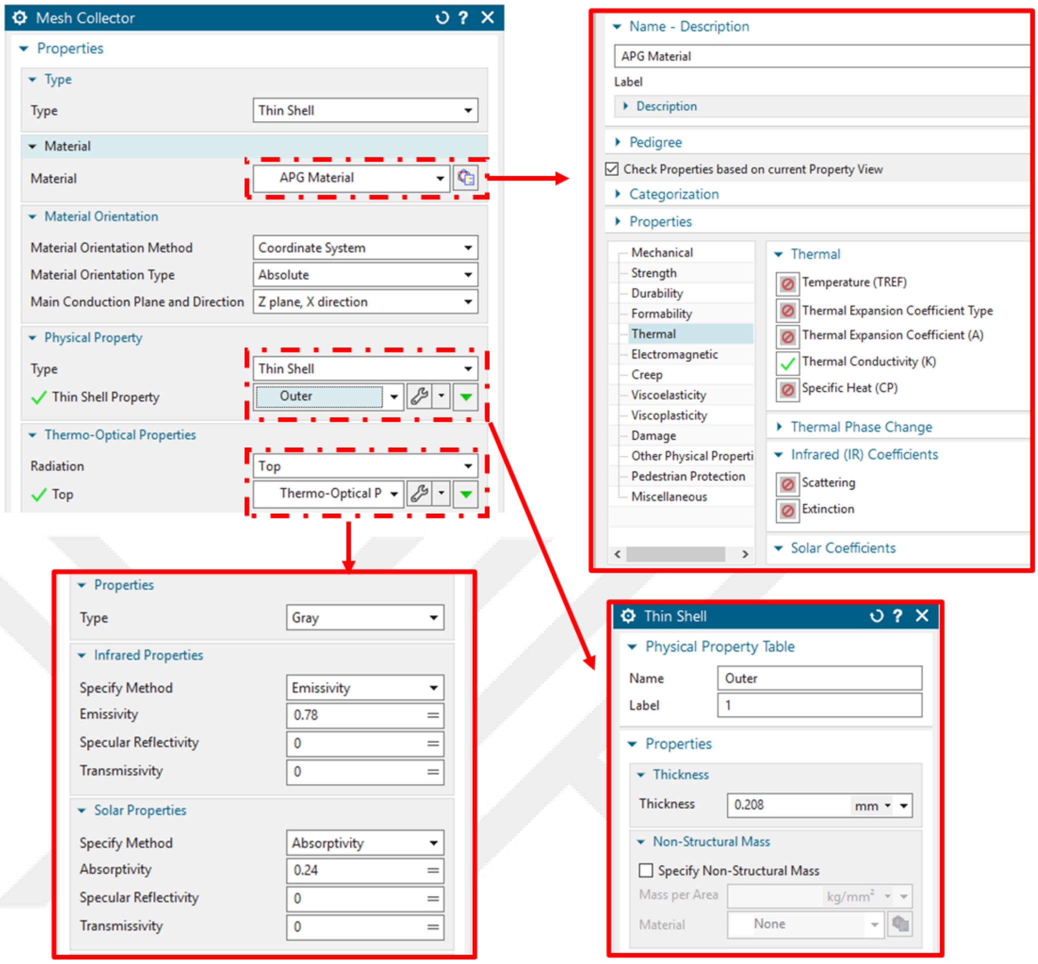

Figure 4.5: *Mesh Collector Information*

4.1.3 Thermal Analysis

Following the completion of the geometric modeling, meshing, and assignment of physical and thermo-optical properties, the thermal simulation setup is performed. In this stage, thermal couplings between elements, orbital heat fluxes (e.g., solar heating), external radiation conditions, and internal heat loads from onboard equipment are defined within the simulation environment, as illustrated in Figure 4.6. Additionally, solution parameters are configured, including the ambient temperature of the radiator environment and the analysis type. For the case studies presented in this work, a steady-state thermal analysis is performed, as shown in Figure 4.7.

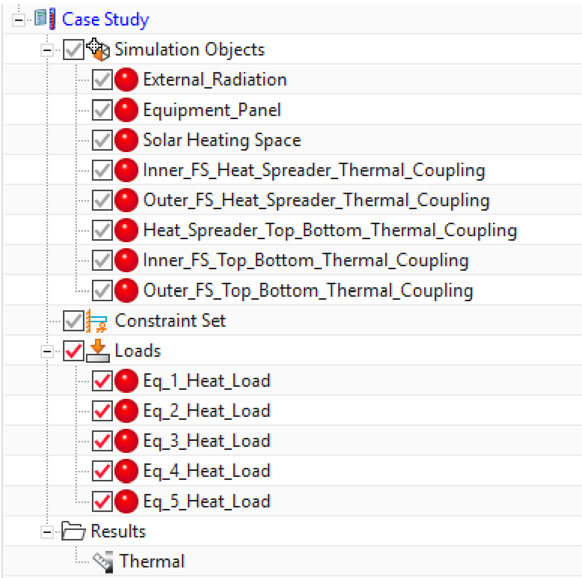

Figure 4.6: *Simulation Objects and Thermal Loads*

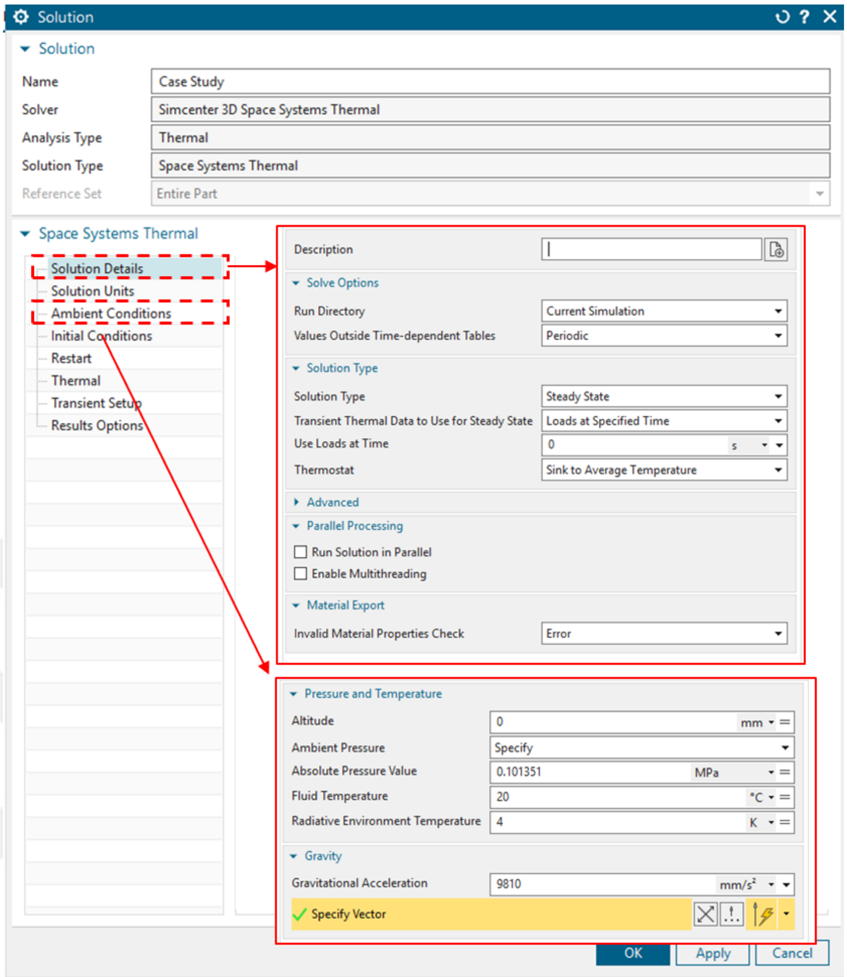

Figure 4.7: *Solution Parameters*

As illustrated in Figure 4.8, radiation coupling is established by selecting the outer facesheet— the surface exposed to space— for radiative exchange analysis. The Monte Carlo method is used to calculate the view factors, and the associated parameters are also detailed in Figure 4.8.

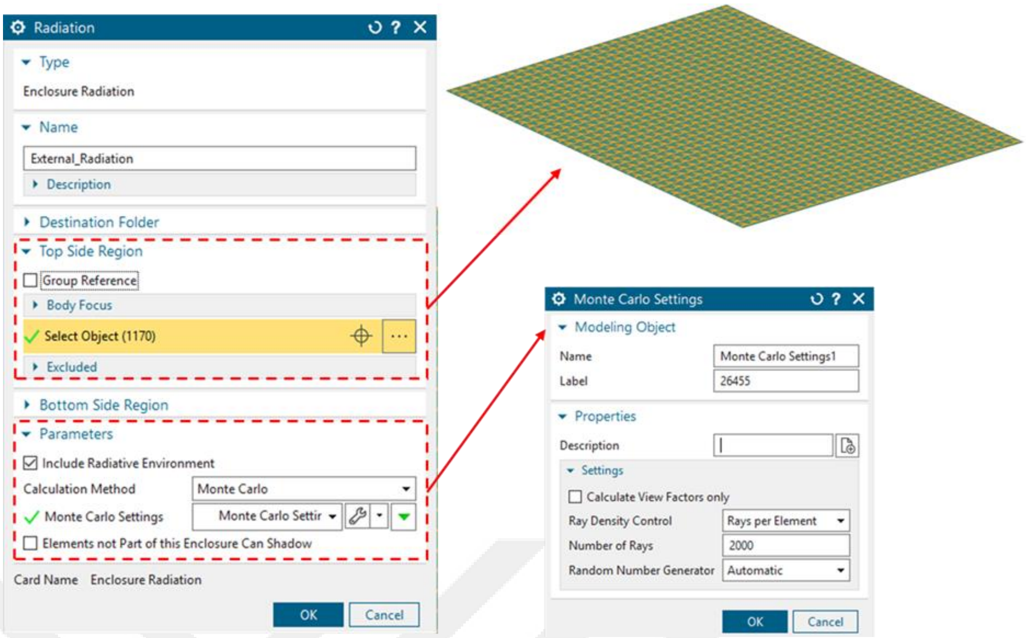

Figure 4.8: *Radiation Definition*

As illustrated in Figure 4.9, thermal coupling between the equipment and the inner facesheet is defined within the simulation. The magnitude of this coupling is determined by the thermal conductivity of the filler material situated between the equipment and the inner facesheet.

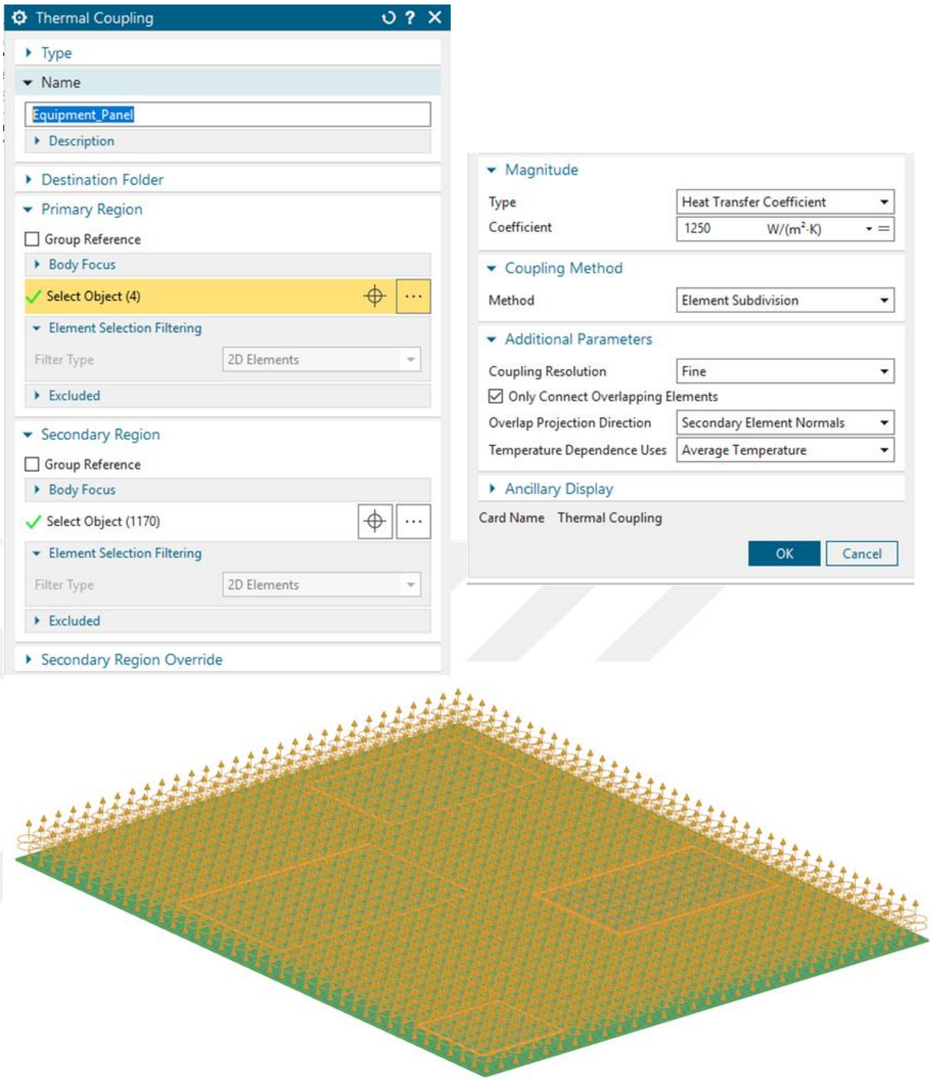

Figure 4.9: *Thermal Coupling Between Equipment and Inner FS*

As illustrated in Figure 4.10, the solar heating environment is defined by selecting the outer facesheet elements exposed to deep space. The model orientation and solar flux parameters—which depend on the time of year and local solar time—are specified accordingly.

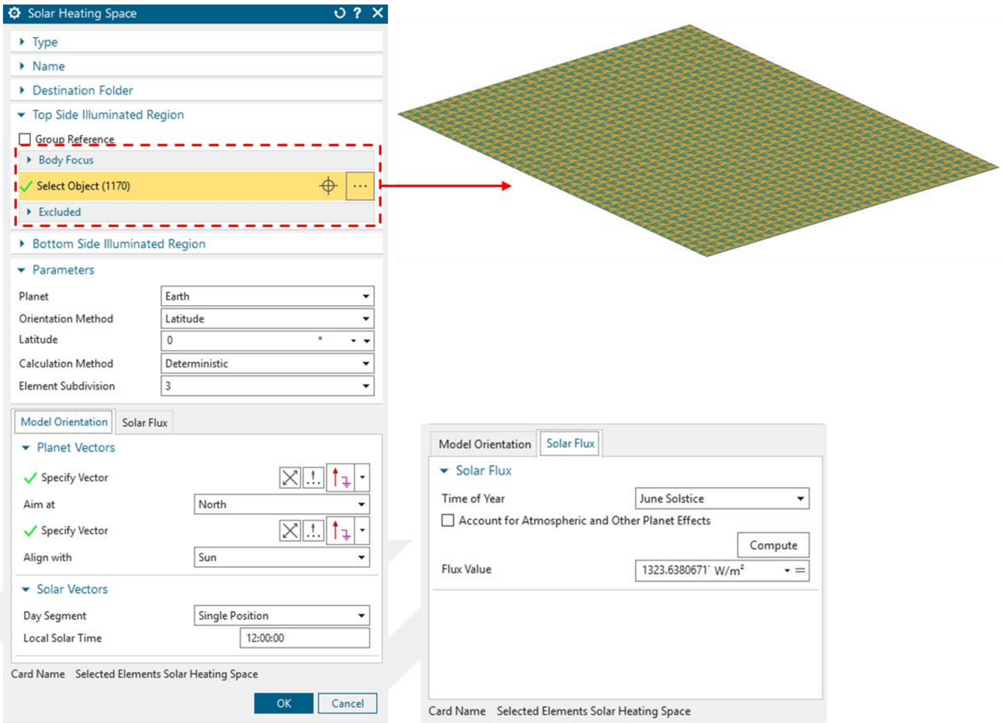

Figure 4.10: *Solar Heating Space Definition*

As illustrated in Figure 4.11, thermal coupling between the inner facesheet elements and the heat spreader is defined. The coupling parameters are applied exclusively to the overlapping elements to ensure accurate thermal interactions.

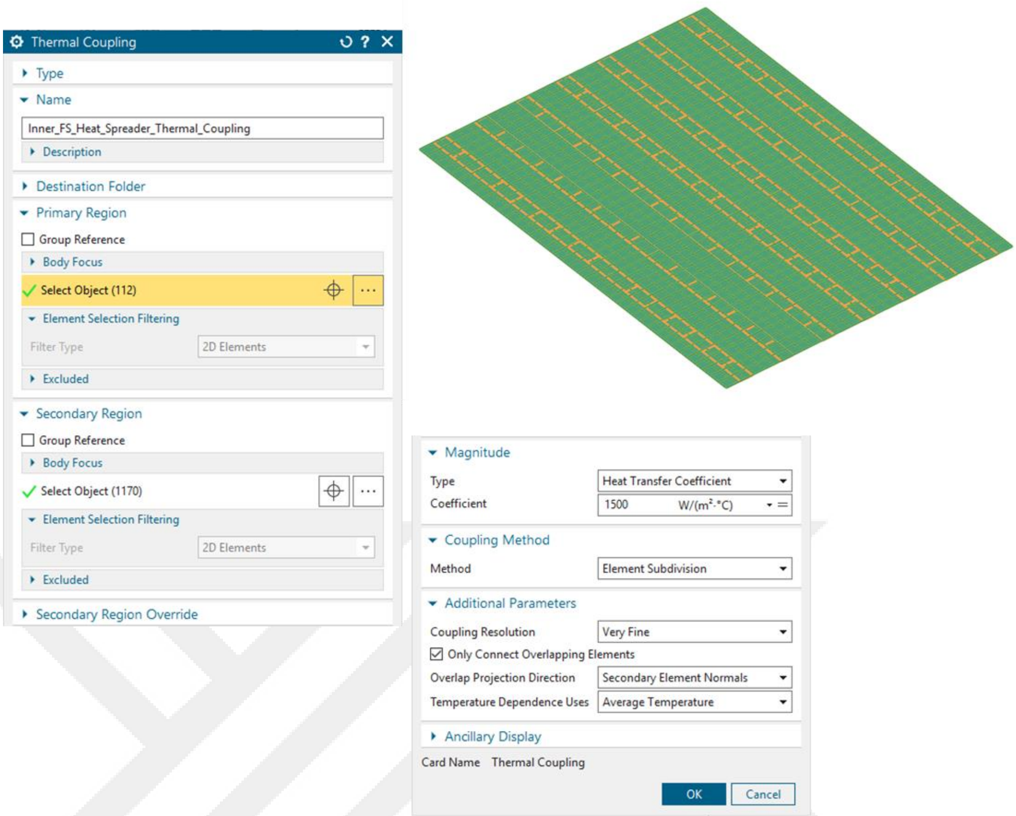

Figure 4.11: *Thermal Coupling Between Inner FS and HS Top*

As illustrated in Figure 4.12, thermal coupling between the outer facesheet elements and the heat spreader is defined. The coupling parameters are applied exclusively to the overlapping elements to ensure accurate thermal interactions.

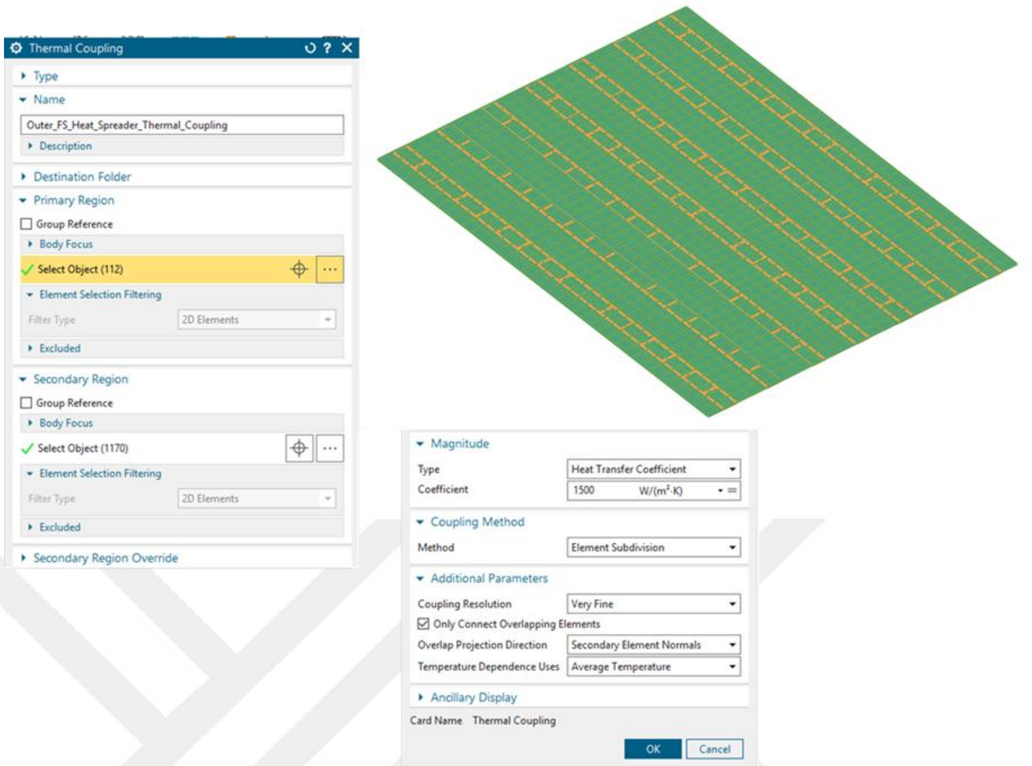

Figure 4.12: *Thermal Coupling Between Outer FS and HS Bottom*

As illustrated in Figure 4.13, thermal coupling between the top and bottom surfaces of the heat spreader is defined based on the material's thermal conductivity. Similarly, the thermal coupling between the top and bottom surfaces of the inner and outer facesheets is defined by the material’s cross-plane thermal conductivity.

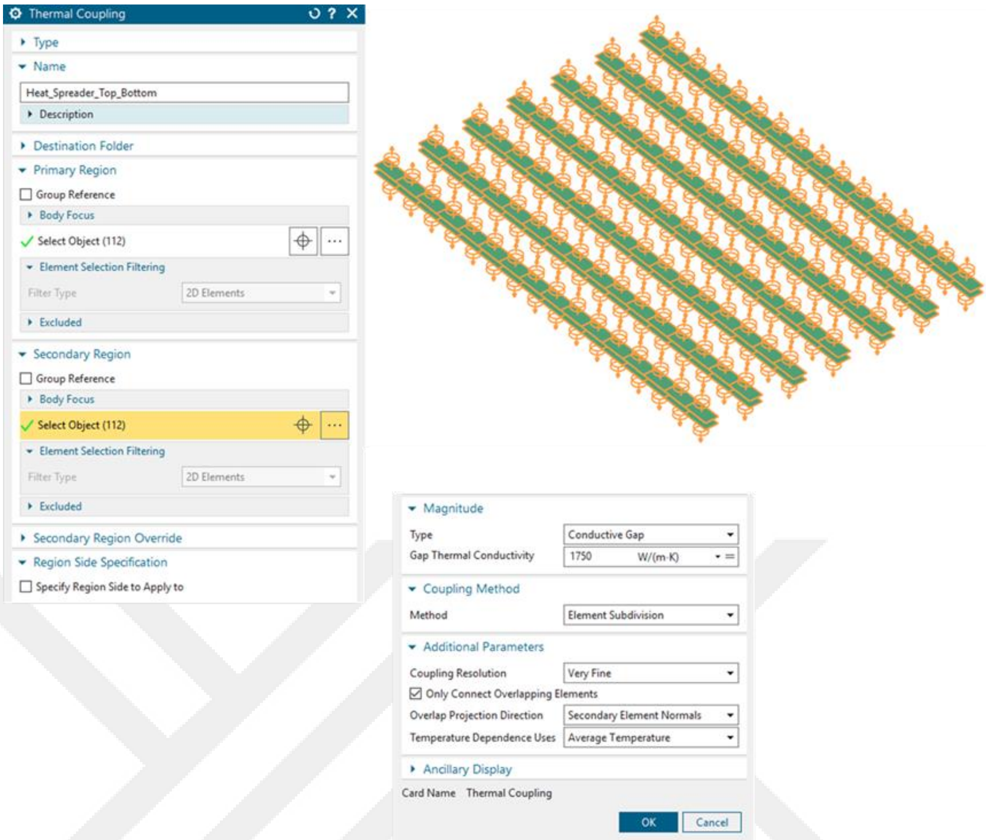

Figure 4.13: *Thermal Coupling Between Top and Bottom of HS*

Finally, the heat load for each equipment component is defined individually, as illustrated in Figure 4.14.

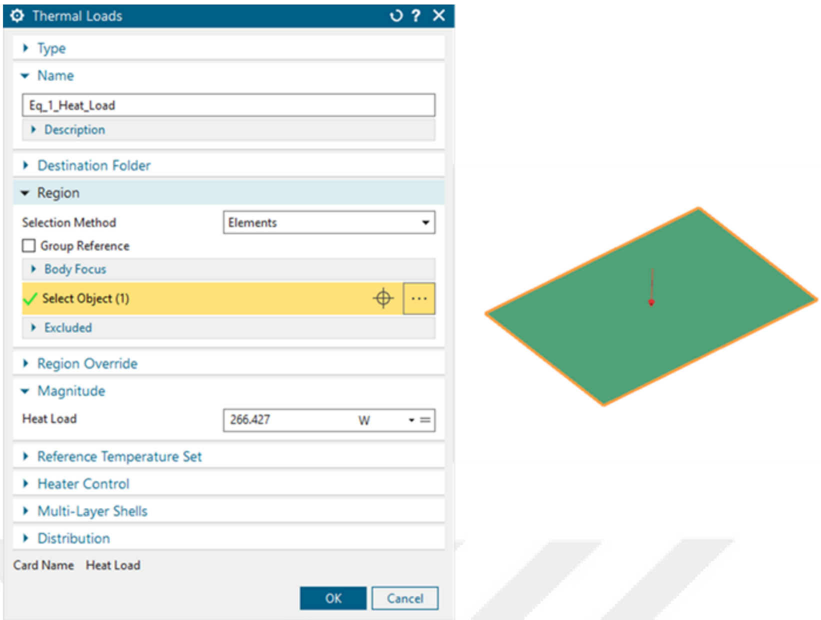

Figure 4.14: *Heat Load Definition for Equipment*

4.2 Case Study Analysis

To evaluate and demonstrate the performance of the proposed approach, two case studies are presented to illustrate the effectiveness of DROC. These scenarios involve different equipment input parameters and constraints. In the first case, DROC is tested with a smaller number of equipment items. In the second case, a larger number of equipment items is provided as input to DROC.

4.2.1 Case Study-1

4.2.1.1 Problem Statement for Case Study-1

In the preliminary design phase of the GEO spacecraft, four distinct equipment is intended to be placed on the north radiator panel. The input information for the equipment configuration is provided in Table 4.1.

Table 4.1: *Equipment Information for Case Study-1*

	Heat Dissipation (W)	Baseplate Area (m^2)	Maximum Design Temperature Limit (°C)
Eq_1	266.43	0.18	50
Eq_2	34.65	0.12	45
Eq_3	221.94	0.12	45
Eq_4	28.71	0.05	55

The selected coating for the space exposed surface of the radiator is the optical solar reflector (OSR). At the end of life, the thermo-optical property of the OSR is 0.24 for solar absorptivity (α_S) and 0.78 for infrared emissivity (ε). Table 4.2 summarizes the thermal conductivity and density values of the materials selected for the facesheets and heat spreader—both made of annealed pyrolytic graphite (APG)—and the honeycomb core, which is made of AL5056. Due to the anisotropic nature of APG, the orientation of its graphene layers differs between the facesheet and the heat spreader. The high-conductivity axis (1750 W/mK) lies along the plane of the facesheet but through the thickness in the heat spreader, as their graphene layer orientations are perpendicular to each other, resulting in interchanged in-plane and cross-plane directions.

Table 4.2: *Material Properties Used in Case Study*

Material	In-Plane Thermal Conductivity (W/mK)	Cross-Plane Thermal Conductivity (W/mK)	Density (kg/m^3)
APG	1750	10	2200
AL5056	116	116	2700

The heat transfer coefficient between the heat spreader and the facesheet, including the adhesive, is 1500 W/m²K. A thermal filler is applied between the equipment and the inner facesheet, with a heat transfer coefficient of 1250 W/m²K. The thickness of inner facesheet is 10 mm. The distance between the inner and the outer facesheets is 15.4 mm, which can be considered as the thickness of the honeycomb and heat spreader. The width of the heat spreader ($2L_p$) is 50 mm.

The radiator design is limited to a maximum width of 3600 mm and a maximum length of 1200 mm. These constraints ensure compatibility with the launcher's envelope and enable effective integration with other spacecraft components and accommodated equipment dimensions. Additionally, the radiator's heat rejection capacity must align with the required waste heat rejection to maintain equipment temperatures within design limits. It is also required that the transverse heat dissipation through each heat spreader remains below 90 W.

The design space for the variables associated with the radiator components is given in Table 4.3. A maximum of 16 heat spreaders is allowed, providing 16 discrete options for the number of heat spreaders. The aspect ratio is defined within a range of 1.0 to 7.3 in increments of 0.1, resulting in 64 possible values. The outer facesheet thickness varies from 0.203 mm to 1.016 mm. For the core structure, 16 different honeycomb types are considered, each characterized by specific cell size, ribbon thickness, and density. The optimal combination of these design variables is expected to minimize mass, ensure adequate heat rejection capability, and satisfy all defined constraints.

Table 4.3: *Design Space for Radiator Design Variables for Case Study-1*

Outer Facesheet Thickness (mm)	Honeycomb			Quantity of Heat Spreader	Aspect Ratio
	Cell Size (mm)	Ribbon Thickness (µm)	Density (kg/m³)		
0.203	3.8	21.1	35	1	1.0
0.254	3.8	30.2	51	2	1.1
0.305	3.8	45.2	69	3	1.2
0.406	3.8	60.3	92	4	1.3
0.508	4.5	20.0	33	5	1.4
0.635	4.5	28.6	48	6	1.5
0.813	4.5	42.9	67	7	1.6
1.016	4.5	57.2	87	8	1.7
	4.5	71.4	107	9	⋮
	5.2	27.5	43	10	6.7
	5.2	41.3	60	11	6.8
	5.2	55.0	78	12	6.9
	5.2	68.8	94	13	7.0
	5.2	82.6	111	14	7.1
	6.1	36.3	61	15	7.2
	6.1	48.4	76	16	7.3

4.2.1.2 Results for Case Study-1

The DROC receives input information containing the design variables of the radiator, equipment input, and GA parameters. Radiator configurations are represented by chromosomes of length 17, while equipment layouts—determined by the selected radiator configuration—are represented by chromosomes of length 16. Equipment temperature limits are calculated by DROC, as shown in Table 4.4. This table indicates that Equipment-3 is the most critical item, requiring a lower inner facesheet temperature than the other equipment. Consequently, the target temperature of the inner facesheet is set according to Equipment-3's requirement, which is 43.35 °C. This input guides the generation of candidate solution sets.

Table 4.4: *Equipment Temperature Limits for Case Study-1*

Equipment	Maximum Design Temperature Limit (°C)	Maximum Allowed Inner FS Temperature (°C)
Equipment-1	50	48.68
Equipment-2	45	44.74
Equipment-3	**45**	**43.35**
Equipment-4	55	54.45

In DROC, twelve different sets of GA parameters (population size, crossover probability and mutation probability) are employed to evaluate their impact on performance, as illustrated in Table 4.5. The DROC was executed on a PC equipped with an Intel(R) Core (TM) i7-4710HQ CPU operating at 2.50 GHz.

Table 4.5: *GA Parameters Set for the DROC*

GA Sets	Population Size	Two Point Crossover Probability	Mutation Probability
GA-1	40	0.8	0.1
GA-2	40	0.9	0.1
GA-3	40	0.8	0.05
GA-4	40	0.9	0.05
GA-5	50	0.8	0.1
GA-6	50	0.9	0.1
GA-7	50	0.8	0.05
GA-8	50	0.9	0.05
GA-9	60	0.8	0.1
GA-10	60	0.9	0.1
GA-11	60	0.8	0.05
GA-12	60	0.9	0.05

The optimization procedure is terminated based on the minimum number of iterations and convergence criteria. The minimum number of iterations was set to 50 for both radiator configuration and equipment layout. The convergence criteria involve analyzing the average fitness of the five best-fit chromosomes within the population across successive iterations. If this average remains constant for 10 consecutive generations, it indicates that the algorithm is unable to find a better chromosome, thereby satisfying the convergence condition. An elitist strategy is employed to immediately transfer the five best chromosomes to the next generation.

The results of DROC using these parameter sets are then compared to assess their effects, with a focus on selecting candidate radiator configuration that have the lowest mass, as illustrated in Table 4.6.

Table 4.6: *Best Radiator Configurations with GA Variations for Case Study-1*

GA Sets	$t_{Outer\ FS}$ (mm)	S (mm)	δ (µm)	ρ_{HC} $\left(\frac{kg}{m^3}\right)$	AR	ℓ (mm)	N	m_R (kg)	Solution Time (min:sec)
GA-1	0.406	4.5	57.2	87	1.8	107.86	7	63.52	05:00
GA-2	**0.203**	**4.5**	**20**	**33**	**1.3**	**135.14**	**7**	**59.91**	**04:35**
GA-3	0.406	4.5	28.6	48	1.4	106.75	8	63.03	04:45
GA-4	0.254	3.8	60.3	92	1.3	112.13	8	62.46	04:37
GA-5	**0.203**	**4.5**	**20**	**33**	**1.3**	**135.14**	**7**	**59.91**	**06:12**
GA-6	**0.203**	**4.5**	**20**	**33**	**1.3**	**135.14**	**7**	**59.91**	**06:13**
GA-7	0.406	4.5	20	33	1.4	106.75	8	62.76	06:11
GA-8	**0.203**	**4.5**	**20**	**33**	**1.3**	**135.14**	**7**	**59.91**	**06:15**
GA-9	**0.203**	**4.5**	**20**	**33**	**1.3**	**135.14**	**7**	**59.91**	**06:08**
GA-10	**0.203**	**4.5**	**20**	**33**	**1.3**	**135.14**	**7**	**59.91**	**07:55**
GA-11	0.203	3.8	21.1	35.5	1.4	106.75	8	62.00	08:55
GA-12	0.254	3.8	60.3	92	1.3	112.13	8	62.46	08:06

The equipment layout optimization was conducted utilizing the GA parameters corresponding to the selected radiator configuration, shown in green font in Table 4.6. A comparison of results from various GA parameter sets is performed to examine their impact on equipment layout design. The analysis focuses on selecting configurations that yield the lowest standard deviation in heat load among the heat spreaders, which enhances the uniformity of temperature distribution. Table 4.7 presents the comparative results, with the highest-performing configurations highlighted in green.

Table 4.7: *Best Equipment Layouts with GA Variations for Case Study-1*

GA Sets	Eq_1		Eq_2		Eq_3		Eq_4		Std Dev (W)	Solution Time (min:sec)
	P	O	P	O	P	O	P	O		
GA-1	4	V	1	H	1	V	5	V	9.33	07:17
GA-2	4	V	1	H	1	V	5	V	9.33	07:20
GA-3	4	V	1	H	1	V	5	V	9.33	06:12
GA-4	4	V	2	H	1	V	5	V	9.95	08:43
GA-5	**4**	**V**	**1**	**V**	**1**	**V**	**6**	**V**	**7.18**	**9:54**
GA-6	4	V	2	H	1	V	6	H	8.40	11:14
GA-7	4	V	1	H	1	V	6	H	7.66	08:48
GA-8	**4**	**V**	**1**	**V**	**1**	**V**	**6**	**V**	**7.18**	**10:08**
GA-9	4	V	2	H	1	V	6	H	8.40	12:20
GA-10	**4**	**V**	**1**	**V**	**1**	**V**	**6**	**V**	**7.18**	**10:18**
GA-11	4	V	1	H	1	V	6	H	7.66	09:52
GA-12	4	V	1	V	1	V	5	V	8.25	10:13

Figure 4.15 illustrates the convergence behavior of GA-5 for the equipment layout design problem in Case Study-1. The blue curve represents the best objective function value across generations, with elitism applied to ensure a non-increasing trend. As observed from the curve, convergence is effectively achieved around the 8th generation.

However, in accordance with the predefined termination criteria, the algorithm was executed up to the 50th generation to allow sufficient exploration of the solution space.

The orange curve shows the corresponding results obtained from Simcenter 3D analyses, conducted in parallel with the DROC simulations. The close agreement and consistent downward trend between the two curves indicate that the improvements achieved by DROC are reliably reflected in the detailed Simcenter 3D analyses, confirming both convergence stability and strong model correlation.

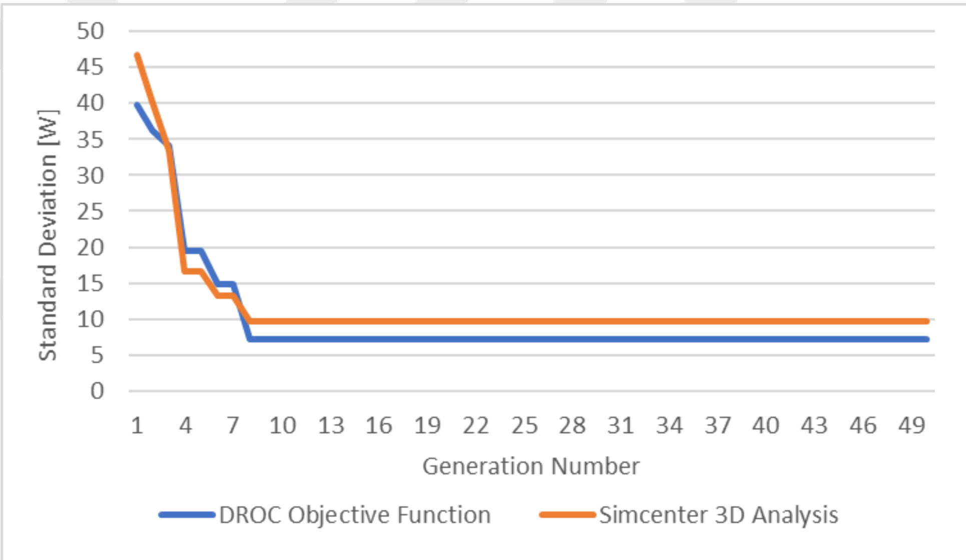

Figure 4.15: *GA-5 Convergence Curve – Case Study-1 Equipment Layout Design*

4.2.1.3 Verification Using Finite Element Method for Case Study-1

The thermal and geometrical mathematical models are constructed based on the radiator design variables provided by DROC. The thermal mathematical model is discretized into 2,568 2-D elements, representing the physical properties of the radiator components and equipment. In the final stage, heat load, orbit definitions, and thermal couplings are defined in SST for perform the steady-state thermal analysis.

The optimal radiator configuration, which achieves a balance between lightweight design and effective thermal performance, was determined using the DROC. This configuration, summarized in Table 4.8, includes parameters such as outer facesheet thickness, number of heat spreaders, spacing between heat spreaders, radiator dimensions, and honeycomb specifications.

Table 4.8: *Design Parameters of Selected Radiator Configuration – Case Study-1*

GA-5 Radiator Configuration	Value	Unit
Outer FS Thickness ($t_{Outer\ FS}$)	0.203	mm
Honeycomb Cell Size (S)	4.5	mm
Honeycomb Cell Thickness (δ_{HC})	20	µm
Honeycomb Density (ρ_{HC})	33	kg/m^3
Heat Spreader Quantity (N)	7	-
Heat Spreader Spacing ($2L_F$)	60.07	mm
Radiator Section (ℓ)	135.14	mm
Width of Heat Spreader ($2xL_p$)	50.0	mm
Length of Radiator (L_R)	1.191	m
Width of Radiator (W_R)	1.548	m

Equipment locations on the inner facesheet were determined based on the results of the DROC, which focuses on the optimal equipment placement to minimize heat flux non-uniformities. The optimal equipment layout, including the location and orientation parameters for each piece of equipment, is presented in Table 4.9.

Table 4.9: *Selected Equipment Layout Design Parameters – Case Study-1*

Eq_1		Eq_2		Eq_3		Eq_4	
O	**P**	**O**	**P**	**O**	**P**	**O**	**P**
V	4	V	1	V	1	V	6

The radiator and its associated equipment are modeled utilizing SIEMENS SIMCENTER 3D SST. A thermal analysis is conducted to evaluate its performance. Figure 4.16 and Figure 4.17 illustrate the geometrical and thermal models, respectively.

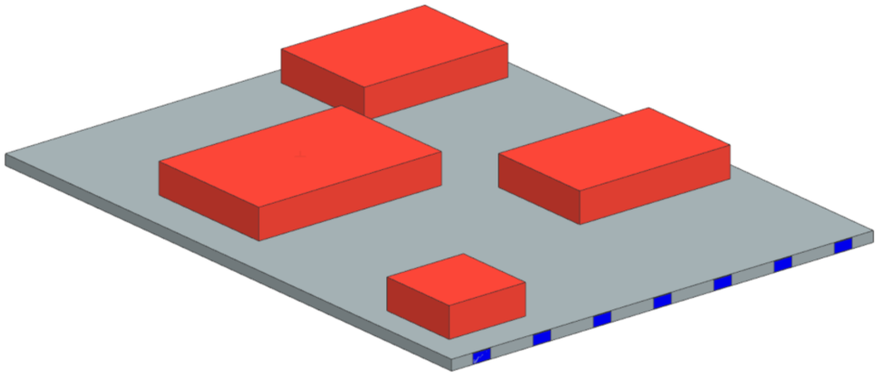

Figure 4.16: *Radiator Geometric Model in Siemens NX – Case Study-1*

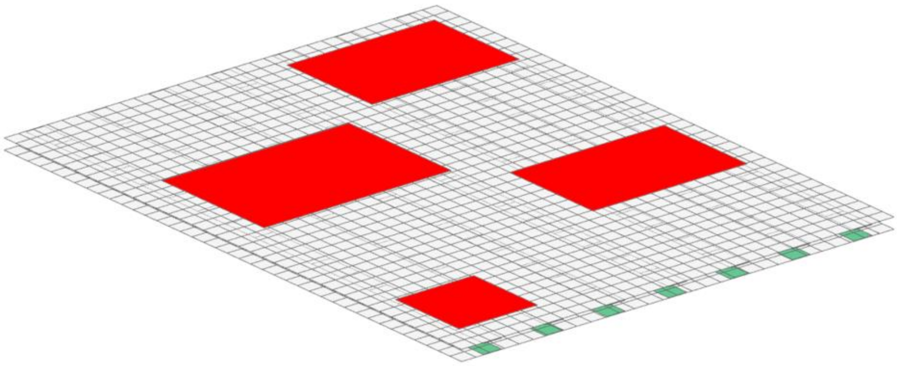

Figure 4.17: *Radiator Thermal Model in Simcenter 3D – Case Study-1*

The radiator design variables were fine-tuned by the DROC to maintain the inner facesheet temperature below 43.35 °C, ensuring that the accommodated equipment remains within its maximum design temperature limits, as shown in Table 4.4. This objective was successfully achieved and verified through simulations conducted in SIMCENTER 3D SST, as illustrated in Figure 4.18 and Figure 4.19.

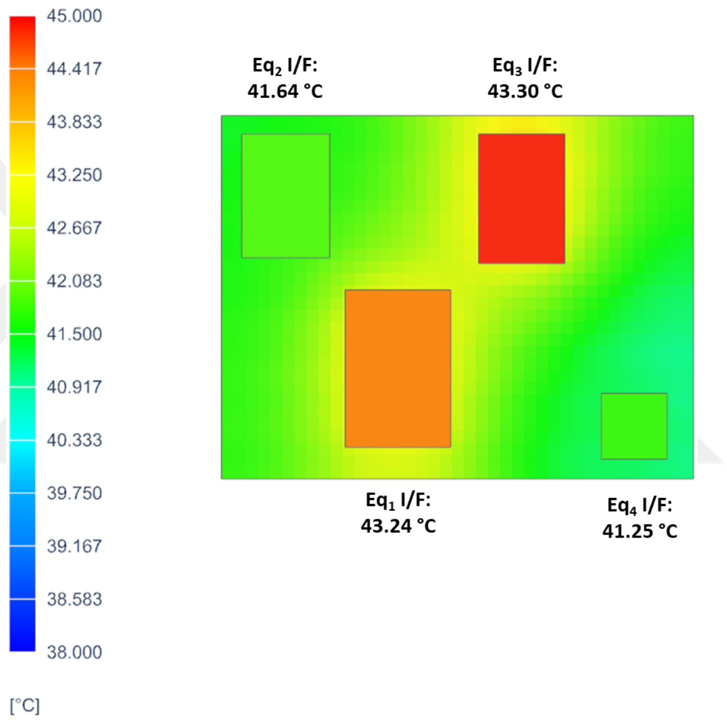

Figure 4.18: *Inner FS Temperature in Simcenter 3D SST – Case Study-1*

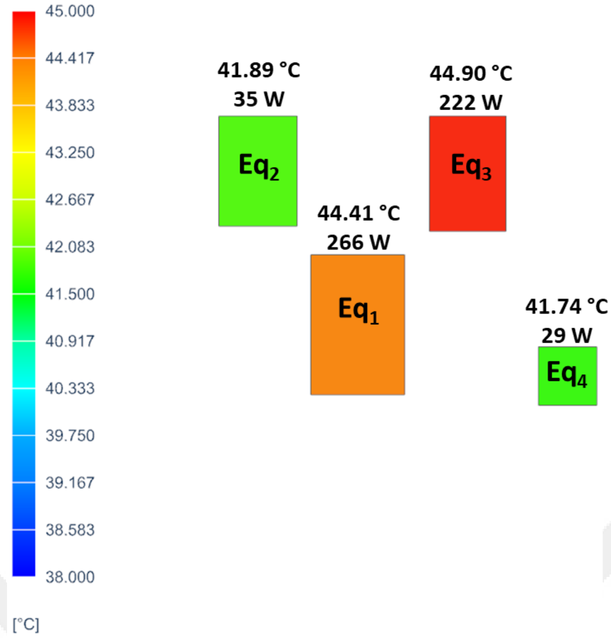

Figure 4.19: *Temperatures of Equipment in Simcenter 3D SST – Case Study-1*

Table 4.10 illustrates the heat distribution across each section (ℓ) of the radiator, corresponding to individual heat spreaders, with all values remaining within the specified transverse heat transfer limit of 90 W.

Table 4.10: *Heat Distribution Across Radiator Sections – Case Study-1*

ℓ_1 (W)	ℓ_2 (W)	ℓ_3 (W)	ℓ_4 (W)	ℓ_5 (W)	ℓ_6 (W)	ℓ_7 (W)
82	82	82	80	70	88	68

Table 4.11 provides a summary of the analysis results for Case Study-1, including the equipment and their corresponding interface temperatures. All of these temperatures remain within the specified temperature limits.

Table 4.11: *Results of Thermal Analysis – Case Study-1*

	Equipment		Interface	
	Maximum Design Temperature Limit (°C)	**Analysis Results (°C)**	**Maximum Allowed I/F Inner FS Temperature (°C)**	**Analysis Results (°C)**
Eq-1	50	**44.41**	48.68	**43.24**
Eq-2	45	**41.89**	44.74	**41.64**
Eq-3	45	**44.90**	43.35	**43.30**
Eq-4	55	**41.74**	54.45	**41.25**

4.2.2 Case Study-2

4.2.2.1 Problem Statement for Case Study-2

To evaluate the performance of DROC under more complex conditions, the number of equipment units is increased to sixteen, as detailed in Table 4.12. This increase introduces additional complexity to the problem, as each unit has distinct heat dissipation rates, baseplate areas, and maximum allowable design temperatures. All equipment units are intended to be positioned on the north radiator panel.

Table 4.12: *Equipment Information – Case Study-2*

	Heat Dissipation (W)	Baseplate Area (m^2)	Maximum Design Temperature Limit (°C)
Eq_1	266	0.179	50
Eq_2	100	0.053	40
Eq_3	360	0.087	45
Eq_4	187	0.082	55
Eq_5	201	0.038	50
Eq_6	90	0.017	55
Eq_7	185	0.087	50
Eq_8	165	0.100	45
Eq_9	211	0.036	55
Eq_{10}	153	0.045	55
Eq_{11}	169	0.085	40
Eq_{12}	65	0.035	45
Eq_{13}	33	0.009	40
Eq_{14}	141	0.081	55
Eq_{15}	74	0.046	50
Eq_{16}	96	0.028	40

The material properties, thermal conductance between radiator components, and the thickness values for the honeycomb and inner facesheet are kept consistent with Case Study-1. The radiator design is constrained by a maximum length of 2000 mm and a maximum width of 7000 mm. The width of heat spreader ($2L_p$) is 15 mm. The thermal filler applied between the equipment and the inner facesheet is the same as that used in Case Study-1. It is required that the transverse heat dissipation through each heat spreader remains below 250 W.

The design space for the radiator component variables is given in Table 4.13. The number of heat spreaders can range from 7 to 22, resulting in 16 discrete design options. The aspect ratio is defined within a range of 1.0 to 7.3, in increments of 0.1, yielding 64 possible values. The outer facesheet thickness ranges from 0.203 mm to 1.016 mm. For the core structure, 16 different honeycomb configurations are considered, each characterized by specific cell size, ribbon thickness, and density. The objective is to identify the optimal combination of these design variables to minimize mass, ensure sufficient heat rejection, and satisfy the defined constraints.

Table 4.13: *Design Space for Radiator Design Variables – Case Study-2*

Outer Facesheet Thickness (mm)	Honeycomb			Quantity of Heat Spreader	Aspect Ratio
	Cell Size (mm)	Ribbon Thickness (μm)	Density (kg/m^3)		
0.203	3.8	21.1	35	7	1.0
0.254	3.8	30.2	51	8	1.1
0.305	3.8	45.2	69	9	1.2
0.406	3.8	60.3	92	10	1.3
0.508	4.5	20.0	33	11	1.4
0.635	4.5	28.6	48	12	1.5
0.813	4.5	42.9	67	13	1.6
1.016	4.5	57.2	87	14	1.7
	4.5	71.4	107	15	⋮
	5.2	27.5	43	16	6.7
	5.2	41.3	60	17	6.8
	5.2	55.0	78	18	6.9
	5.2	68.8	94	19	7.0
	5.2	82.6	111	20	7.1
	6.1	36.3	61	21	7.2
	6.1	48.4	76	22	7.3

4.2.2.2 Results for Case Study-2

The design variables of the radiator, equipment inputs, and GA parameters are imported into DROC. For Case Study-2, radiator configurations are encoded as chromosomes of length 17, while the equipment layouts, influenced by the selected radiator configuration, were represented by chromosomes of length 80. Equipment temperature limits, calculated by DROC and presented in Table 4.14, indicate that Equipment-13 is the most thermally critical component, requiring a lower inner facesheet temperature than the others. Consequently, the target inner facesheet temperature is set to 37.07 °C. This input guides the generation of candidate solution sets.

Table 4.14: *Equipment Temperature Limits for Case Study-2*

Equipment	Maximum Design Temperature Limit (°C)	Maximum Allowed Inner FS Temperature (°C)
Equipment-1	50	48.81
Equipment-2	40	38.50
Equipment-3	45	41.68
Equipment-4	55	53.18
Equipment-5	50	45.71
Equipment-6	55	50.73
Equipment-7	50	48.31
Equipment-8	45	43.69
Equipment-9	55	50.29
Equipment-10	55	52.27
Equipment-11	40	38.40
Equipment-12	45	43.53
Equipment-13	**40**	**37.07**
Equipment-14	55	53.61
Equipment-15	50	48.72
Equipment-16	40	37.25

In DROC, different sets of GA parameters (population size, crossover probability, and mutation probability) are employed for Case Study-2. The same stopping criteria used in Case Study-1 are also applied. The results obtained with these parameter sets are compared to assess their effects, with a focus on selecting candidate radiator configurations that achieve the lowest mass, as presented in Table 4.15.

Table 4.15: *Best Radiator Configurations with GA Variations – Case Study-2*

GA Sets	$t_{Outer\ FS}$ (mm)	S (mm)	δ (μm)	ρ_{HC} $\left(\frac{kg}{m^3}\right)$	AR	ℓ (mm)	N	m_R (kg)	Solution Time (min:sec)
GA-1	0.203	4.5	20	33	2.6	103.5	16	252.85	05:59
GA-2	0.203	4.5	20	33	2.9	104.7	15	252.41	05:16
GA-3	0.406	4.5	20	33	3.3	105.2	14	256.48	06:27
GA-4	0.305	4.5	20	33	3.8	97.0	17	263.71	05:46
GA-5	**0.203**	**4.5**	**20**	**33**	**2.5**	**105.8**	**16**	**252.03**	**07:20**
GA-6	0.203	4.5	20	33	2.6	103.5	16	252.85	08:43
GA-7	0.203	5.2	27.5	43	2.6	103.5	16	254.07	08:36
GA-8	0.203	4.5	28.6	48	2.5	105.8	16	253.87	07:30
GA-9	**0.203**	**4.5**	**20**	**33**	**2.5**	**105.8**	**16**	**252.03**	**11:09**
GA-10	**0.203**	**4.5**	**20**	**33**	**2.5**	**105.8**	**16**	**252.03**	**11:30**
GA-11	0.406	3.8	21.1	35.5	3.4	103.4	14	255.25	10:30
GA-12	0.406	3.8	21.1	35.5	3.4	103.4	14	253.16	09:46

The equipment layout optimization was carried out using the selected radiator configuration, highlighted in green in Table 4.15. The results obtained from different GA parameter sets are compared to evaluate their influence on layout design. Particular attention is given to identifying candidate equipment layout configurations that minimize the standard deviation of heat load across the heat spreaders, thereby promoting a more uniform temperature distribution. The comparative results are presented in Table 4.16, with the best-performing configuration highlighted in green.

Table 4.16: *Best Equipment Layouts with GA Variations for Case Study-2*

GA Sets	Std Dev (W)	Solution Time (min:sec)
GA-1	29.53	26:05
GA-2	34.03	23:28
GA-3	28.19	24:55
GA-4	38.7	23:24
GA-5	31.41	30:14
GA-6	29.43	31:36
GA-7	25.93	30:14
GA-8	25.87	31:08
GA-9	**24.66**	**37:10**
GA-10	33.63	36:11
GA-11	31.88	35:29
GA-12	28.62	35:22

Figure 4.20 illustrates the convergence behavior of GA-9 for the equipment layout design problem in Case Study-2. The blue curve represents the best objective function value across generations, with elitism applied to ensure a non-increasing trend. As observed from the curve, convergence is effectively achieved around the 19th generation. However, in accordance with the predefined termination criteria, the algorithm was executed up to the 50th generation to allow sufficient exploration of the solution space.

The orange curve shows the corresponding results obtained from Simcenter 3D analyses, conducted in parallel with the DROC simulations. The close agreement and consistent downward trend between the two curves indicate that the improvements achieved by DROC are reliably reflected in the detailed Simcenter 3D analyses, confirming both convergence stability and strong model correlation.

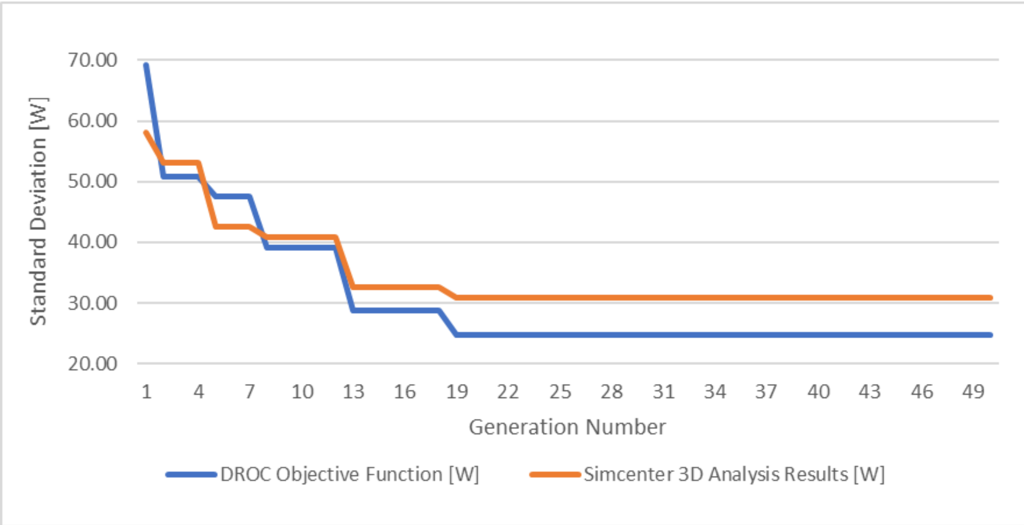

Figure 4.20: *GA-9 Convergence Curve – Case Study-2 Equipment Layout Design*

4.2.2.3 Verification Using Finite Element Method for Case Study-2

Geometrical and thermal mathematical models are constructed based on the outcomes of DROC for verification purposes. The thermal mathematical model is discretized into 13,200 2-D elements, representing the physical properties of the radiator components and equipment. The optimal radiator configuration, which achieves a balance between lightweight design and effective thermal performance, was identified using DROC. This configuration, detailed in Table 4.17, includes parameters such as facesheet thickness, number of heat spreaders, spacing between them, radiator dimensions, and honeycomb specifications.

Table 4.17: *Design Parameters of Selected Radiator Configuration – Case Study-2*

Radiator Configuration	**Value**	**Unit**
Outer FS Thickness ($t_{Outer\ FS}$)	0.203	mm
Honeycomb Cell Size (S)	4.5	mm
Honeycomb Cell Thickness (δ_{HC})	20.0	µm
Honeycomb Density (ρ_{HC})	33.0	kg/m^3
Heat Spreader Quantity (N)	16	-
Heat Spreader Spacing ($2L_F$)	105.81	mm
Radiator Section (ℓ)	120.81	mm
Width of Heat Spreader ($2xL_p$)	15.0	mm
Length of Radiator (L_R)	1.933	m
Width of Radiator (W_R)	4.833	m

Equipment locations on the inner facesheet were determined using the results from DROC, which aims to optimize placement in order to minimize heat flux nonuniformities. The resulting optimal equipment layout, including the location and orientation of each equipment unit, is presented in Table 4.18.

Table 4.18: *Selected Equipment Layout Design Parameters – Case Study-2*

Equipment	P	O
Equipment-1	10	H
Equipment-2	1	V
Equipment-3	14	V
Equipment-4	3	V
Equipment-5	5	V
Equipment-6	12	V
Equipment-7	7	V
Equipment-8	2	H
Equipment-9	13	H
Equipment-10	15	V
Equipment-11	6	V
Equipment-12	8	H
Equipment-13	4	V
Equipment-14	9	V
Equipment-15	1	H
Equipment-16	1	H
Standard Deviation (W)		24.66

The radiator and its associated equipment were modeled utilizing SIEMENS SIMCENTER 3D SST. Figure 4.21 and Figure 4.22 illustrate the geometrical and thermal models, respectively.

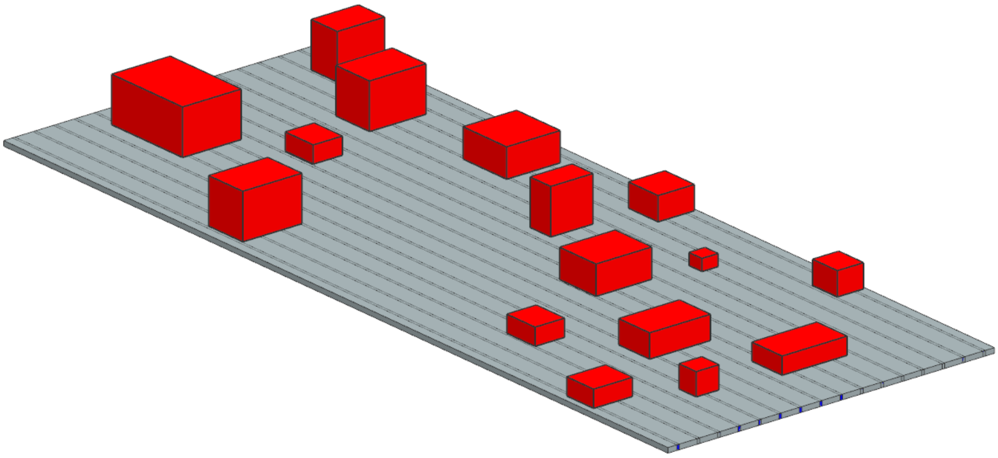

Figure 4.21: *Radiator Geometric Model in Siemens NX – Case Study-2*

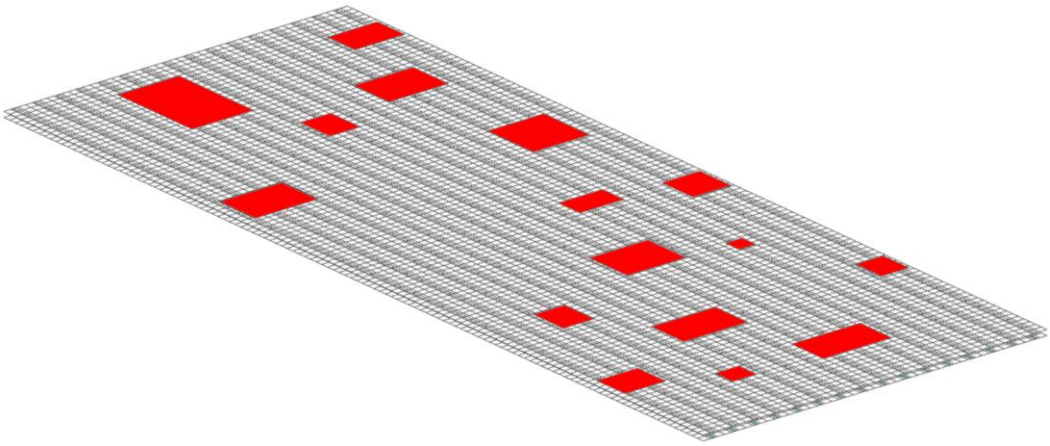

Figure 4.22: *Radiator Thermal Model in Simcenter 3D – Case Study-2*

The next step involves performing thermal analysis using SIMCENTER 3D SST. The results, including the inner facesheet temperature (with equipment interface temperatures indicated) and the equipment temperatures along with their corresponding heat loads, are presented in Figure 4.23 and Figure 4.24, respectively.

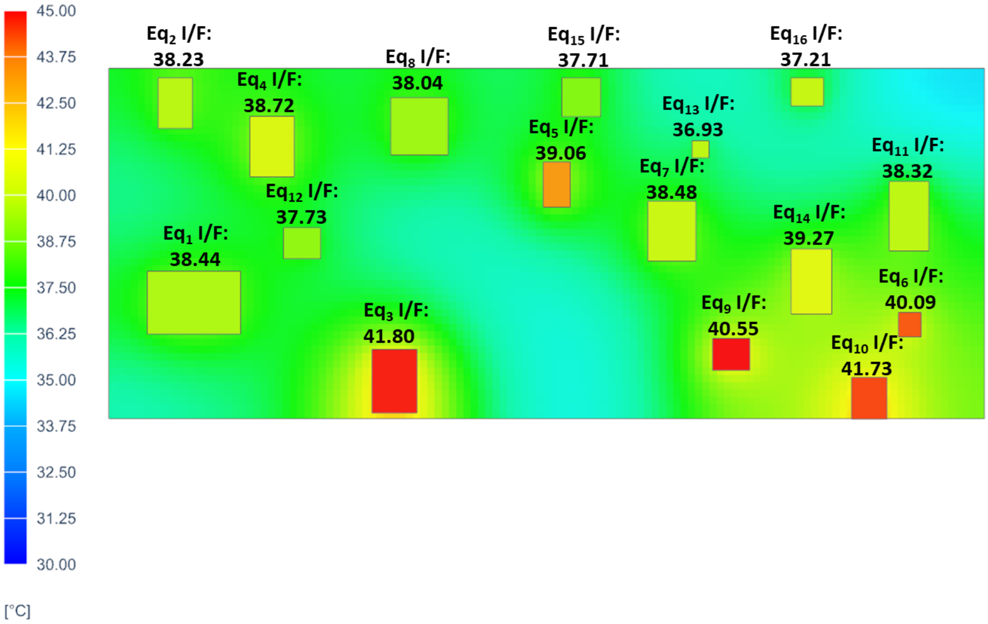

Figure 4.23: *Inner FS Temperature in Simcenter 3D SST – Case Study-2*

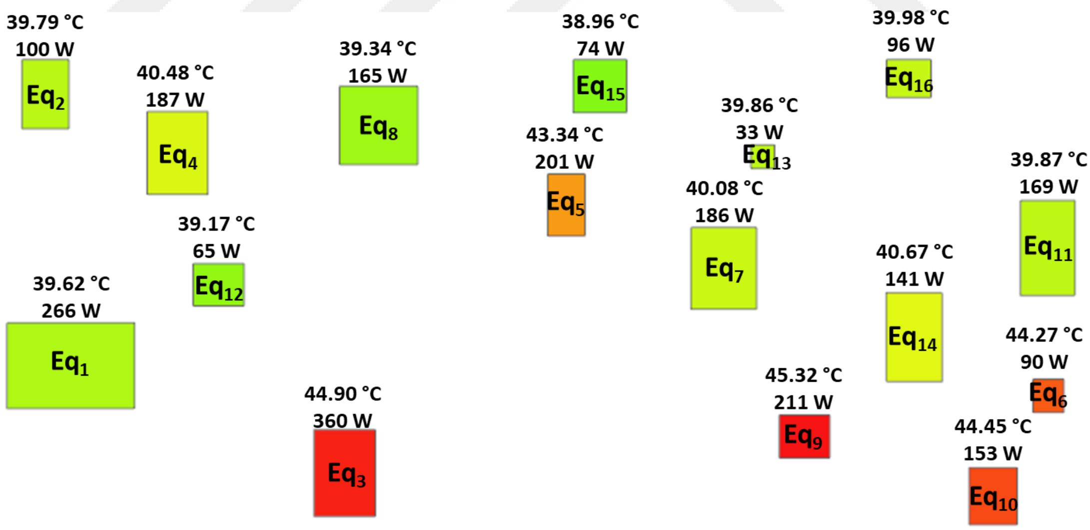

Figure 4.24: *Temperatures of Equipment in Simcenter 3D SST – Case Study-2*

Table 4.19 illustrates the heat distribution across each section (ℓ) of the radiator, corresponding to individual heat spreaders, with all values remaining within the specified transverse heat transfer limit of 250 W.

Table 4.19: *Heat Distribution Across Radiator Sections – Case Study-2*

ℓ_1 (W)	ℓ_2 (W)	ℓ_3 (W)	ℓ_4 (W)	ℓ_5 (W)	ℓ_6 (W)	ℓ_7 (W)	ℓ_8 (W)	ℓ_9 (W)	ℓ_{10} (W)	ℓ_{11} (W)	ℓ_{12} (W)	ℓ_{13} (W)	ℓ_{14} (W)	ℓ_{15} (W)	ℓ_{16} (W)
140	160	139	147	144	141	137	146	155	130	123	168	203	204	179	179

Table 4.20 provides a summary of the analysis results for case study-2, including the equipment and their corresponding interface temperatures. All of these temperatures remain within the specified temperature limits.

Table 4.20: *Results of Thermal Analysis – Case Study-2*

	Equipment		**Interface**	
	Maximum Design Temperature Limit (°C)	**Analysis Results (°C)**	**Maximum Allowed I/F Inner FS Temperature (°C)**	**Analysis Results (°C)**
Eq-1	50	**39.62**	48.81	**38.44**
Eq-2	40	**39.79**	38.50	**38.23**
Eq-3	45	**44.90**	41.68	**41.80**
Eq-4	55	**40.48**	53.18	**38.72**
Eq-5	50	**43.34**	45.71	**39.06**
Eq-6	55	**44.27**	50.73	**40.09**
Eq-7	50	**40.08**	48.31	**38.48**
Eq-8	45	**39.34**	43.69	**38.04**
Eq-9	55	**45.32**	50.29	**40.55**
Eq-10	55	**44.45**	52.27	**41.73**
Eq-11	40	**39.87**	38.40	**38.32**
Eq-12	45	**39.17**	43.53	**37.73**
Eq-13	40	**39.86**	37.07	**36.93**
Eq-14	55	**40.67**	53.61	**39.27**
Eq-15	50	**38.96**	48.72	**37.71**
Eq-16	40	**39.98**	37.25	**37.21**

4.3 Discussion

This section presents the results obtained from the two case studies. The first case study includes four distinct pieces of equipment, while the second involves sixteen, each with different thermal requirements. The presence of varied thermal demands in both cases adds complexity to the optimization problem and serves to evaluate the efficiency and robustness of DROC under scenarios with both smaller and larger equipment quantities. To verify the accuracy and applicability of DROC, the radiator configurations and equipment layouts generated for each case study were modeled, and thermal analyses were conducted using SIMCENTER 3D SST, which employs the FEM.

As observed in the case studies, certain equipment acts as design drivers, meaning that the inner facesheet temperature is determined based on their thermal requirements. In Case Study-1, Equipment-3 significantly influences the design due to its requirement for a lower inner facesheet temperature of 43.35 °C—lower than that of any other equipment. The simulation results confirm that the maximum temperature of Equipment-3 reaches 44.90 °C, which remains below its threshold limit of 45.0 °C. Furthermore, all other equipment operates within its respective maximum design temperature limits. In Case Study-2, Equipment-13 is identified as the most critical component, necessitating a lower inner facesheet temperature of 37.07 °C. The results show that the temperature of Equipment-13 is 39.86 °C, remaining below its design limit of 40.0 °C. All other equipment in this case study also meets its respective design temperature constraints.

Data obtained through the DROC approach using various genetic algorithm parameters indicate that the optimal spacing length between heat spreaders lies within the range of 100 mm to 135 mm. Shorter distances lead to a significant increase in mass with minimal improvement in heat rejection capability, while larger distances require a wider radiator to meet heat rejection constraints, increasing overall mass. As a result, when the design solutions are evaluated based on their fitness (defined by total mass in this study), configurations with heat spreader spacings outside this optimal range are gradually eliminated through the evolutionary process of the algorithm. Therefore, positioning heat spreaders at distances significantly lower or higher than this range is inadvisable, as it compromises mass efficiency without offering meaningful thermal benefits.

The shape of the embedded heat spreader radiator generally evolves into a rectangular form during the optimization process, as the greater longitudinal length allows the heat spreader to transfer heat over a wider area owing to its higher thermal conductivity and thickness; however, this also results in an increase in the overall radiator mass. Furthermore, the AR limitation is primarily determined by the specified transversal heat transfer limit of the heat spreaders, the dimensional constraints of the radiator, and the physical dimensions and layout of the equipment. In Case Study-1, the maximum heat load on a single heat spreader in the selected DROC design is calculated as 88 W, which approaches but remains below the predefined transversal heat transfer limit of 90 W. Similarly, in Case Study-2, the corresponding value reaches 203 W, remaining below the predefined transversal heat transfer limit of 250 W. Therefore, the AR and, consequently, the radiator width (W_R) remained within a certain range to avoid reducing the number of heat spreaders, which could lead to exceeding the heat transfer limit.

Uniform heat distribution across the radiator panel is often unachievable due to variations in the dimensions, positions, and heat dissipation characteristics of the equipment. In both case studies, the heat spreaders generally carry comparable thermal loads; however, variations in equipment properties and placement lead to noticeable differences in individual heat spreader loads. Despite these disparities, the inner facesheet temperature distribution remains relatively uniform in both cases, indicating effective thermal performance of the optimized radiator configurations.

The parameters of the GA, including population size, crossover probability, mutation probability, influence the algorithm's performance and results. The findings indicate that multiple GA parameter sets should be evaluated to determine the most effective solution, as demonstrated in the case studies. The case studies indicate that solution time increases with population size due to the need to solve all equations for each population member. While this leads to longer computation times, it also expands the search space, potentially yielding better results. The study also reveals that higher mutation rates further extend solution times, as mutations may generate chromosomes that violate constraints, necessitating additional iterations to produce valid solutions. However, mutation contributes to a broader search space, enhancing the exploration of potential solutions.

5. CONCLUSION

This study proposes a methodology for designing embedded heat spreader GEO radiator panels and equipment layouts, utilizing a Python-based GA code for the preliminary design phase of spacecraft projects. Essential components of the radiator, including the honeycomb structure, facesheets, and heat spreader, are carefully selected to meet minimal mass, heat rejection requirements, and other limits that restrict manufacturability. Furthermore, the equipment on the radiator is placed to ensure uniform heat dissipation, considering the thermal transfer capacity of the heat spreaders.

The methodology was validated through case studies. The radiator configuration and equipment layout from DROC were modeled in SIEMENS NX and thermally analyzed in SIMCENTER 3D SST. Analysis results show that the radiator configuration and equipment layout meet case study objectives. The slight difference between the required temperature and the temperature obtained from the simulation demonstrates that the radiator is effectively designed, indicating that it is not overdesigned. Overdesign would otherwise lead to increased mass and cost for the spacecraft. Therefore, the case study not only confirms the accuracy of the DROC results but also demonstrates its applicability in spacecraft projects.

In conclusion, the developed methodology proves to be highly beneficial for the preliminary design phase of embedded heat spreader radiator panels, particularly when numerous conceptual designs and thermal analyses are required. It streamlines the design iteration process, resulting in superior conceptual designs as a starting point for development compared to traditional methods. The method provides the thermal control subsystem engineer with the flexibility to select the radiator configuration among optimal design alternatives.

6. FUTURE WORK

For future work, in order to reduce the overall mass of the radiator, heat pipes are planned to replace the currently used APG solid heat spreaders. Due to their high thermal conductivity and low mass, heat pipes offer significant advantages, especially in applications requiring efficient heat transfer over extended distances. Moreover, heat pipes enable the use of thinner facesheets by providing adequate in-plane thermal conductivity, thereby contributing further to mass reduction. The existing thermal model can be modified accordingly, incorporating the thermal resistance network approach developed by Saygan et al. [54, 55] for heat pipe systems, thereby improving modeling accuracy and agreement with experimental results. Additionally, the equipment layout will be configured so that one section of each heat pipe functions as the evaporator, while the remaining sections serve as the adiabatic region and the condenser.

7. REFERENCES

[1] "Annual number of objects launched into space," Our World in Data, Feb. 28, 2025. [Online]. Available: https://ourworldindata.org/grapher/yearly-number-of-objects-launched-into-outer-space (accessed Aug. 23, 2025).

[2] A. Cermak, “Chapter 2: Reference systems - NASA Science,” NASA Science, Jan. 16, 2025. [Online]. Available: https://science.nasa.gov/learn/basics-of-space-flight/chapter2-1/ (accessed Aug. 23, 2025).

[3] M. Bulut, S. Demirel, S. Gulgonul, and N. Sozbir, “Battery thermal design conception of Turkish satellite,” in *Proc. 6th Int. Energy Conversion Engineering Conf. (IECEC)*, Cleveland, OH, USA, Jun. 2008, doi: 10.2514/6.2008-5787.

[4] K. F. C. H. Sam and Z. Deng, “Optimization of a space based radiator,” *Applied Thermal Engineering*, vol. 31, no. 14–15, pp. 2312–2320, Apr. 2011, doi: 10.1016/j.applthermaleng.2011.03.029.

[5] J. Meseguer, I. Pérez-Grande, and A. Sanz-Andrés, *Spacecraft Thermal Control*. Amsterdam, Netherlands: Elsevier, 2012.

[6] European Cooperation for Space Standardization (ECSS), "Space Engineering-Thermal Control General Requirements," ECSS-E-ST-31C, Mar. 2008.

[7] D. Gilmore, *Spacecraft Thermal Control Handbook, Volume I: Fundamental Technologies*. El Segundo, CA, USA: The Aerospace Press, 2002, doi: 10.2514/4.989117.

[8] C. Atar and M. Aktaş, “Advances in thermal modeling and analysis of satellites,” *Gazi University Journal of Science*, vol. 35, no. 1, pp. 42–58, Mar. 2021, doi: 10.35378/gujs.840191.

[9] “Thermal solver guides,” Maya HTT. [Online]. Available: https://help.mayahtt.com/tmg/topics/thermal_solver_guides.html (accessed Aug. 23, 2025).

[10] P. C. Wise, J. Raisch, W. Kelly, and S. P. Sharma, "Thermal design verification of a high-power direct broadcast satellite," in *Proc. AIAA/ASME 4th Joint Thermophysics and Heat Transfer Conf.*, San Diego, CA, USA, Jun. 1986, doi: 10.2514/6.1986-1339.

[11] R. Reda, Y. Ahmed, I. Magdy, H. Nabil, M. Khamis, and M. Refaey, et al., "Basic principles and mechanical considerations of satellites: A short review," *Transactions on Aerospace Research*, vol. 2023, no. 3, pp. 40–54, 2023.

[12] M. Ralphs, M. Sinfield, H. Mortensen, and M. Felt, “Advances in thermal technologies using pyrolytic graphite sheet,” in *Proc. Thermal & Fluids Analysis Workshop (TFAWS)*, Cleveland, OH, USA, Aug. 2023. [Online]. Available: https://digitalcommons.usu.edu/sdl_pubs/324 (accessed Aug. 23, 2025).

[13] A. Lécossais, F. Jacquemart, G. Lefort, E. Dehombreux, F. Beck and V. Frard, “Deployable panel radiator,” in *Proc. 47th Int. Conf. Environmental Systems (ICES)*, Charleston, SC, USA, Jul. 2017. [Online]. Available: http://hdl.handle.net/2346/72955 (accessed Aug. 23, 2025).

[14] T. Iwata et al., “NIRS3: the near infrared spectrometer on Hayabusa2,” *Space Science Reviews*, vol. 208, no. 1–4, pp. 317–337, Mar. 2017, doi: 10.1007/s11214-017-0341-0.

[15] W. H. Kelly and J. H. Reisenweber, “Thermal performance of embedded heat pipe spacecraft radiator panels,” *SAE Technical Paper 932158*, Jul. 1993, doi: 10.4271/932158.

[16] B. Zohuri, *Heat Pipe Applications in Fission Driven Nuclear Power Plants*, Cham, Switzerland: Springer Nature, 2019.

[17] R. C. Consolo Jr. and S. K. S. Boetcher, “Advances in spacecraft thermal control,” *Advances in Heat Transfer*, vol. 56, Amsterdam, Netherlands: Elsevier, 2023, pp. 1–50, doi: 10.1016/bs.aiht.2023.04.001.

[18] H. Alijani, B. Çetin, Y. Akkuş, and Z. Dursunkaya, “Effect of design and operating parameters on the thermal performance of aluminum flat grooved heat pipes,” *Applied Thermal Engineering*, vol. 132, pp. 174–187, Feb. 2018, doi: 10.1016/j.applthermaleng.2017.12.085.

[19] M. G. Sahab, V. V. Toropov, and A. H. Gandomi, “A review on traditional and modern structural optimization,” *Evolutionary Algorithms and Metaheuristics in Civil Engineering and Construction*, Amsterdam, Netherlands: Elsevier, Jan. 2013, pp. 25–47, doi: 10.1016/B978-0-12-398364-0.00002-4.

[20] J. D. Bagley, *The Behavior of Adaptive Systems Which Employ Genetic and Correlation Algorithms*, Ph.D. dissertation, Univ. of Michigan, Ann Arbor, MI, USA, Jan. 1967, doi: 10.7302/10207.

[21] J. H. Holland, *Adaptation in Natural and Artificial Systems*. Ann Arbor, MI, USA: Univ. of Michigan Press, 1975. [Online]. Available: https://dl.acm.org/citation.cfm?id=129194 (accessed Aug. 23, 2025).

[22] K. A. De Jong, *An Analysis of the Behavior of a Class of Genetic Adaptive Systems*, Ph.D. dissertation, Univ. of Michigan, Ann Arbor, MI, USA, 1975.

[23] J. Grefenstette, “Optimization of control parameters for genetic algorithms,” *IEEE Transactions on Systems Man and Cybernetics*, vol. 16, no. 1, pp. 122–128, Jan. 1986, doi: 10.1109/TSMC.1986.289288.

[24] J. E. Baker, "Reducing bias and inefficiency in the selection algorithm," in *Proc. 2nd Int. Conf. Genetic Algorithms*, Hillsdale, NJ, USA: L. Erlbaum Associates, Oct. 1987, pp. 14–21. [Online]. Available: http://dblp.uni-trier.de/db/conf/icga/icga1987.html#Baker87 (accessed Aug. 23, 2025).

[25] D. E. Goldberg, *Genetic Algorithms in Search, Optimization, and Machine Learning*. Reading, MA, USA: Addison-Wesley, 1989.

[26] A. Chehouri, R. Younes, J. Perron, and A. Ilinca, “A constraint-handling technique for genetic algorithms using a violation factor,” *Journal of Computer Science*, vol. 12, no. 7, pp. 350–362, Jul. 2016, doi: 10.3844/jcssp.2016.350.362.

[27] H. Chang, “Optimization of a heat pipe radiator design,” in *Proc. 30th Thermophysics Conf.*, Snowmass, CO, USA, Jun. 1984, doi: 10.2514/6.1984-1718.

[28] S. J. Mertesdorf, "Development of a generalized radiator weight optimization design code for high power spacecraft applications," in *Proc. AIAA/ASME 4th Joint Thermophysics and Heat Transfer Conf.*, Boston, MA, USA, 1986, Paper no. AIAA-86-1268.

[29] D. G. T. Curran and T. T. Lam, “Weight optimization for honeycomb radiators with embedded heat pipes,” *Journal of Spacecraft and Rockets*, vol. 33, no. 6, pp. 822–828, Nov. 1996, doi: 10.2514/3.26844.

[30] S. K. Roy and B. L. Avanic, “Optimization of a space radiator with energy storage,” *International Communications in Heat and Mass Transfer*, vol. 33, no. 5, pp. 544–551, Feb. 2006, doi: 10.1016/j.icheatmasstransfer.2006.01.011.

[31] T. Y. Kim, S.-Y. Chang, and S. S. Yong, “Optimizing the design of space radiators for thermal performance and mass reduction,” *Journal of Aerospace Engineering*, vol. 30, no. 3, Oct. 2016, doi: 10.1061/(ASCE)AS.1943-5525.0000676.

[32] S. Katoch, S. S. Chauhan, and V. Kumar, “A review on genetic algorithm: past, present, and future,” *Multimedia Tools and Applications*, vol. 80, no. 5, pp. 8091–8126, Oct. 2020, doi: 10.1007/s11042-020-10139-6.

[33] I. Codreanu, D. Besnea, F. Dragomir, and I. Voda, "Use of genetic algorithms in heat transfer problems," in *Proc. 2004 Int. Semiconductor Conf. (CAS 2004)*, vol. 2, Sinaia, Romania, Oct. 2004, pp. 1031–1034, doi: 10.1109/SMICND.2004.1436706.

[34] D. Hengeveld, J. Braun, E. Groll, and A. Williams, "Optimal placement of electronic components to minimize heat flux non-uniformities," in *Proc. 54th AIAA/ASME/ASCE/AHS/ASC Structures, Structural Dynamics, Materials Conf.*, Palm Springs, CA, USA, May 2009, doi: 10.2514/6.2009-2223.

[35] M. Akpinar, “Application of genetic algorithm for optimization of heat-transfer parameters,” *Sakarya University Journal of Science*, vol. 23, no. 6, pp. 1123–1130, Aug. 2019, doi: 10.16984/saufenbilder.500643.

[36] B. S. Mekki, J. Langer, and S. Lynch, “Genetic algorithm based topology optimization of heat exchanger fins used in aerospace applications,” *International Journal of Heat and Mass Transfer*, vol. 170, p. 121002, Feb. 2021, doi: 10.1016/j.ijheatmasstransfer.2021.121002.

[37] V. K. Koumousis and C. P. Katsaras, “A saw-tooth genetic algorithm combining the effects of variable population size and reinitialization to enhance performance,” *IEEE Transactions on Evolutionary Computation*, vol. 10, no. 1, pp. 19–28, Jan. 2006, doi: 10.1109/tevc.2005.860765.

[38] M. Pelikan, D. E. Goldberg, and E. Cantu-Paz, "Bayesian optimization algorithm, population sizing, and time to convergence," Lawrence Livermore National Laboratory, Livermore, CA, USA, Jan. 2000. [Online]. Available: https://www.osti.gov/biblio/790398 (accessed Aug. 23, 2025).

[39] A. Piszcz and T. Soule, "Genetic programming: optimal population sizes for varying complexity problems," in *Proc. 8th Annual Genetic and Evolutionary Computation Conference (GECCO 2006)*, Seattle, WA, USA, 2006, pp. 953–954.

[40] F. G. Lobo and D. E. Goldberg, “The parameter-less genetic algorithm in practice,” *Information Sciences*, vol. 167, no. 1–4, pp. 217–232, Mar. 2004, doi: 10.1016/j.ins.2003.03.029.

[41] X.-S. Yang, *Nature-Inspired Optimization Algorithms*, Amsterdam, Netherlands: Elsevier Science Publishers, 2014.

[42] P. A. Diaz-Gomez and D. F. Hougen, "Initial population for genetic algorithms: A metric approach," in *Proc. 2007 Int. Conf. Genetic and Evolutionary Methods*

(GEM), Las Vegas, NV, USA: CSREA Press, 2007, pp. 43–49. [Online]. Available: http://cameron.edu/~pdiaz-go/GAsPopMetric.pdf (accessed Aug. 23, 2025).

[43] C.-Y. Lin and P. Hajela, "Genetic Algorithms in optimization problems with discrete and integer design variables," *Engineering Optimization*, vol. 19, no. 4, pp. 309-327, Jun. 1992, doi: 10.1080/03052159208941234.

[44] S. Datta, C. Garai, and R. Das, "Efficient genetic algorithm on linear programming problem for fittest chromosomes," *Journal of Global Research in Computer Science*, vol. 3, no. 6, pp. 1–7, Jun. 2012.

[45] A. Konak, D. W. Coit, and A. E. Smith, "Multi-objective optimization using genetic algorithms: A tutorial," *Reliability Engineering & System Safety*, vol. 91, no. 9, pp. 992–1007, Sep. 2006, doi: 10.1016/j.ress.2005.11.018.

[46] N. N. Erdogmus, B. Ervural, and H. Hakli, "Comparative analysis of genetic crossover operators for the p-median facility location problem," *Selçuk Univ. J. Eng. Sci.*, vol. 21, no. 1, pp. 32–38, 2022. [Online]. Available: https://sujes.selcuk.edu.tr/sujes/article/view/587 (accessed Aug. 23, 2025).

[47] X.-S. Yang, *Nature-Inspired Metaheuristic Algorithms*, 2nd ed. Frome, UK: Luniver Press, 2010.

[48] J. E. Smith and T. C. Fogarty, "Operator and parameter adaptation in genetic algorithms," *Soft Computing*, vol. 1, no. 2, pp. 81–87, Jun. 1997.

[49] J. Hesser and R. Männer, "Towards an optimal mutation probability for genetic algorithms," *Parallel Problem Solving from Nature – PPSN ’90*, H. P. Schwefel and R. Männer, Eds. Berlin, Germany: Springer, 1991, pp. 23–32.

[50] T. Bäck, "Optimal mutation rates in genetic search," in *Proc. 5th Int. Conf. on Genetic Algorithms*, S. Forrest, Ed. San Mateo, CA, USA: Morgan Kaufmann, 1993, pp. 2–8.

[51] T. C. Fogarty, "Varying the probability of mutation in the genetic algorithm," in *Proc. 3rd Int. Conf. on Genetic Algorithms*, J. D. Schaffer, Ed. San Mateo, CA, USA: Morgan Kaufmann, 1989, pp. 104–109.

[52] G. Rudolph, *Convergence Properties of Evolutionary Algorithms.* Hamburg, Germany: Verlag Dr. Kovac, 1997.

[53] Z. Michalewicz, *Genetic Algorithms + Data Structures = Evolution Programs*. Berlin, Germany: Springer, 1996.

[54] S. Saygan, Y. Akkuş, Z. Dursunkaya, and B. Çetin, “Fast and predictive heat pipe design and analysis toolbox: H-PAT,” *Isı Bilimi ve Tekniği Dergisi*, vol. 42, no. 1, pp. 141–156, 2022, doi: 10.47480/isibted.1107492.

[55] S. Saygan, Y. Akkuş, Z. Dursunkaya, and B. Çetin, “Capillary boosting for enhanced heat pipe performance through bifurcation of grooves: Numerical assessment and experimental validation,” *International Communications in Heat and Mass Transfer*, vol. 137, art. no. 106162, Oct. 2022, doi: 10.1016/j.icheatmasstransfer.2022.106162.